ORNL/TM-2023/2924

R-matrix Resolved Resonance Region Evaluation of ^{140,142}Ce

Chris W. Chapman
Marco T. Pigni
Klaus Guber
Goran Arbanas

November 2023

OAK RIDGE National Laboratory

ORNL IS MANAGED BY UT-BATTELLE LLC FOR THE US DEPARTMENT OF ENERGY

ORNL/TM-2023/2924

Nuclear Energy and Fuel Cycle Division

R-matrix Resolved Resonance Region Evaluation of ^{140,142}Ce

Chris W. Chapman
Marco T. Pigni
Klaus Guber
Goran Arbanas

November 2023

Prepared by
OAK RIDGE NATIONAL LABORATORY
Oak Ridge, TN 37831
managed by
UT-Battelle LLC
for the
US DEPARTMENT OF ENERGY
under contract DE-AC05-00OR22725

CONTENTS

LIST OF FIGURES

LIST OF TABLES

ABBREVIATIONS

ORNL	Oak Ridge National Laboratory
JENDL	Japanese Evaluated Nuclear Data Library
WPEC	Working Party on International Nuclear Data Evaluation Co-operation
GELINA	Geel Electron Linear Accelerator
RM	Reich–Moore
RRR	resolved resonance region
ENDF	Evaluated Nuclear Data File
TOF	time of flight
MACS	Maxwellian stellar-averaged capture cross section
MLBW	multilevel Breit–Wigner
URR	unresolved resonance region
DSD	direct-semidirect
DC	direct capture

ABSTRACT

Oak Ridge National Laboratory completed the resolved resonance region (RRR) evaluation of the two most abundant cerium isotopes, ^{140}Ce (88.45%) and ^{142}Ce (11.11%) [1], as requested by the US Nuclear Criticality Safety Program [2]. These evaluations are based on recent high-resolution transmission and capture measurements performed on ^{nat}Ce and highly enriched ^{142}Ce samples at the JRC-Geel Linear Accelerator facility, as well as measured thermal constants available from the EXFOR database [3]. Starting from the resonance parameters of the ENDF/B-VIII.0 library [4] followed by a preliminary *R*-matrix analysis [5], an updated set of resonance parameters and corresponding covariance information were derived by fitting these measured data using the Reich–Moore approximation of the *R*-matrix theory, as implemented in the SAMMY code system [6]. The ^{140}Ce RRR upper energy limit was kept at 200 keV, whereas the ^{142}Ce resonance region was extended from 13 to 26 keV. Updated statistical properties were obtained for the new evaluations and compared to those derived from the ENDF/B-VIII.0 nuclear data library. The new evaluation work improved some of the discrepancies found in previous work, such as the capture resonance integral and stellar Maxwellian-averaged cross sections. These integral quantities were mainly derived from the fit of the latest measured data, especially the neutron capture yield data for ^{142}Ce isotope.

1. INTRODUCTION

Cerium has multiple applications to the fields of nuclear energy and nuclear criticality safety. In 2008, the Hanford Plutonium Finishing Plant specifically identified the need for improved cerium cross section data, as cerium is found in chemical processing streams due to its use as a catalyst or additive for chemical applications such as glass polishing powder. For this reason, cerium appears as an admixed material in process streams. Additionally, several prominent primary fission products such as ^{140}Ba ($\tau_{1/2}$=12.7 days) and ^{140}La ($\tau_{1/2}$=1.7 days), produced in the fission of both ^{235}U and ^{239}Pu, β^- decay into ^{140}Ce, making it a prominent secondary fission product. Therefore, cerium is also likely to be found in spent fuel arrays.

Besides applied science interest, cerium interaction with neutrons is important to nuclear astrophysics, particularly for the nucleosynthesis of heavy elements. In fact, the majority of elements heavier than iron are thought to be made in different stellar environments by a chain of subsequent neutron captures followed by β-decays. Due to the increasing Coulomb barriers and decreasing binding energy per nucleon, the fusion of charged particles by nucleosynthesis is no longer a viable process for nuclei heavier than ≈60 atomic mass unit (amu). Because of this, three stellar nucleosynthesis processes are responsible for heavy element synthesis: *s*-process, *r*-process, and *p*-process [7]. Of particular interest is the slow neutron capture process (*s*-process) that occurs in thermally pulsed asymptotic giant branch (AGB) stars, which have a relatively low neutron density, meaning the nucleosynthesis process is constrained to the valley of β stability. Therefore, the *s*-process abundances can be calculated using observed isotopic abundances, β decay rates, and Maxwellian averaged neutron capture cross sections. Of special interest are the so called *s*-only nuclei, which are shielded against contribution from the *r*-process by its stable isobar and can thus be produced only by the *s*-process. Likewise, certain unstable isotopes in the nucleosynthesis path are important because certain conditions from the s-process can be deduced; these are called called branching points. If the unstable isotope lives long enough, then the nucleosynthesis path can branch and bypass certain isotopes, as is the case in the cerium–neodymium region. Due to a closed neutron shell ^{140}Ce has a rather small neutron capture cross section, and, consequently, ^{140}Ce is located on s-process peak of the solar abundance. ^{142}Ce is the next stable isotope and shields ^{142}Nd from contribution of the r-process, making it an s-only isotope, an interesting calibration point for the *s*-process calculations. Accurate ^{140}Ce and ^{142}Ce Maxwellian averaged

capture cross sections are crucial in understanding the *s*-process path branching in this cerium–neodymium region.

The first set of resonance parameters for the ^{140}Ce isotope was evaluated for the release of the Japanese Evaluated Nuclear Data Library JENDL-2 [8, 9]. This evaluation was based on neutron widths measured by Hacken [10] and Camarda [11], as well as the radiation widths measured by Musgrove [12]. Later revisions of the Japanese library included experimental data measured by Ohkubo [13]. For the ^{142}Ce isotope, the resonance parameters were predominately adopted from Ohkubo [13], including some variations in the neutron and capture average widths estimated by Mughabghab, as reported in the ATLAS of neutron resonances [14]. The set of resonance parameters of ^{140,142}Ce included in the US ENDF/B-VII.0 nuclear data library [15] was based on the recommendations of the WPEC Subgroup 23 [16]. Here, the recommended set of resonance parameters was primarily adopted from the ATLAS compilation [14]. In that compilation as well as in the corresponding evaluated data reported in the ENDF/B-VIII.0 library, two ^{142}Ce neutron widths between 1 and 2 keV appear to be reported with the wrong units, resulting in large discrepancies with the ^{nat}Ce [17] and ^{142}Ce [18] measured data in that energy range. With these and additional available experimental data, a new set of resonance parameters was evaluated for ^{140,142}Ce. Additional resonance levels for ^{140}Ce were included while keeping the existing resolved resonance region (RRR) upper energy range at 200 keV. Because of the excellent resolution of the measurement performed on the highly enriched ^{142}Ce sample, it was possible to extend the RRR upper energy range from 13 to 26 keV. Moreover, the Bayesian fitting procedure used for the optimization of the resonance parameters provided the corresponding covariance information for both ^{140,142}Ce, which is of fundamental importance to support sensitivity and uncertainty analyses, for instance, on reactivity coefficients.

A summary of some properties of the cerium isotopes is given in Table 1, where E_{inel} is the inelastic scattering threshold energy important to define the upper limit of the RRR evaluations, as inelastic neutron scattering was not measured.

Table 1. Properties of cerium isotopes[(a)]

Isotope	I^{π}	Mass (amu)	Abundance (%)	E_{inel} (keV)
^{136}Ce	0^+	135.9071294	0.185	522.2
^{138}Ce	0^+	137.9059890	0.251	788.7
^{140}Ce	0^+	139.9054464	88.450	1596
^{142}Ce	0^+	141.9092499	11.114	641.3

[(a)]Due to the lack of high-resolution experimental data and very low isotopic abundances in ^{nat}Ce (<0.5%), ^{136,138}Ce are not included in this analysis.

A description of the experimental data used for the evaluation is given in Section 2, and details about the evaluation methodology are provided in Section 3. Finally, some concluding thoughts and potential areas for improvement are given in Section 4.

2. EXPERIMENTAL DATA

Although several transmission experiments were performed on cerium isotopes, most were performed over a limited neutron energy range. Only a few data sets from Hacken [10], Camarda [11], Ohkubo [13], and Newson [19] were found to have a sufficient upper neutron energy limit and, in some cases, sufficient resolution to determine spectroscopic resonance information. For neutron capture experiments, only a set of ^{140}Ce measured data reported by Musgrove [12] exists. Therefore, the available experimental data for ^{140,142}Ce in the EXFOR database is quite limited despite their being the most common isotopes of the rare earth elements. This also motivated the experimental campaign performed at GELINA within NCSP as a nuclear data need; results are reported in the next subsections.

2.1 EXFOR DATABASE

The high-resolution total cross section (or transmission data) and capture yield data considered in this analysis are listed in Table 2 summarizing the analyzed experiments as well as some properties of the experiments such as thickness, sample, and energy range.

Table 2. Available experimental data sets.

Author (year)	Sample	Data type	Experimental[(a)]		Evaluated[(a)]		Thickness[(b)]
			E_{min}	E_{max}	E_{min}	E_{max}	(10^{-3} a/b)
Hacken (1974)[(c)]	$^{140}CeO_2$	Total	1	68	2.5	63	4.76 21.51
Ohkubo (1993)[(c)]	$^{140}CeO_2$	Total	0.709	182	2.5	55.11	N/A
	$^{142}CeO_2$	Total	0.709	182	1.2	49.25	N/A
Guber (2016)	^{nat}Ce metal	Transmission	0.1	500	1	200	5.530(2)
			0.1	897.7	1	200	28.71(1)
		Capture yield	0.1	1000	1	200	5.530(2)
Guber (2019)	$^{142}CeO_2$	Transmission	0.2	300	1	200	4.523(2)
		Capture yield	0.1	1000	1	200	4.523(2)

(a) All energies are in units of keV.
(b) Uncertainties are listed such that 5.530(2) corresponds to 5.530±0.002. Measurements with no provided uncertainties will have no parenthetical note.
(c) Excluded from the *R*-matrix analysis.

Analysis of both sets of Hacken's measured data revealed anomalous resonances at 5.9 and 35 keV, corresponding to well-known neutron resonances of ^{27}Al. Because the measurements were performed on a cerium oxide sample, the aluminum contamination came most likely from the sample holder used to encapsulate the powdered sample of cerium oxide.

The theoretical cross sections were calculated both with and without the oxygen resonance parameters taken from Sayer [20]. The inclusion of oxygen parameters did not show an appreciable difference in the calculated cross sections, suggesting that oxygen contribution for such a sample configuration was negligible. The same test was performed with the aluminum resonance parameters, which, on the contrary, showed a noticeable difference. To demonstrate this, the aluminum resonance parameter was added for each sample, and then the values of the resonance widths were manually adjusted until the magnitude of the peaks were reached between the two samples. This is shown below in Fig. 1. Because the magnitude of the adjustments was significantly different between the two samples (0.8 for the thick sample and 2.5 for the thin sample), this strongly suggests that the data were not appropriately corrected for the presence of aluminum. Additionally,

there were no reported uncertainties in the EXFOR entry, nor any attempt to quantify uncertainties in the publication. For these reasons, Hacken's data had to be excluded from the present resonance analysis.

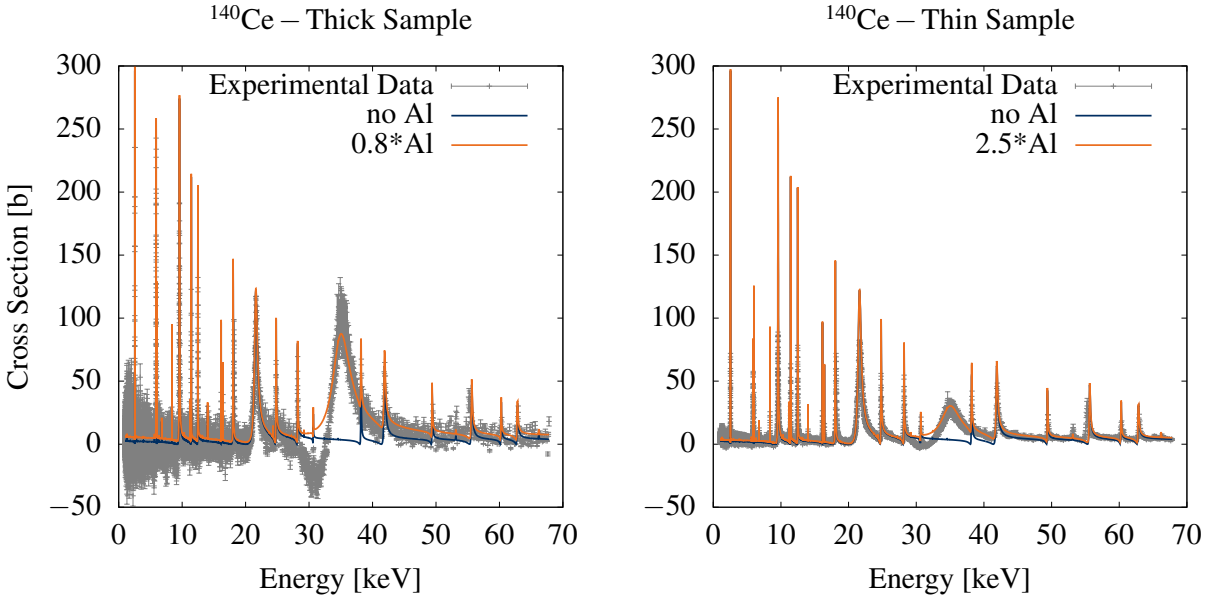

Figure 1. n+^{140}Ce total cross sections measured by Hacken [10] compared with the cerium resonance parameters in ENDF/B-VIII.0 without aluminum (blue line), and with a best guess estimate of the aluminum concentration (orange line).

The EXFOR entries referring to Ohkubo's measured cross sections did not contain sample thickness information. This is consistent with the source publication stating the measurements were performed with varying thicknesses. Since it is practically impossible to derive the sample thicknesses for this set of data, and, additionally, without error analysis information, Ohkubo's data were excluded form the present analysis.

2.2 GELINA MEASUREMENTS

The experiments were performed at the Geel Electron Linear Accelerator (GELINA) time-of-flight (TOF) facility [21] at the Joint Research Center of the European Union in Geel, Belgium (JRC-Geel). Neutron production at GELINA begins with a pulsed beam of electrons accelerated to 150 MeV. The pulsed electron beam is further compressed to a pulse width of 1 ns using a bunching magnet located before the neutron production target. The compressed electron pulses impinge on a rotating target of depleted uranium, producing high-energy γ-rays when stopped. The neutrons are released from the uranium target via the (γ,n) and (γ,fission) reactions. Two beryllium canned water containers mounted above and below the uranium target serve as a moderator for the neutrons. This produces a neutron spectrum with energies in the range of 10 meV–20 MeV. The long flight paths at GELINA (up to 400 m) coupled with the electrons' short pulse width result in an excellent TOF and hence neutron energy resolution, facilitating the resolution of individual resonances in the neutron cross sections to high neutron energies. For cerium, two kinds of experiments were performed at GELINA: neutron capture and transmission using different samples.

2.2.1 Samples

For neutron-induced cross section measurements, the preferred material composition is a metallic sample to avoid and reduce background effects from the sample. In many cases, however, enriched isotopes are manufactured as compounds, the most likely form being either an oxide or a carbonate. Unfortunately, neutrons are highly likely to scatter from the oxygen or carbon in those samples, which can in the case of a capture experiment lead to the capture of the neutron in the close surroundings of the experimental setup and produce an unwanted signal that can falsify the observed capture yield. Additionally, oxides are hygroscopic and can absorb water to form hydroxide. This can also lead to results which can be misinterpreted [22]. The process to convert those ceramic compounds into metallic samples is complicated and often cost-prohibitive.

For these reasons, the ^{140}Ce experiments were conducted using two metallic disks with different thicknesses, each containing a natural abundance of ^{140}Ce. Metallic cerium is slightly reactive in air and oxidizes over time. Because of this, the samples were encapsulated in thin-walled aluminum containers. The corresponding empty aluminum containers were also measured for background corrections. Conversely, for ^{142}Ce, an enriched $^{142}CeO_2$ sample was leased from Oak Ridge National Laboratory (ORNL) and used for the ^{142}Ce experiments to limit the cost of the samples. The sample was heated to a high temperature to remove all moisture from the oxide before it was pressed to a self-supporting disk. To further protect the oxide disk from absorbing water, it was also encapsulated in a thin-walled aluminum container. The exact sample characteristics of the three samples are given in Table 3.

Table 3. Sample properties of GELINA experiments.

Sample composition	Diameter [cm]	Thickness [cm]	Thickness [10^{-3} a/b]	Mass [g]	Ce-Abundance [%] 136	138	140	142
^{nat}Ce Metal	5.985(1)	0.993(1)	28.71(1)	187.975(1)	0.19	0.25	88.45	11.11
^{nat}Ce Metal	5.985(1)	0.185(1)	5.530(2)	34.975(1)	0.19	0.25	88.45	11.11
$^{142}CeO_2$	6.000(1)	0.285(1)	4.523(2)	37.014(1)	0.00186	0.002	7.93	92.07

2.2.2 Determination of the capture yield

The neutron capture experiments were performed at the GELINA 60 m flight path station using four deuterated benzene (C_6D_6) detectors. The four detectors were mounted in a backward angle of 125°relative to the neutron beam. The pulse height weighting method was applied to the detected γ-rays. The weighting functions were calculated for each sample using MCNP [23]. Details about the calculations including the detector materials, geometry, and environments can be found in Borella [24] and the references therein. For the pulse height weighting technique used by the GELINA detectors, a systematic uncertainty of less than 2% was estimated [25].

The thin natural cerium sample was positioned in the neutron beam at a distance of 58.85(1) m from the neutron production target, whereas the enriched $^{142}CeO_2$ sample was placed at 58.68(1) m from the target. A ^{10}B-loaded ionization chamber located approximately 80 cm upstream of the sample was used to determine the neutron flux shape. At the time of the capture experiments, GELINA was operating with an 800 Hz repetition rate and a 1 ns pulse width. A ^{10}B slab was used as a frame overlap filter to prevent the counting of low-energy neutrons from the previous neutron pulse. Additionally, a lead slab reduced the effect of high-energy γ-rays (bremsstrahlung) emitted by the neutron production target when the electrons get stopped.

Supplemental measurements included the empty aluminum container, empty sample holder, and a carbon scattering sample to account for background effects from sample scattered neutrons. Those neutrons can get captured in the area surrounding the detectors and produce an unwanted capture signal, which can produce false capture events if it occurs within the TOF width of the resonance. For the natural cerium sample runs with ^{10}B, sodium and sulfur background filters were included to have calibration points for the background correction; additionally, a run was performed with a ^{10}B overlap filter only. The data with only the ^{10}B filter were used in the analysis of the natural cerium sample. The ^{142}Ce data were obtained with two different filter combinations: ^{10}B, W, Co, Na; and ^{10}B, Co, and S filters in the beam. The latter combination was used for data analysis.

A dedicated experiment using natural iron sample was performed to obtain the capture yield of the 1.15 keV resonance of ^{56}Fe. This resonance is well studied and has been shown in the literature to be a good candidate to obtain a normalization factor for the acquired cerium neutron capture experiments. The data reduction procedures for the iron experiments were the same as described for the cerium yield, except that the empty holder instead of the aluminum container was used as open beam data.

The experimental capture yield in dependence of TOF is calculated from the count rate of the C_6D_6 detectors corrected for background and divided by the neutron fluence. In brief, the dead time corrected and weighted data for the aluminum container and scattering sample are subtracted from the weighted cerium data after normalizing all to the same neutron counts, which were obtained with a BF_3 counter in the neutron production hall. The capture yield is given as

$$Y_{\mathrm{exp}} = N_{\mathrm{exp}} \frac{C_{\mathrm{exp}} - B_{\mathrm{exp}}}{\varphi}\,, \tag{1}$$

where the time-dependent C_{exp} and B_{exp} are the dead time corrected, weighted, and normalized count rate from the sample and background, respectively, as detailed in [24]. N_{exp} is the normalization factor determined from the dedicated iron sample experiment, which is known to be better than 2%. The time-dependent neutron flux $\varphi \equiv \varphi(t)$ is determined by the ^{10}B ion chamber, using the ^{10}B (n,α) cross section from the ENDF/B-VIII.0 library. A detailed description about the data correction and reduction can be found in Schillebeeckx [25].

To achieve a sufficient count rate, neutron capture cross sections experiments are ideally performed with a thin sample. However, due to the low capture cross section of ^{140,142}Ce, thicker samples were required. This, in addition to the fact that scattering is the dominant reaction, leads to several experimental corrections that need to be accounted for in the data analysis program (e.g., self-shielding, multiple scattering, neutron energy resolution function). These corrections can be quite sizeable and can require reliable neutron widths as input to the data analysis programs. The lack of this information can result in erroneous capture cross section data, as shown in Koehler [26].

2.2.3 Determination of the transmission data

Transmission measurements were performed using a ^{6}Li loaded glass scintillator 0.635 cm thick to detect sample-transmitted neutrons. The detector was placed 49.33(1) m from the neutron production target in flight path number 4. The photo multiplier tube of neutron detector was mounted outside of the neutron beam in such a way that only GELINA neutrons illuminated the lithium glass. The neutron beam at the sample was collimated to a diameter slightly smaller than the diameter of the sample under investigation.

A computer-controlled sample changer cycled the samples in and out of the beam synchronized with the accelerator pulses. This approach helps to reduce systematic effects from changes of detector efficiencies and beam intensities over time. The background for this kind of TOF experiment consists of a time-dependent and time-independent component. Details of these background compositions, determinations, and corrections are given in Schillebeeckx [25]. The technique to measure these backgrounds is by inserting different materials used as filters into the neutron beam path while collecting the data counts for the transmission measurements; the background is determined because of the saturated resonances found in these filters (e.g., W, Co, Na, S). Due to the setup and geometry, all neutrons are scattered out of the beam at these energies and provide points to fit the shape of the background. Dedicated runs were done with tungsten, cobalt, and sodium background filters to obtain the background shape, which was normalized to the transmission data obtained with only a cobalt filter. This kept the interference of the background filters with the data to a minimum. The experimental transmission is given by

$$T_{\text{exp}} = N\frac{C_{\text{in}} - B_{\text{in}}}{C_{\text{out}} - B_{\text{out}}}\,, \tag{2}$$

where time-dependent $C_{\text{in/out}}$ are the dead time corrected count rates of sample in and sample out, with $B_{\text{in/out}}$ as their corresponding backgrounds. The backgrounds were obtained using dead time corrected and normalized TOF spectra with black resonance filters. N is an energy-independent normalization factor for the ratio of sample in and sample out, determined by the count rate of a BF_3 ion chamber located in the ceiling of the neutron production target hall. A typical uncertainty for this ratio is less than 0.5%. Details about the background determination and data reduction for the transmission experiments and related uncertainties can be found in Schillebeeckx [25].

With the transmission data, a complete set of resonance parameters can be obtained for the resolved cerium resonances, which enables calculation of the appropriate correction factors for the capture yield using the resonance analysis program SAMMY [6].

2.2.4 Reduction Analysis

All pulse height and TOF information from transmission, capture, and flux measurements were stored in list mode (containing information about each event, including TOF, pulse height, etc.) on disk together with a report file that stores scalers for various controls (e.g., t0, neutron flux count, etc.). These scalers are used to determine which list mode runs are included in the data analysis.

While sorting the data, stability checks using scalers and counts for different TOF windows were made to exclude unstable runs. The accepted runs were sorted into TOF spectra for transmission depending on sample in, sample out, and background filtered runs. The same procedure was applied to the capture runs after applying gain shift corrections and pulse height weighting for the capture data, respectively. Known resonance energies from background filters and other materials in the beam such as aluminum or lead were used to calibrate the neutron energy scale of the TOF spectra.

The Analysis of Geel Spectra (AGS) software was used for data reduction analysis, which consists of converting recorded count rates into observables such as transmission and reaction yield data. The AGS code also performs a full uncertainty propagation including both uncorrelated uncertainties due to counting statistics and correlated uncertainty components such as those from normalization factors. The full covariance information after each operation is stored in vectorized way [27]. AGS code is also used for background and dead time effect corrections as well as normalization. In the final step for capture measurements, the yield data are normalized using the 1.15 keV resonance in ^{56}Fe obtained from the iron capture yield runs.

3. RESONANCE ANALYSIS

The multilevel multichannel *R*-matrix analysis of the measured data was performed by using the SAMMY code [6]. Unlike the extant ENDF/B-VIII.0 ^{140,142}Ce evaluations that were performed within the superseded multilevel Breit–Wigner (MLBW) formalism, this work used the Reich–Moore (RM) approximation of the R-matrix theory. For the analyzed nuclei, RM is commonly accepted as the recommended method to perform resonance parameter evaluations [28] since the capture widths can be approximated by an average value proportional to the sum of all possible gamma transitions. Additionally, this work generated, by design, covariance information that is not reported in the ENDF/B-VIII.0 library and is often needed for sensitivity studies. Together with obvious corrections, the set of resonance parameters from the ENDF/B-VIII.0 library was purely used as prior information to fit the selected suite of measured data. The major inconsistencies to be addressed in ENDF/B-VIII.0 resonance parameters were related to three resonances between 1 and 2 keV. Although these levels belong to the minor isotope ^{142}Ce, due to their large widths, they are also visible in transmission data measured on ^{nat}Ce sample—namely, at 1.15, 1.28, and 1.68 keV. Especially for the levels at 1.15 and 1.68 keV, the significant discrepancy with the measured data derives from the incorrect compilation of the spin group in the ENDF/B-VIII.0 library. In fact, visual inspection indicates that both 1.15 and 1.68 keV levels are most likely related to p-wave resonances, but both are listed as s-wave resonances in ENDF/B-VIII.0 library. The s-wave spin assignment is highly unlikely due to the lack of negative interference between potential and resonant scattering, and it is also not supported by the average s-wave level spacing value of 1.5 keV for ^{142}Ce. As reported by Ohkubo [13], the level at 1.15 keV resonance was considered a very small probable p-wave level, slightly higher (2.8 eV) than the 1.15 keV resonance level of ^{56}Fe. Its neutron width was not specified by Ohkubo, but the value of 50 eV given in Mughabghab [14] is significantly larger than one would expect for a small p-wave. Therefore, the small width value was considered a transcription error that should have been listed as 50 meV. The neutron width for the 1.68 keV resonance level was first reported Anufriev [29] to be 10 eV. The other resonance widths in this publication appear to be of the correct magnitude, so it is unclear why this one specifically also appears to be off by 3 orders of magnitude. An image of the ^{nat}Ce thick sample transmission data reconstructed from the resonance parameters with and without these corrections is given below in Fig. 2. Throughout the rest of this report, all results with ENDF/B-VIII.0 parameters are assumed to be the corrected values unless explicitly stated otherwise. After the spin assignment and related corrections were performed, the quantification of the external levels discussed in subsection 3.1 was followed by a sequential Bayesian fit including the suite of measured data. This generated a set of evaluated resonance parameters based on SAMMY input files as reported in Appendix A and SAMMY par file reported in Appendix B. The resulting fit to the experimental data is shown in a series a plots in Appendix C for several energy ranges to magnify the quality of the fit in comparison to the ENDF/B-VIII.0 evaluation together with the point-by-point residual, denoted as σ_R.

3.1 EXTERNAL LEVEL QUANTIFICATION

The *R*-matrix analysis depends on resonance levels existing above and below the analyzed RRR energy range. These are usually called external levels [28], and their contribution can be approximated by using broad resonances whose widths are based on the statistics of the resonance parameters. This approximation is valid assuming that the average gamma width is much smaller than the RRR energy region as for ^{140,142}Ce. As shown by Fröhner [30], the energy and neutron width of the two broad resonances can be approximated by

$$E_{\pm} \cong \frac{E_{\max} + E_{\min}}{2} \pm \frac{\sqrt{3}}{2} I, \tag{3}$$

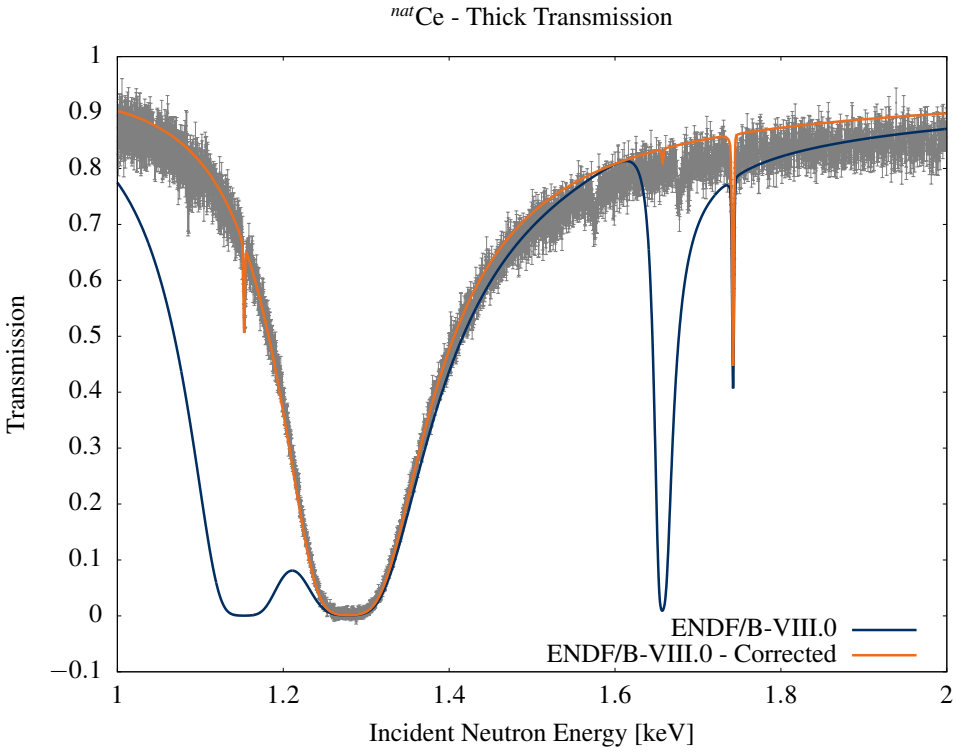

Figure 2. Comparison of ^{nat}Ce transmission data from the ENDF/B-VIII.0 library (blue), and corrected resonance parameters (orange).

$$\Gamma_{n\pm} \cong \frac{3}{2} I S_0 \sqrt{\frac{|E_\pm|}{1[\mathrm{eV}]}}, \tag{4}$$

where $E_{\max}$ is defined to be the energy of the last resonance in the RRR plus the average level spacing $\langle D \rangle$, $E_{\min}$ is the energy of the first resonance in the RRR minus the average level spacing, I is the energy range defined by $E_{\max} - E_{\min}$, and S_0 is the dimensionless s-wave strength function.

Although using two broad resonances is a good approximation, the resulting elastic scattering cross section will deviate from the analytical definition near the edges of the energy range. A further improvement on this approximation can be made by fitting two additional resonances closer to the bounds of the energy range. Two additional resonances were added at E=$E_{\min}$ and E=$E_{\max}$ with neutron widths equal to 1% of the values calculated for E_- and E_+, respectively. These resonances were then fitted to the analytical cross section calculated from the pole strength parameter

$$s_c = \frac{S_0}{2 k_c a_c} \sqrt{\frac{E}{1[\mathrm{eV}]}}, \tag{5}$$

where k_c is the wavenumber of the entrance channel c, and a_c is the channel radius. After defining the parameters of the external contribution as detailed in [5], the RRR evaluation proceeds by testing or deriving the spin assignment of each resonance level according to the χ^2 metric assuming available spin populations up to p-wave. This assumption was based on the energy-dependent penetrability factor for four partial waves

calculated over the anticipated energy region range of 1–200 keV. As shown in Fig. 3, the penetrability factors for the d- and f-wave can be considered negligible over the entire energy range and, therefore, excluded in the quantum number definition of each particle pair.

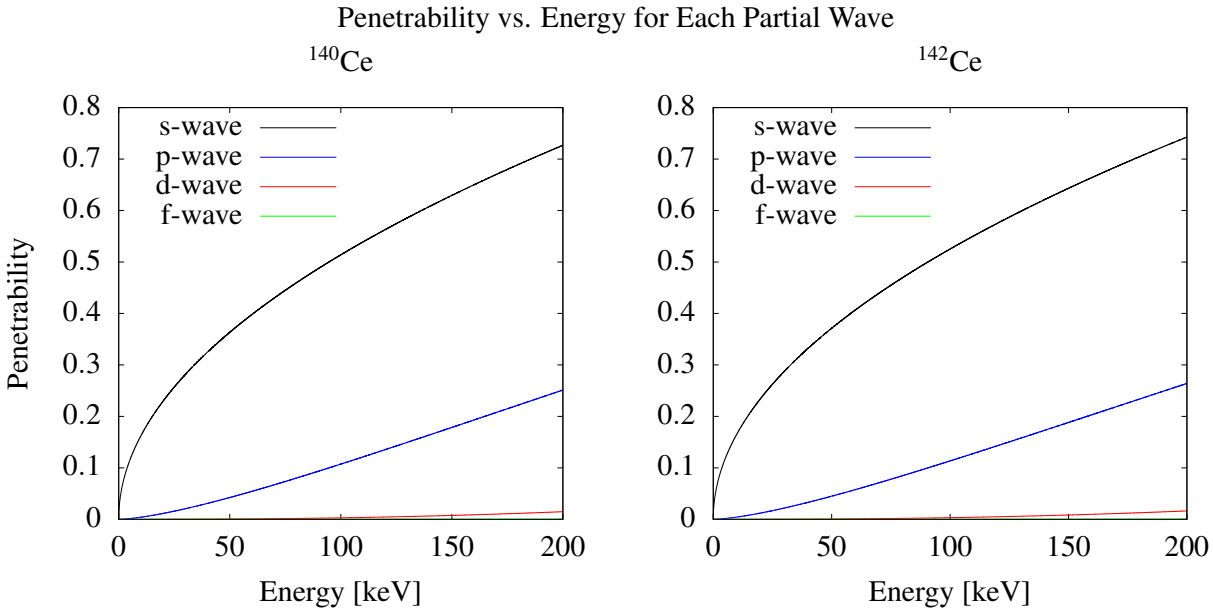

Figure 3. n+^{140,142}Ce energy-dependent penetrability factors for four partial waves.

3.2 DETAILS ON THE FIT OF ^{NAT}CE MEASURED DATA

To provide an idea of the impact of both the correction applied to the ENDF/B-VIII.0 set of parameters and the improved fit to the measured data, the χ^2 values for three experimental data sets for natural samples are given in Table 4. In this publication, unless explicitly stated otherwise, all reported values of χ^2 are really χ^2/N, where N represents the number of data points in the fitting procedure. As expected, an overall improvement is seen especially for transmission measurements even after accounting for the corrected library.

Table 4. Resonance parameter comparison according to the χ^2 metric for ^{nat}Ce measured data.

Measurement	**ENDF/B-VIII.0**		**ORNL**
	(original)	(corrected)	
Transmission (thick)	75	30	1.8
Transmission (thin)	17	2.1	0.74
Capture Yield	1.9	1.9	1.2

These data were primarily used for the fitting ^{140}Ce parameters, since ^{140}Ce is the most abundant isotope. The quantification of the external levels for ^{140}Ce in the ENDF/B-VIII.0 library was defined by 9 s-wave and 22 p-wave resonances above 200 keV from the Ohkubo measurements [13]. These were not included in the new ORNL evaluation, as the external levels were defined by four large s-wave resonances, as described in Section 3.1. In the RRR analyzed energy range up to 200 keV, 1 new s-wave and 19 new p-wave resonances

were added. The thick transmission sample is where the most notable improvements were found, mainly because the overall transmission data compared to the ENDF/B-VIII.0 evaluation either slightly overestimates the experimental data—for instance, as shown in Fig. 15—or reports mis-assigned spins, for instance, as shown in Fig. 16, near 11 keV. Other imperfections are found in misaligned resonances as in Fig. 16, near 18 keV, or missing resonances as in Fig. 19, between 100 and 120 keV. The thin transmission sample shows less significant differences between the two libraries, apart from some slight differences from misaligned resonances and the inclusion of several resonances above 100 keV to improve the overall fit to the measurement. The thin sample was primarily used to confirm spin assignments for p-wave resonances.

One area of particular interest is two spurious resonance features in Fig. 14 at 1.58 and 1.68 keV. These features cannot be seen in any of the other samples at these energies in Figs. 21, 28, 33, and 40. It is conceivable that these could be resonances in the minor cerium isotopes ^{136,138}Ce. Attempts made at fitting these resonances showed that each resonance could be described by a combination of ^{136,138}Ce s-wave resonances, but no justification could be made as to which resonance corresponds to which specific isotope. Because of this, no further attempt was made to fit them.

The capture yield results show a less significant improvement than the transmission data. This can be attributed to the fact that the capture cross section for both cerium isotopes is very small, leading to a very weak capture yield signal. This also results in very large uncertainties in the experimental data (in some areas over 100%), most notably at higher incident energies and between strong capture resonances where the capture cross section is at its minimum.

3.3 DETAILS ON THE FIT OF ^{142}CE DATA

Similarly to the ^{nat}Ce set of measured data, a table reporting χ^2 values for two selected measurements is given below showing an overall improvement.

Table 5. Resonance parameter comparison according to the χ^2 metric for ^{142}Ce measured data.

Measurement	**ENDF/B-VIII.0**		**ORNL**
	(original)	(corrected)	
Transmission	48	2.0	1.3
Capture Yield	1.8	1.9	1.1

Significant work was performed in extending the RRR of ^{142}Ce up to 26 keV. By comparison, the ENDF-B/VIII.0 evaluation has an RRR range from 0-13 keV, and URR range from 13-100 keV. The current evaluation has an RRR range from 0-26 keV and URR range from 26-200 keV. The ENDF/B-VIII.0 URR parameters from 26-100 keV were accepted in the current evaluation, and 39 s-waves and 159 p-waves were added to the RRR. Many of these resonances exist in the URR range, so they will not be present in the current evaluation. These levels are included in the SAMMY .par file listed in Appendix B in case higher resolution measurements of ^{142}Ce are conducted that allow for the extension of the RRR further.

Several ^{142}Ce transmission plots show a noticeable increase of the residuals in the energy region between 1 and 2 keV. This is particularly evident for the thick target measurement shown in Fig. 33. The large resonance width in combination with the target thickness leads to a saturated resonance in the energy range that can be properly fitted only thanks to the thin ^{nat}Ce transmission measurement (as in Fig. 21) designed to accurately measured the resonance amplitude.

Many improvements in the fitting of ^{142}Ce transmission data came from the inclusion of resonance information above 50 keV as shown in Figs. 37–38. Because the data are significantly noisier than the ^{nat}Ce data, small p-wave resonances were difficult to identify. The only resonances added were those for which a clear resonance structure in the measured data was seen. Due to their small magnitude, the capture yield measurement suffers from similar issues as the ^{nat}Ce capture yield data. Additionally, the data are associated with significantly large uncertainties at 30, 78, and 100 keV, as shown in Fig. 39. This is because of strong resonances present in the lead and sulfur filter, which eliminates neutrons at these energies, and thus only background is counted at these energies for which the data are corrected.

3.4 THERMAL CROSS SECTION EVALUATION

Thermal capture and scattering cross section values were compiled from available sources as reported in Tables 6 and 7. Several criteria, such as measurement technique together with the reliability and documentation of the measured data, were used to assign a weight applied to calculate the best estimate for the thermal constant values. Experiments were excluded if no uncertainties were provided.

Table 6. ^{140}Ce Thermal Values (in barns)

Quantity	Author & Year	Value	Weight
2200 m/s capture xs	Panikkath (2017) [31]	0.44 ± 0.01	0.4
		0.44 ± 0.02	0.4
	de Corte (1988) [32]	0.576 ± 0.006912	0.2
	Alian (1973) [33]	0.68∗	0
	Best Estimate	0.467 ± 0.001	
2200 m/s scattering xs	NIST (1992) [34]	2.94 ± 0.11	0.5
	ATLAS (2018) [14]	2.96 ± 0.11	0.5
	Best Estimate	2.95 ± 0.08	
Resonance Integral	Panikkath (2017) [31]	0.55 ± 0.03	0.33
	Torrel (2012) [35]	0.55 ± 0.02	0.27
	Heft (1978) [36]	0.483 ± 0.005	0.2
	Alian (1973) [33]	0.66∗	0
	Alstad (1967) [37]	0.49 ± 0.05	0.13
	Lantz (1964) [38]	0.48 ± 0.05	0.07
	Best Estimate	0.524 ± 0.011	

(*)No uncertainties were reported.

Table 7. ^{142}Ce Thermal Values (in barns)

Quantity	Author & Year	Value	Weight
2200 m/s capture xs	de Corte (1988) [32]	0.974 ± 0.01	1.0
	Best Estimate	0.974 ± 0.01	
2200 m/s scattering xs	NIST (1992) [34]	2.84 ± 0.11	0.5
	ATLAS (2018) [14]	2.85 ± 0.11	0.5
	Best Estimate	2.85 ± 0.08	
Resonance Integral	Torrel (2012) [35]	1.25 ± 0.06	0.33
	Heft (1978) [36]	1.66 ± 0.15	0.33
	Alstad (1967) [37]	1.6 ± 0.20	0.33
	Best Estimate	1.503 ± 0.085	

An additional negative resonance was tuned specifically to fit the available thermal values for elastic scatter-

ing, capture, and total cross section data. Instead of a single energy value at the thermal energy E=25.3 meV, artificial data was generated on an energy grid of equi-spaced values between 20 and 30 meV. For the capture channel, the standard $1/\sqrt{E}$ energy dependence was assumed differently from the elastic scattering data that were assumed with a flat energy dependence. Because the closest resonance for each isotope is above 1 keV, this would not significantly alter the energy dependence shape assumed for the thermal cross section.

For the thermal capture fit, several sources were used to fit ^{140}Ce [31, 32]. The value calculated by [33] was not included due to a lack of reported uncertainties. The mean value of these data is 0.467 ± 0.009, which was used as the prior for the fit. Unfortunately, only one source could be found to fit ^{142}Ce [32], meaning the prior was set to its value of 0.974 ± 0.010.

For the scattering fit, the values were calculated from an average of the measurements of the bound coherent scattering length from Mughabghab [14] and NIST [34] (because both ^{140,142}Ce are even-even nuclei, there is no incoherent contribution to thermal scattering, meaning the scattering is entirely described by the coherent contribution).

Table 8. n+^{140,142}Ce thermal cross sections (in barn).

Isotope	Source	Capture	Scattering
^{140}Ce	Experiment	0.467 ± 0.009	2.95 ± 0.08
	ENDF/B-VIII.0	0.577	3.62
	ORNL	0.463	3.07
^{142}Ce	Experiment	0.974 ± 0.010	2.85 ± 0.08
	ENDF/B-VIII.0	0.815	2.86
	ORNL	0.974	2.87

This thermal evaluation method leads to newly evaluated thermal constant values which differ from the ENDF/B-VIII.0 library. The fitted values predict a reduction of about 20% in the capture reaction channel for ^{140}Ce and an increase of about the same amount for ^{142}Ce, leading to a 15% reduction of the capture thermal value for ^{nat}Ce. There is a relatively small remaining discrepancy between the experimental and fitted thermal scattering cross section of ^{140}Ce that is about 15% lower than ENDF/B-VIII.0 value.

3.5 DIRECT-SEMIDIRECT CAPTURE CALCULATIONS

Since the ^{140}Ce nucleus has a closed neutron shell with a neutron number N=82, direct-semidirect (DSD) capture processes are expected to contribute a relatively large fraction of the total thermal neutron capture cross section [39]. Indeed, a calculation of the ^{140}Ce DSD capture cross section for a thermal neutron energy of 25.3 meV using the CUPIDO [40, 41] code yields 840 mb, overestimating the measured thermal neutron capture value of 467 mb. We point out that such an overestimation has been conventionally explained by a simple model of (destructive) interference between the direct and the compound nuclear resonant capture amplitudes for capture into each bound capturing level [42].

The CUPIDO methodology uses binding energies of the capturing bound states in ^{141}Ce, their single-particle quantum numbers, and their spectroscopic factors taken from [43]. The direct capture (DC) amplitude is computed as the expectation value of electromagnetic multipole transition operator between the incoming channel and the capturing bound state wave function, and the semidirect capture amplitude accounts for a two-step capture via a giant dipole resonance. It was found that the vast majority of the DC of thermal energy s-wave neutrons is due to the electric dipole capture into two excited bound states of orbital angular

momentum l=1 and relatively large single-particle spectroscopic factors. In fact, the calculated DSD thermal neutron capture into the two excited states of ^{141}Ce alone accounts for approximately 500 mb.

For comparison, a calculation of the thermal neutron DC alone* on ^{140}Ce into discrete bound levels using the TALYS-1.95 code and its database of calculated bound states yielded 955 mb, about 14% larger than CUPIDO calculations; such a discrepancy is well within the range of large uncertainties of the bound level energies and their spectroscopic factors.

For ^{142}Ce, the DC thermal capture cross section calculated by TALYS-1.95 yielded 700 mb which, as expected, is smaller than the DC value calculated for ^{140}Ce. This is because ^{142}Ce has two additional neutrons in an otherwise empty neutron shell that are expected to decrease (1) the binding energies and (2) the single-particle spectroscopic factors of the capturing states, where each of these decreases alone would cause the capture to decrease. This decrease in DC is completely analogous to the case for ^{132}Sn and ^{134}Sn as discussed by Chiba [39] for the same closed neutron shell N=82. We have not computed DSD capture on ^{142}Ce using the CUPIDO code because of the absence of any published bound state spectroscopic data of ^{143}Ce needed as input for CUPIDO calculation of DSD capture on ^{142}Ce.

Ideally, the DSD process and compound resonant capture should be fitted simultaneously to account for their interference in a phenomenological R-matrix formalism in which all capture processes are parameterized simultaneously [44]. Since the thermal neutron capture cross sections computed by both the CUPIDO code for the DSD process and TALYS-1.95 for the DC process are 40–50% higher than the averaged measured values reported in Table 8, this would indicate a strong correlation between the direct and compound mechanism. However, since the direct mechanism is expected to dominate for nuclei like cerium isotopes, a normalization factor >50% to account for a weak compound mechanism seems inconsistent and requires additional investigation. Therefore, although SAMMY has the capability to include DC cross sections in the fit procedure, the direct contribution was included by using negative resonances. Recent work has been conducted suggesting a novel way to parameterize the DC process such that it can be included in the R-matrix formalism [44]. This would be ideal since the correlation between the direct and compound process would be implicitly taken into account and, at the same time, this would greatly simplify the uncertainty quantification.

Table 9. n+^{140,142}Ce direct thermal cross sections (in mb).

Source	^{140}Ce	^{142}Ce
CUPIDO	840	N/A
TALYS	955	700
ATLAS	500	485

3.6 VALIDATION TEST

Integral measured data such as reactivity coefficients are usually used as benchmarks to validate nuclear data libraries. However, the lack of integral experiments containing appreciable amounts of cerium makes the validation of these nuclear data evaluations difficult. Instead, as integral quantities, we relied on resonance integrals and stellar-averaged capture cross sections to test the accuracy of the newly generated resonance parameters.

*the TALYS code does not yet compute the semidirect contribution to the capture cross section.

3.6.1 Capture Resonance Integral

The resonance integral is a metric used to approximate the epithermal absorption in a typical nuclear reactor. This metric is especially important for the ^{140}Ce isotope, being a stable secondary fission product. It is defined as

$$I_\gamma = \int_{E_3}^{\infty} \frac{\sigma_\gamma(E)}{E} dE\,, \tag{6}$$

where the lower limit of the integral is E_3=0.5 eV, the resonance integrals for ORNL evaluation work were calculated by NJOY2016 [45] and reported in Table 10 together with other values found in literature. The label experimental refers to an average value compiled by using the values found in previous work [31, 35, 36, 37, 38] for ^{140}Ce and elsewhere [35, 36, 37] for ^{142}Ce, similarly to the method described in Section 3.4.

Table 10. Capture Resonance Integrals (in barn)

Source	^{140}Ce	^{142}Ce
Experimental	0.524 ± 0.011	1.503 ± 0.085
ATLAS	0.54 ± 0.05	1.15 ± 0.05
ENDF/B-VIII.0	0.303	0.861
ORNL	0.296	1.010

There is clear disagreement between evaluated and measured data. As expected, the ^{140}Ce resonance integral value agrees with the ENDF/B-VIII.0 evaluation since the low-lying resonances were already in good agreement with the transmission data. It is unlikely that this discrepancy would be caused by the lack of DC contribution, since the integral accounts only for values above 0.5 eV, where the DC cross section is negligible.

The significant change in the ^{142}Ce resonance integral is likely due to the corrections of the resonance parameters in the 1–2 keV region. Although this is an increased value, the evaluated value is about 33% lower than the averaged experimental value by almost six standard deviations. Due to the relatively small thermal capture cross section values, the related integral is difficult to accurately measure, leading to discrepant results, as seen in Table 7.

3.6.2 Stellar-Averaged Capture Cross Sections

The Maxwellian stellar-averaged capture cross section (MACS) calculated at the temperature T (in Kelvin) is defined by

$$\left\langle \sigma(E)\sqrt{E} \right\rangle_{k_B T} = \frac{2}{\sqrt{\pi}(k_B T)^2} \int_0^{\infty} \sigma_{n,\gamma}(E) E e^{-E/k_B T} dE\,, \tag{7}$$

where k_B is the Boltzmann constant. For both isotopes, Table 11 reports evaluated values of the ENDF/B-VIII.0 library together with ORNL and ATLAS work, as well as measured values found in the KADoNiS database [46]. The ORNL values are calculated using the SAMMY code for a constant value $k_B T = 30$ keV, as this matches the value provided in the KADoNiS database. The SAMMY code calculates MACS using capture cross section reconstructed from resolved and unresolved resonance parameters (file MF=2) and, above the unresolved resonance range, capture cross section data (reported in file MF=3). In this work, capture cross sections taken from File MF=3 of the ENDF/B-VIII.0 library were used. Table 11 also reports the values for the KADoNIS database updated by the latest ^{197}Au(n,γ) data [47], as these data were used as reference cross sections for their measurements. When applied to both isotopes, this correction results in about a 5% increase. Comparing the updated values to the ORNL work, there are notable differences

between 20 and 25%. For the ^{142}Ce isotope, the increased value with respect to ENDF/B-VIII.0 library is

Table 11. Maxwellian averaged thermal cross section (in mb).

Source	^{140}Ce	^{142}Ce
KADoNiS	11.73 ± 0.44	29.9 ± 1.0
KADoNiS-new Au	12.32 ± 0.46	31.4 ± 1.1
ATLAS	9.7 ± 0.9	19.6 ± 1.1
ENDF/B-VIII.0	7.77 ± 0.22	20.29 ± 0.26
ORNL	15.43 ± 0.15	25.73 ± 0.13

related to the extension of the RRR from 13 to 26 keV and the fit of newly measured capture data. Therefore, the discrepancy with the KADoNIS database may reside in the URR above 26 keV, despite the fact that a large majority of the Maxwellian spectrum is less than 30 keV. This might indicate that a re-evaluation of the URR for ^{142}Ce is warranted.

3.7 STATISTICAL PROPERTIES OF THE RESONANCE PARAMETERS

In this section, we report the statistical properties of the resonance parameters for the ENDF/B-VIII.0 library and the ORNL evaluated work. These include average level spacing, average radiative width, and neutron strength function.

3.7.1 Cumulative Levels and Average Level Spacing

The cumulative level function for a given orbital angular momentum l is expected to increase linearly as a function of energy. As the incident neutron energy increases, the number of levels will deviate from the linear behavior because of the limited experimental resolution to measure closer and closer energy levels. Plots of the energy-dependent cumulative levels are shown in Figs. 4-7.

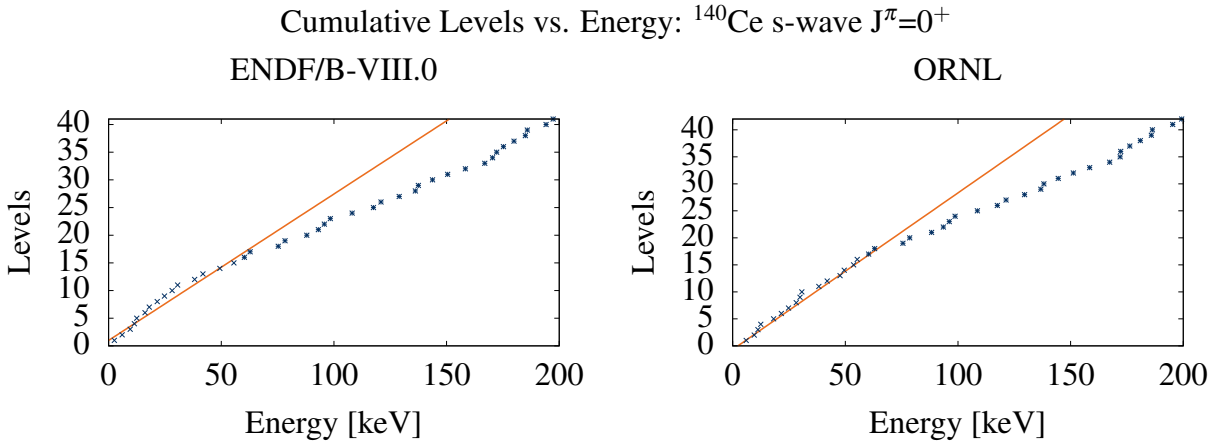

Figure 4. Energy-dependent cumulative levels for ^{140}Ce s-wave resonance parameters.

Both ^{140}Ce plots show a deviation away from the linear fit, although the deviation is more gradual in the s-wave distribution compared to the p-wave distribution. The deviation point occurs at 63 keV for the

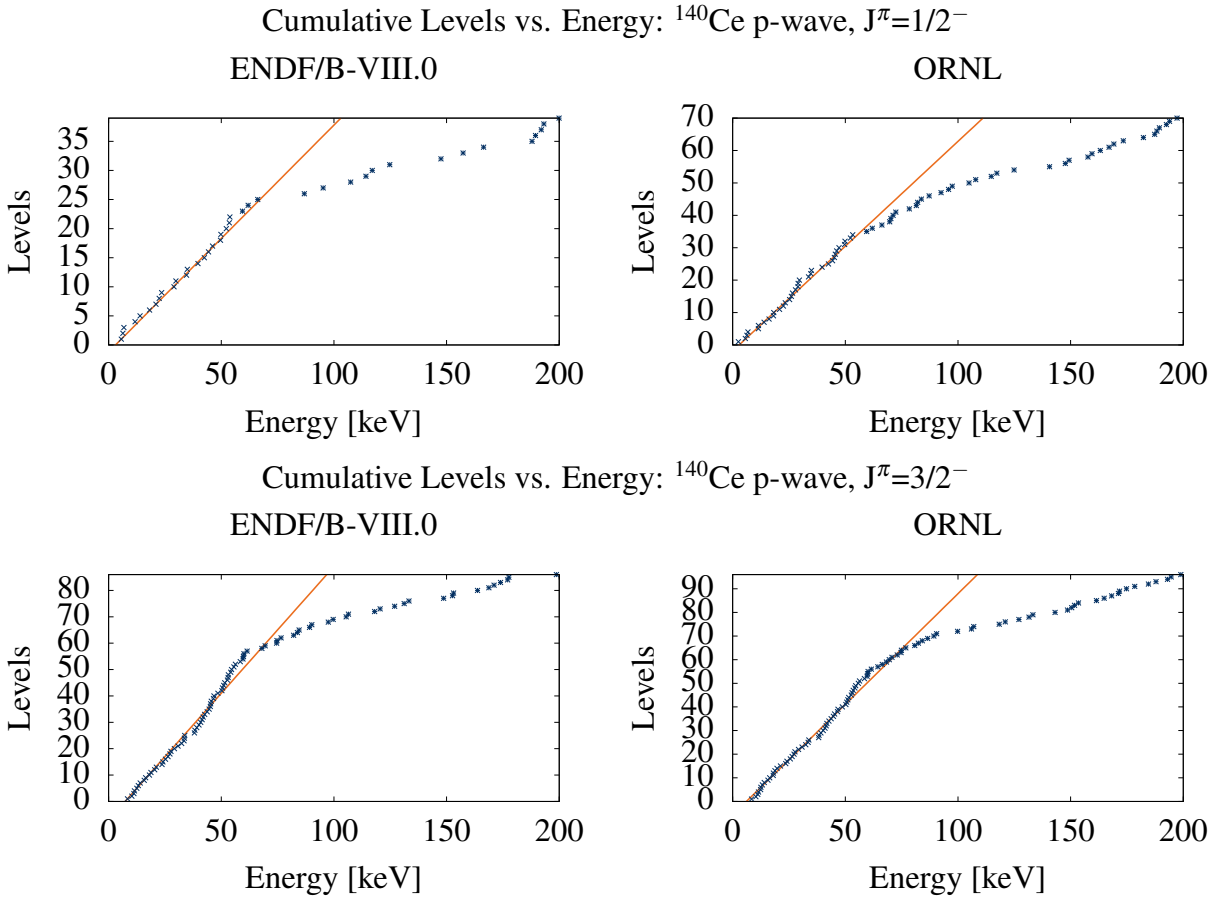

Figure 5. Energy-dependent cumulative levels for ^{140}Ce p-wave resonance parameters.

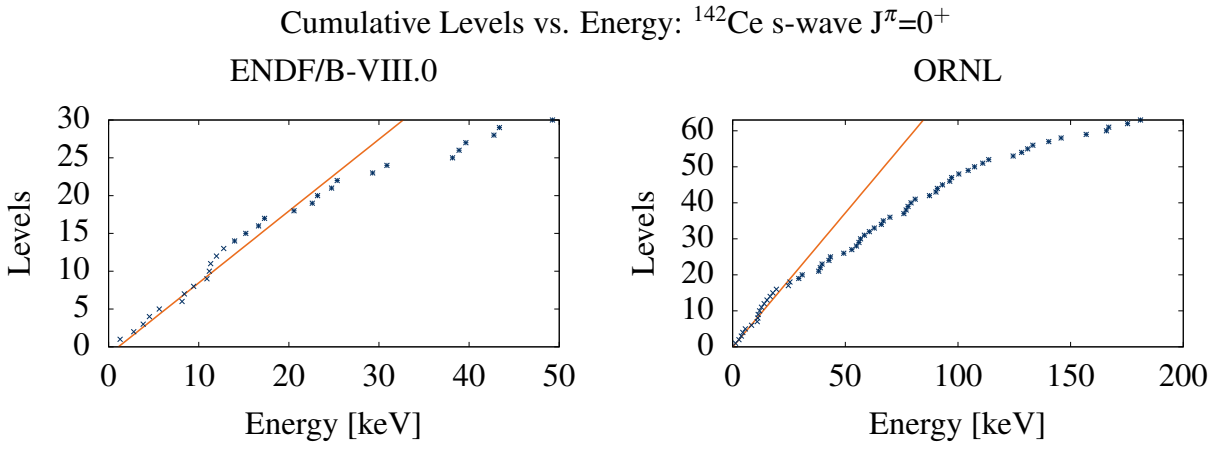

Figure 6. Energy-dependent cumulative levels for ^{142}Ce s-wave resonance parameters.

ENDF/B-VIII.0 library and 80 keV for the ORNL evaluation. This may be due to the fact that ENDF/B-VIII.0 resonances are primarily based on two measurements, one below 63 keV [10] and one spanning the

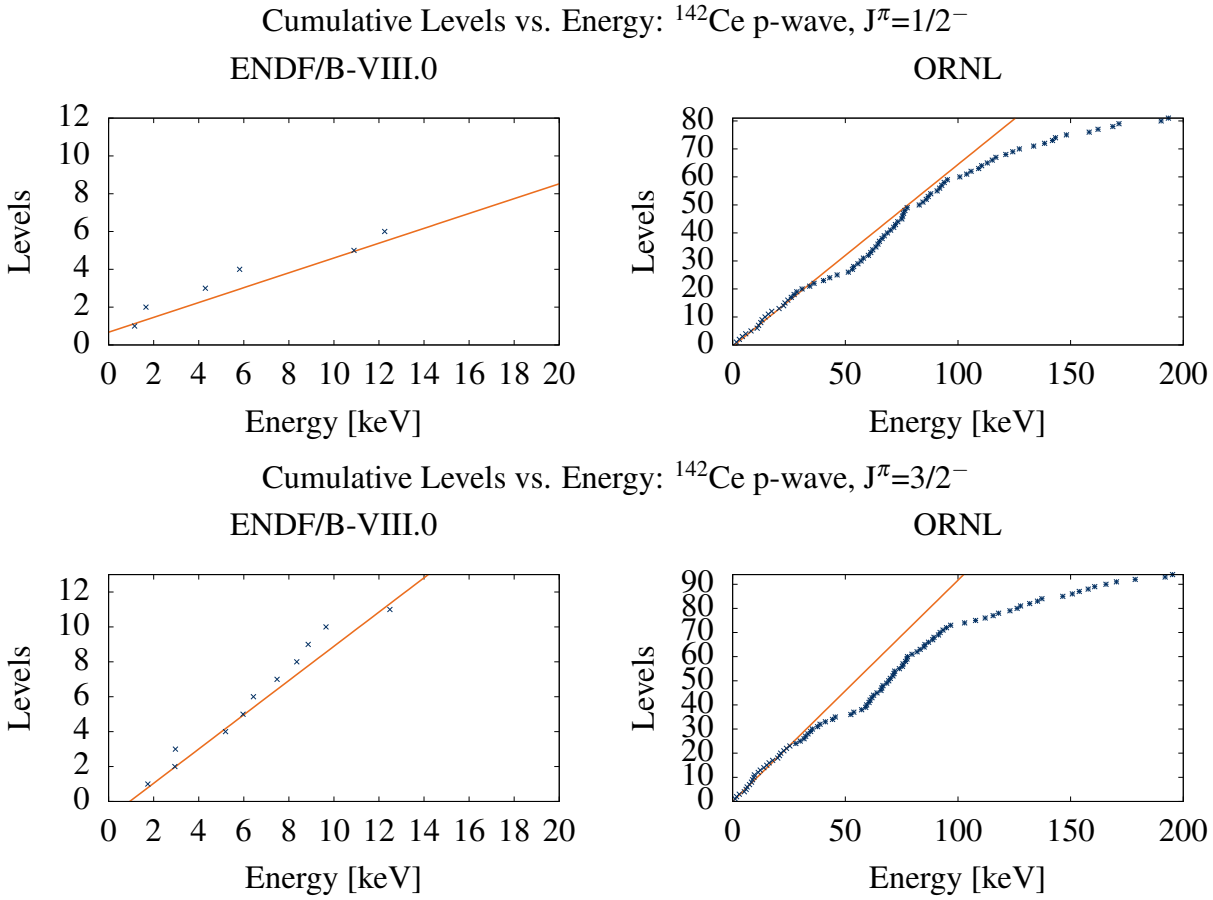

Figure 7. Energy-dependent cumulative levels for ^{142}Ce p-wave resonance parameters.

entire energy range [13]. It can be assumed that the former assigned more levels in their evaluation and is, therefore, a more faithful representation of the true level density. The new ORNL evaluation extended that point up to 80 keV but was unable to resolve significantly additional resonances above that point. The decision was made to keep the upper energy limit of the RRR at 200 keV, even though the level spacing statistics suggest that the limit should be closer to 80 keV.

The ^{142}Ce plots also show an expected gradual deviation from linearity for both s-wave and p-wave distributions. In the present evaluation, there were noticeable changes in the average level spacing for the ^{142}Ce s-wave parameters. This is largely due to the re-assignment of several low-energy ^{142}Ce s-waves to either ^{142}Ce p-waves or ^{140}Ce s-waves. There is a curious gap in the ORNL p-wave distribution near 50 keV, where there appear to be missing p-wave resonances, as the slope from 60 to 100 keV looks very similar to the slope below 26 keV. No resonances could be seen in this area, shown in Figs. 36–37. However, it is possible that additional p-wave resonances could be measured by increasing the experimental resolution.

The average level spacings derived from the slopes of the energy-dependent cumulative levels are reported in Table 12 together with $E_{\max}$ used as upper energy limit for the linear fit of the cumulative levels. The average level spacing for l=1 levels was obtained as the average of the J=1/2 and J=3/2 level spacings.

Table 12. ^{140,142}Ce average level spacing (in keV). E_{max} (in keV) is the upper energy limit used in the fit to obtain the average level spacing.

Isotope	Library	E_{max}	l=0	l=1
^{140}Ce	ATLAS	N/A	3.730 ± 0.470	1.550 ± 0.110
	ENDF/B-VIII.0	63	3.938	0.7875
		200	5.000	1.612
	ORNL	80	4.211	0.754
		200	4.878	1.212
^{142}Ce	ATLAS	N/A	1.490 ± 0.155	N/A
	ENDF/B-VIII.0	13	0.866	1.000
		50	1.563	3.333
	ORNL	26	1.529	0.684
		200	3.225	1.149

The ^{140}Ce s-wave level spacing for ENDF/B-VIII.0 agree favorably with the reported in Mughabghab [14], while the ORNL library is slightly larger than the reported value at the cutoff values of 63 and 80 keV, respectively. Both of these values significantly increase when the upper energy limit is raised to 200 keV, further indicating that levels are not being observed in the measured data above the cutoff value. It is curious to note that, for both the ENDF/B-VIII.0 and ORNL files, the p-wave level spacing at their cutoff value does not agree with the values reported in Mughabghab [14], but the level spacing at 200 keV does agree.

For ORNL ^{142}Ce s-wave and p-wave level spacings, there are significant deviations from the ENDF/B-VIII.0 s-wave distribution but reasonable agreement with the ATLAS value. This is likely the result of several low-lying s-wave resonances that were miscategorized (including the 1–2 keV issue mentioned earlier), as well as setting the upper energy cutoff at 13 keV instead of 50 keV (where the final resonance is located). It is difficult to discern any meaningful information from the ENDF-B/VIII.0 p-wave distribution, as there were only 16 p-wave resonances reported in the ENDF-B/VIII.0 file compared to the 175 p-wave resonances reported in this work.

3.7.2 Average Radiative Widths

Average radiative widths were calculated from the resonance parameters, and they are listed in Table 13. There is a large increase (above 50%) of the average radiative width for both isotopes from the ORNL parameterization in comparison to the ATLAS and previous ENDF compilations. This can be seen as a direct effect from the fit of the recently measured data, particularly for the ^{142}Ce isotope.

Table 13. ^{140,142}Ce average radiative widths (in meV).

Isotope	Library	l=0	l=1
^{140}Ce	ATLAS	43 ± 11	22 ± 2
	ENDF/B-VIII.0	39 ± 9	23 ± 0.3
	ORNL	120 ± 25	76 ± 15
^{142}Ce	ATLAS	N/A	N/A
	ENDF/B-VIII.0	30 ± N/A	30 ± N/A
	ORNL	79 ± 15	94 ± 21

3.7.3 Neutron Strength Function

The strength function can be calculated by the ratio of the average reduced neutron width to the average level spacing. Among other parameters, this quantity is used to generate average cross sections in the URR. The values are reported in Table 14 in units of 10^{-4}.

Table 14. ^{140,142}Ce neutron strength function (in 10^{-4} unit).

Isotope	Library	*l*=0	*l*=1
^{140}Ce	ATLAS	1.16 ± 0.34	0.34 ± 0.05
	ENDF/B-VIII.0	1.16	0.26
	ORNL	0.96	0.84
^{142}Ce	ATLAS	3.4 ± 0.7	0.13 ± 0.7
	ENDF/B-VIII.0	4.2	0.63
	ORNL	2.9	1.2

Comparing the two isotopes, it's clear that the s-wave strength functions are in agreement with the values reported in the ATLAS compilation. While the ^{140}Ce s-wave strength function is in worse agreement when compared to the ENDF/B-VIII.0 value, they are both within the statistical uncertainty reported in the ATLAS. Conversely, the ^{142}Ce s-wave function is in closer agreement to the reported value, most likely because of the aforementioned issue between 1–2 keV.

While the s-wave strength functions are in agreement with the reference value, the same cannot be said for the p-wave functions. Both the ^{140,142}Ce p-wave strength functions are significantly larger than both what's reported in the ATLAS and what's calculated from the ENDF/B-VIII.0 libraries. It is currently not clear why there is a significant increase in the ^{140}Ce p-wave strength function, as an overall agreement with p-wave resonances is seen in the ^{nat}Ce transmission data. It's possible this might be due to some p-waves assigned to the wrong spin groups.

The increase in the ^{142}Ce p-wave strength function is in large part due to the several large p-wave resonances between 20 and 25 keV, which can be seen in Fig. 36. Because the upper energy limit of this analysis is 26 keV, it incorporated these resonances and sharply increased the summed strength function used to calculate these values. A more accurate value could be found with higher resolution measurements.

4. CONCLUSIONS AND FUTURE WORK

An evaluated set of resonance parameters for ^{140,142}Ce isotopes was generated by significantly improving the agreement with available experimental data. In addition to key corrections to the ENDF/B-VIII.0 evaluation, as shown in Fig. 2, resonance parameters were fitted to recent transmission and capture yield data measured on ^{nat}Ce and ^{142}Ce samples at the GELINA facility as well as to thermal neutron constants available from the EXFOR database. The resulting best estimate parameters and corresponding covariance matrix were submitted to update the existing ENDF/B-VIII.0 repository at the National Nuclear Data Center and selected for inclusion into the next US ENDF/B nuclear data library release. The upper RRR energy limit of ^{140}Ce was kept at 200 keV, whereas the limit for ^{142}Ce was extended from 13 to 26 keV.

There are several areas for potentially improving this set of resonance parameters. One of these areas is the quantification of the interference effects between direct and compound effects. As discussed in Section 3.5, DC, and DSD calculations suggest strong interference effects, although the direct contribution should be dominant for nuclei like ^{140,142}Ce. In the absence of a formal theoretical framework able to include interference effects between the two mechanisms in *R*-matrix analyses, the direct contribution was effectively included in resonance parameters of a negative resonance. This decision simplified the assembly of the evaluated resonance parameters in ENDF format, as the direct-semidirect contribution, including its covariance information, would have been added as a background.

Although transmission and capture yield data were recently measured at the GELINA facility, more experimental data is needed to improve the evaluations. Previous measurements [10] [13] are reported with significant issues that precluded them from being included in the evaluation. Specifically, measurements of ^{142}Ce above 26 keV would allow for the potential of further increasing the RRR and a revised evaluation of the extant URR. In addition to the dearth of cross section measurements, the lack of integral benchmark experiments containing appreciable amounts of cerium significantly limits the validation effort to affirm the accuracy of the newly evaluated parameters. Attempts to incorporate the capture resonance integrals and MACS into the evaluation procedure led to contradictory results compared to the thermal cross section values and current values reported in available compilations such as ATLAS and KADoNIS. This may be partly due to the small thermal capture cross section, as evident by the spread in the values of capture resonance integrals and MACS reported in Tables 10–11, respectively.

This work was supported by the Nuclear Criticality Safety Program, funded and managed by the National Nuclear Security Administration for the Department of Energy.

5. REFERENCES

[1] Juris Meija, Tyler B. Coplen, Michael Berglund, Willi A. Brand, Paul De Bièvre, Manfred Gröning, Norman E. Holden, Johanna Irrgeher, Robert D. Loss, Thomas Walczyk, and Thomas Prohaska. Isotopic compositions of the elements 2013 (IUPAC Technical Report). *Pure and Applied Chemistry*, 88(3):293–306, 2016.

[2] Angela Chambers. 5-Year Execution Plan for the Mission and Vision of the United States Department of Energy Nuclear Criticality Safety Program - FY21 through FY25. https://ncsp.llnl.gov/sites/ncsp/files/2021-10/fy21-25_ncsp_five-year_execution_plan.pdf_rev_2_final.pdf, September 2021.

[3] V.V. Zerkin and B. Pritychenko. The experimental nuclear reaction data (EXFOR): Extended computer database and Web retrieval system. *Nuclear Instruments and Methods in Physics Research Section A: Accelerators, Spectrometers, Detectors and Associated Equipment*, 888:31–43, 2018.

[4] D.A. Brown, M.B. Chadwick, R. Capote, A.C. Kahler, A. Trkov, M.W. Herman, A.A. Sonzogni, Y. Danon, A.D. Carlson, M. Dunn, D.L. Smith, G.M. Hale, G. Arbanas, R. Arcilla, C.R. Bates, B. Beck, B. Becker, F. Brown, R.J. Casperson, J. Conlin, D.E. Cullen, M.-A. Descalle, R. Firestone, T. Gaines, K.H. Guber, A.I. Hawari, J. Holmes, T.D. Johnson, T. Kawano, B.C. Kiedrowski, A.J. Koning, S. Kopecky, L. Leal, J.P. Lestone, C. Lubitz, J.I. Márquez Damián, C.M. Mattoon, E.A. McCutchan, S. Mughabghab, P. Navratil, D. Neudecker, G.P.A. Nobre, G. Noguere, M. Paris, M.T. Pigni, A.J. Plompen, B. Pritychenko, V.G. Pronyaev, D. Roubtsov, D. Rochman, P. Romano, P. Schillebeeckx, S. Simakov, M. Sin, I. Sirakov, B. Sleaford, V. Sobes, E.S. Soukhovitskii, I. Stetcu, P. Talou, I. Thompson, S. van der Marck, L. Welser-Sherrill, D. Wiarda, M. White, J.L. Wormald, R.Q. Wright, M. Zerkle, G. erovnik, and Y. Zhu. ENDF/B-VIII.0: The 8th Major Release of the Nuclear Reaction Data Library with CIELO-project Cross Sections, New Standards and Thermal Scattering Data. *Nuclear Data Sheets*, 148:1–142, 2018. Special Issue on Nuclear Reaction Data.

[5] Chris W. Chapman, Marco T. Pigni, and Klaus H. Guber. PROGRESS ON 140,142CE NEUTRON CROSS SECTION RESOLVED RESONANCE REGION EVALUATIONS. 11th International Conference on Nuclear Criticality Safety (ICNC 2019), Paris, France, September 15-20, 2019.

[6] N.M. Larson. Updated Users' Guide for SAMMY: Multilevel R-Matrix Fits to Neutron Data Using Bayes' Equations. Technical Report ORNL/TM-9179/R8, Oak Ridge National Laboratory, Oak Ridge, TN, USA, ORNL, 2008.

[7] E. Margaret Burbidge, G. R. Burbidge, William A. Fowler, and F. Hoyle. Synthesis of the Elements in Stars. *Rev. Mod. Phys.*, 29:547–650, Oct 1957.

[8] Yasuyuki Kikuchi, Tsuneo Nakagawa, Tetsuo Asami, Masayoshi Kawai, Hiroyuki Matsunobu, and Yukinori Kanda. Second Version of Japanese Evaluated Nuclear Data Library (JENDL-2). *Journal of Nuclear Science and Technology*, 22(8):593–603, 1985.

[9] Yasuyuki Kikuchi, Orihiko Togawa, and Tsuneo Nakagawa. Evaluation of resonance parameters of Mo, Tc, Te, Ba, La, Ce, Pr, Nd, Pm, Sm and Eu isotopes for JENDL-2 fission product file, Mar 1986.

[10] G. Hacken, H. Liou, W. Makofske, F. Rahn, J. Rainwater, , and U. Singh. Cross Section, Resonance Parameters, and Strength Function of Cerium-140. Technical Report USND-11, USAEC, 1974.

[11] H. S. Camarda. Neutron total cross section measurement on ^{140}Ce. *Phys. Rev. C*, 18:1254–1261, Sep 1978.

[12] A. R. de L Musgrove, B. J. Alien, and R. L. Macklin. Resonance Neutron Capture in ^{138}Ba and ^{140}Ce and the Prompt Neutron Correction to γ-ray Detectors. *Australian Journal of Physics*, 32(3):213–222, 1979.

[13] Makio Ohkubo, Motoharu Mizumoto, and Yutaka Nakajima. Neutron transmission measurements on ^{121}Sb,^{123}Sb, ^{140}Ce and ^{142}Ce in the resonance region, Feb 1993.

[14] S.F. Mughabghab, editor. *Atlas of Neutron Resonances*. Elsevier, Amsterdam, fifth edition, 2006.

[15] M.B. Chadwick, P. Obloinský, M. Herman, N.M. Greene, R.D. McKnight, D.L. Smith, P.G. Young, R.E. MacFarlane, G.M. Hale, S.C. Frankle, A.C. Kahler, T. Kawano, R.C. Little, D.G. Madland, P. Moller, R.D. Mosteller, P.R. Page, P. Talou, H. Trellue, M.C. White, W.B. Wilson, R. Arcilla, C.L. Dunford, S.F. Mughabghab, B. Pritychenko, D. Rochman, A.A. Sonzogni, C.R. Lubitz, T.H. Trumbull, J.P. Weinman, D.A. Brown, D.E. Cullen, D.P. Heinrichs, D.P. McNabb, H. Derrien, M.E. Dunn, N.M. Larson, L.C. Leal, A.D. Carlson, R.C. Block, J.B. Briggs, E.T. Cheng, H.C. Huria, M.L. Zerkle, K.S. Kozier, A. Courcelle, V. Pronyaev, and S.C. van der Marck. ENDF/B-VII.0: Next Generation Evaluated Nuclear Data Library for Nuclear Science and Technology. *Nuclear Data Sheets*, 107(12):2931–3060, 2006. Evaluated Nuclear Data File ENDF/B-VII.0.

[16] P. Obložinský et. al. Evaluated Data Library for the Bulk Fission Products,. Technical Report NEA/WPEC-23, NEA, 2009.

[17] K. Guber, G. Alaerts, J. Heyse, S. Kopecky, C. Paradela, P. Schillebreeckx, and R. Wynants. Results of time-of-flight transmission measurements for ^{nat}Ce samples at GELINA,. Technical Report EUR 28223 EN, GELINA, 2016.

[18] D. H. Moon, C. Paradela, G.Alaerts, V. Chavan, K. Guber, J. Heyse, S. W. Hong, S. Kopecky, P. Schillebeeckx, and R. Wynants. Results of time-of-flight transmission measurements for ^{142}Ce at a 50 m station of GELINA,. Technical Report INDC(EUR)-0038, GELINA, 2021.

[19] Henry W. Newson, J. H. Gibbons, H. Marshak, R. M. Williamson, R. A. Mobley, A. L. Toller, and R. Block. Neutron Resonances in the kev Region: Heavy Even Elements. *Phys. Rev.*, 102:1580–1583, Jun 1956.

[20] R O Sayer, L C Leal, N M Larson, R R Spencer, and R Q Wright. R-Matrix Evaluation of ^{16}O neutron cross sections up to 6.3 MeV. Technical Report ORNL/TM-2000/212, ORNL, August 2000.

[21] M. Flaska, A. Borella, D. Lathouwers, L.C. Mihailescu, W. Mondelaers, A.J.M. Plompen, H. van Dam, and T.H.J.J. van der Hagen. Modeling of the GELINA neutron target using coupled electron-photon-neutron transport with the MCNP4C3 code. *Nuclear Instruments and Methods in Physics Research Section A: Accelerators, Spectrometers, Detectors and Associated Equipment*, 531(3):392 – 406, 2004.

[22] Motoharu Mizumoto and Masayoshi Sugimoto. The influence of water absorption in samples for neutron capture cross section measurements. *Nuclear Instruments and Methods in Physics Research Section A: Accelerators, Spectrometers, Detectors and Associated Equipment*, 282(1):324 – 328, 1989.

[23] J. Goorley, Michael James, et al. Initial MCNP6 Release Overview. Technical Report LA-UR-13-22934, Los Alamos National Laboratory, 2013.

[24] A. Borella, G. Aerts, F. Gunsing, M. Moxon, P. Schillebeeckx, and R. Wynants. The use of C6D6 detectors for neutron induced capture cross-section measurements in the resonance region. *Nuclear*

Instruments and Methods in Physics Research Section A: Accelerators, Spectrometers, Detectors and Associated Equipment, 577(3):626 – 640, 2007.

[25] P. Schillebeeckx, B. Becker, Y. Danon, K. Guber, H. Harada, J. Heyse, A.R. Junghans, S. Kopecky, C. Massimi, M.C. Moxon, N. Otuka, I. Sirakov, and K. Volev. Determination of Resonance Parameters and their Covariances from Neutron Induced Reaction Cross Section Data. *Nuclear Data Sheets*, 113(12):3054 – 3100, 2012. Special Issue on Nuclear Reaction Data.

[26] P. E. Koehler, R. R. Spencer, R. R. Winters, K. H. Guber, J. A. Harvey, N. W. Hill, and M. S. Smith. Resonance neutron capture and transmission measurements and the stellar neutron capture cross sections of ^{134}Ba and ^{136}Ba. *Phys. Rev. C*, 54:1463–1477, Sep 1996.

[27] B. Becker, C. Bastian, J. Heyse, S. Kopecky, and P. Schillebeeckx. AGS - Analysis of Geel Spectra. NEA/DB/DOC (2014)4, 2014.

[28] F. Fröhner. Evaluation and Analysis of Nuclear Resonance Data. Technical Report JEFF Report 18, OECD, 2000.

[29] V. A. Anufriev, S. I. Babich, and S. N. Nkol'skiy. Neutron Resonance Parameters for ^{142}Ce and ^{142}Pr (Half-Life=13.6 Days) Nuclides. In *International Conference on Neutron Physics*, pages 229–231, 1987.

[30] Fritz H. Fröhner and Olivier Bouland. Treatment of External Levels in Neutron Resonance Fitting: Application to the Nonfissile Nuclide ^{52}Cr. *Nuclear Science and Engineering*, 137(1):70–88, 2001.

[31] Priyada Panikkath and P. Mohanakrishnan. Thermal neutron capture cross-section and resonance integral measurements of ^{139}La(n,γ)^{140}La and ^{140}Ce(n,γ)^{141}Ce using a Am-Be neutron source. *The European Physical Journal A*, 53(3):46, Mar 2017.

[32] F. de Corte and A. Simonits. *A compilation of accurately measured 2200 ms-1 Cross-sections for 101 (n,γ) reactions of interest in activation analysis*. International conference on nuclear data for science and technology; Mito, Ibaraki (Japan); 30 May - 3 Jun 1988.

[33] A. Alian, H.-J. Born, and J. I. Kim. Thermal and epithermal neutron activation analysis using the monostandard method. *Journal of Radioanalytical Chemistry*, 15(2):535–546, Sep 1973.

[34] Varley F. Sears. Neutron scattering lengths and cross sections. *Neutron News*, 3(3):26–37, 1992.

[35] S. Torrel and K. S. Krane. Neutron capture cross sections of ^{136,138,140,142}Ce and the decays of ^{137}Ce. *Phys. Rev. C*, 86:034340, Sep 2012.

[36] R. E. Heft. *Consistent set of nuclear-parameter values for absolute INAA*. United States. Conference on computers in activation analysis and gamma-ray spectroscopy; Mayaguez, Puerto Rico; 30 Apr - 4 May 1978.

[37] J. Alstad, T. Jahnsen, and A.C. Pappas. Thermal neutron capture cross section and resonance capture integral of the lanthanide nuclei ^{140}Ce, ^{142}Ce, ^{146}Nd, ^{148}Nd, ^{150}Nd and ^{159}Tb. *Journal of Inorganic and Nuclear Chemistry*, 29(9):2155–2160, 1967.

[38] P. M. Lantz, C. R. Baldock, and L. E. Idom. Thermal-Neutron Capture Cross Section and Resonance Capture Integral of Ce^{140} and Effective Capture Cross Section of Ce^{141}. *Nuclear Science and Engineering*, 20(3):302–306, 1964.

[39] S. Chiba, H. Koura, T. Hayakawa, T. Maruyama, T. Kawano, and T. Kajino. Direct and semi-direct capture in low-energy (n, γ) reactions of neutron-rich tin isotopes and its implications for *r*-process nucleosynthesis. *Phys. Rev. C*, 77:015809, Jan 2008.

[40] G Arbanas, F S Dietrich, and A K Kerman. Direct-Semidirect Neutron Capture Calculations Applied to R-Matrix Data Evaluations in the Resolved Resonance Region. In *AIP Conference Proceedings (the International Conference on Nuclear Data for Science and Technology)*, volume 769, page 296, 2005.

[41] W. E. Parker, M. B. Chadwick, F. S. Dietrich, J. E. Kammeraad, S. J. Luke, K. E. Sale, R. M. Chasteler, M. A. Godwin, L. H. Kramer, G. J. Schmid, H. R. Weller, and A. K. Kerman. Fluctuation effects in radiative capture to unstable final states: A test via the ^{89}Y(p$\rightarrow$,γ) reaction at e_p=19.6 mev. *Phys. Rev. C*, 52:252–266, Jul 1995.

[42] S. Raman, S. Kahane, R. M. Moon, J. A. Fernandez-Baca, J. L. Zarestky, J. E. Lynn, and J. W. Richardson. Thermal-neutron scattering lengths and capture by even calcium isotopes. *Phys. Rev. C*, 39:1297–1306, Apr 1989.

[43] J. E. Park, W. W. Daehnick, and M. J. Spisak. ^{140}Ce$(d, p)^{141}$Ce at 17 mev. *Phys. Rev. C*, 15:587–593, Feb 1977.

[44] Arbanas, Goran, Brown, Jesse, Wiarda, Dorothea, Holcomb, Andrew, Brain, Peter, Barry, Devin, and Danon, Yaron. Parameterization of Direct and Doorway Processes in R-Matrix Formalism. *EPJ Web of Conf.*, 284:03005, 2023.

[45] R.E. MacFarlane and A.C. Kahler. Methods for Processing ENDF/B-VII with NJOY. *Nuclear Data Sheets*, 111(12):2739–2890, 2010. Nuclear Reaction Data.

[46] I Dillmann, R Plag, F Käppeler, and T Rauscher. https://exp-astro.de/kadonis1.0/.

[47] C. Lederer, N. Colonna, C. Domingo-Pardo, F. Gunsing, F. Käppeler, C. Massimi, A. Mengoni, A. Wallner, U. Abbondanno, G. Aerts, H. Álvarez, F. Álvarez-Velarde, S. Andriamonje, J. Andrzejewski, P. Assimakopoulos, L. Audouin, G. Badurek, M. Barbagallo, P. Baumann, F. Bečvář, F. Belloni, E. Berthoumieux, M. Calviani, F. Calviño, D. Cano-Ott, R. Capote, C. Carrapiço, A. Carrillo de Albornoz, P. Cennini, V. Chepel, E. Chiaveri, G. Cortes, A. Couture, J. Cox, M. Dahlfors, S. David, I. Dillmann, R. Dolfini, W. Dridi, I. Duran, C. Eleftheriadis, M. Embid-Segura, L. Ferrant, A. Ferrari, R. Ferreira-Marques, L. Fitzpatrick, H. Frais-Koelbl, K. Fujii, W. Furman, I. Goncalves, E. González-Romero, A. Goverdovski, F. Gramegna, E. Griesmayer, C. Guerrero, B. Haas, R. Haight, M. Heil, A. Herrera-Martinez, M. Igashira, S. Isaev, E. Jericha, Y. Kadi, D. Karadimos, D. Karamanis, M. Kerveno, V. Ketlerov, P. Koehler, V. Konovalov, E. Kossionides, M. Krtička, C. Lampoudis, H. Leeb, A. Lindote, I. Lopes, R. Losito, M. Lozano, S. Lukic, J. Marganiec, L. Marques, S. Marrone, T. Martínez, P. Mastinu, E. Mendoza, P. M. Milazzo, C. Moreau, M. Mosconi, F. Neves, H. Oberhummer, S. O'Brien, M. Oshima, J. Pancin, C. Papachristodoulou, C. Papadopoulos, C. Paradela, N. Patronis, A. Pavlik, P. Pavlopoulos, L. Perrot, M. T. Pigni, R. Plag, A. Plompen, A. Plukis, A. Poch, J. Praena, C. Pretel, J. Quesada, T. Rauscher, R. Reifarth, M. Rosetti, C. Rubbia, G. Rudolf, P. Rullhusen, J. Salgado, C. Santos, L. Sarchiapone, R. Sarmento, I. Savvidis, C. Stephan, G. Tagliente, J. L. Tain, D. Tarrío, L. Tassan-Got, L. Tavora, R. Terlizzi, G. Vannini, P. Vaz, A. Ventura, D. Villamarin, V. Vlachoudis, R. Vlastou, F. Voss, S. Walter, H. Wendler, M. Wiescher, and K. Wisshak. ^{197}Au(n, γ) cross section in the unresolved resonance region. *Phys. Rev. C*, 83:034608, Mar 2011.

APPENDIX A. SAMMY INPUT FILES

APPENDIX A. SAMMY INPUT FILES

```
Ce-nat / Guber(16) total cross section (thick target) - from EXFOR
Cerium-nat 140.11568 1.0000e-5 200403.00    0    1 0  0 0  0 0
reich-moore formalism
generate plot file a
twenty
fgm
ev
print capture area in lpt file
PRINT REDUCED WIDTHS
PUBLISH
energy uncertainties are at end of line in par file
use no cutoff for derivatives or cross sections
quantum numbers are in parameter file
shift GELINA resolution function to center

 295.20000 47.669000 0.0200000 0.0000000 0.0010000
 5.6000000 0.0287130                     0.0000000
transmission

ISOTOPIC ABUNDANCIES AND MASSES
135.907129 1.8500e-3 1.0000E-5 0 1
137.905989 2.5100e-3 1.0000E-5 0 2
139.905446 8.8450e-1 1.0000E-5 0 3 4 5
141.909250 1.1114e-1 1.0000E-5 0 6 7 8
13.0033550 0.1000e-9 1.0000E-5 0 91011121314151617

GEEL RESOLUTION
BURST0     1.0000000 .10010000
TAU  00000 0.        0.        0.        0.       -.77220000 1363.8500-.53220000
TAU  00    1.00000-5 1.00000-5 1.00000-5 1.00000-5 1.00000-5 130.00000 1.00000-5
LAMBD00000 1.4460000 0.        0.        454.97200-.55077000
LAMBD      1.00000-5 1.00000-5 1.00000-6 45.000000 .10000000
A1   00000 0.        0.        .04152000-5.84700-6-.04150000 9.24700-6 .59610000
A1   00    1.00000-6 1.00000-7 1.00000-7 1.00000-6 1.00000-6 1.00000-6 .00100000
EXPON00000 0.        1.0000000 0.       -1.0000000 0.
EXPON      1.00000-5 .10000000 .20000000 .10000000 .00030470
A3sqE00000 0.        0.        0.        0.        .00030470 7.81800-5-2.0110000
A3sqE00    1.00000-5 1.00000-5 1.00000-5 1.00000-5 5.00000-8 1.00000-8 .00100000
A5sqE00000 0.        0.        0.        0.        .00733100 0.        0.
A5sqE00 24 352800.+8 2.0000000 0.5000000 0.0000100 0.0000010 0.0000100 0.0000010
CHANN 0    10.663700 64.000000 .50000000
CHANN 0    27.067200 64.000000 .50000000
CHANN 0    163.55620 64.000000 .50000000
CHANN 0    285.43520  8.000000 .50000000
CHANN 0    405.03600  4.000000 .50000000
CHANN 0    699.45070  4.000000 .50000000
CHANN 0   26349995.8  8.000000 .50000000
```

Figure 8. SAMMY input file for ^{nat}Ce Transmission - Thick Target

```
Ce-nat / Guber(16) total cross section (thin target) - from EXFOR
Cerium-nat 140.11568 1.0000e-5 200403.00    0    1 0  0 0  0 0
reich-moore formalism
generate plot file a
twenty
fgm
ev
print capture area in lpt file
PRINT REDUCED WIDTHS
PUBLISH
energy uncertainties are at end of line in par file
use no cutoff for derivatives or cross sections
quantum numbers are in parameter file
shift GELINA resolution function to center

 295.20000 47.669000 0.0200000 0.0000000 0.0010000
 5.6000000 0.0055340                     0.0000000
transmission

ISOTOPIC ABUNDANCIES AND MASSES
135.907129 1.8500e-3 1.0000E-5 0 1
137.905989 2.5100e-3 1.0000E-5 0 2
139.905446 8.8450e-1 1.0000E-5 0 3 4 5
141.909250 1.1114e-1 1.0000E-5 0 6 7 8
13.0033550 0.1000e-9 1.0000E-5 0 91011121314151617

GEEL RESOLUTION
BURST0     1.0000000 .10010000
TAU  00000 0.        0.        0.        0.       -.77220000 1363.8500-.53220000
TAU  00    1.00000-5 1.00000-5 1.00000-5 1.00000-5 1.00000-5 130.00000 1.00000-5
LAMBD00000 1.4460000 0.        0.        454.97200-.55077000
LAMBD      1.00000-5 1.00000-5 1.00000-6 45.000000 .10000000
A1   00000 0.        0.        .04152000-5.84700-6-.04150000 9.24700-6 .59610000
A1   00    1.00000-6 1.00000-7 1.00000-7 1.00000-6 1.00000-6 1.00000-6 .00100000
EXPON00000 0.        1.0000000 0.       -1.0000000 0.
EXPON      1.00000-5 .10000000 .20000000 .10000000 .00030470
A3sqE00000 0.        0.        0.        0.        .00030470 7.81800-5-2.0110000
A3sqE00    1.00000-5 1.00000-5 1.00000-5 1.00000-5 5.00000-8 1.00000-8 .00100000
A5sqE00000 0.        0.        0.        0.        .00733100 0.        0.
A5sqE00 24 352800.+8 2.0000000 0.5000000 0.0000100 0.0000010 0.0000100 0.0000010
CHANN 0    10.663700 64.000000 .50000000
CHANN 0    27.067200 64.000000 .50000000
CHANN 0    163.55620 64.000000 .50000000
CHANN 0    285.43520  8.000000 .50000000
CHANN 0    405.03600  4.000000 .50000000
CHANN 0    699.45070  4.000000 .50000000
CHANN 0   26349995.8  8.000000 .50000000
```

Figure 9. SAMMY input file for ^{nat}Ce Transmission - Thin Target

```
Ce-nat / Guber(16) capture cross section
Cerium-nat 140.11568 800.00000 19937308.    0    1 0  0 0  0 0
reich-moore formalism
generate plot file a
twenty
fgm
ev
print capture area in lpt file
PUBLISH
energy uncertainties are at end of line in par file
use no cutoff for derivatives or cross sections
quantum numbers are in parameter file
shift GELINA resolution function to center
include double scattering  + single + self
no finite-size corrections to multiple-scattering
do not suppress intermediate printout
chi squared is wanted
normalize as yield rather than cross section
#normalize as cross section rather than yield
print reduced widths

 302.000000 58.58600 0.0167400 0.0000000 0.0010000
 5.60000000 0.005341                     0.0000000
capture
    0.1850      2.99      0.00

ISOTOPIC ABUNDANCIES AND MASSES
135.907129 1.8500e-3 1.0000E-5 0 1
137.905989 2.5100e-3 1.0000E-5 0 2
139.905446 8.8450e-1 1.0000E-5 0 3 4 5
141.909250 1.1114e-1 1.0000E-5 0 6 7 8
13.0033550 0.1000e-9 1.0000E-5 0 91011121314151617

GEEL RESOLUTION
BURST0     1.0000000 .10010000
TAU  00000 0.        0.        0.        0.       -.77220000 1363.8500-.53220000
TAU  00    1.00000-5 1.00000-5 1.00000-5 1.00000-5 1.00000-5 130.00000 1.00000-5
LAMBD00000 1.4460000 0.        0.        454.97200-.55077000
LAMBD      1.00000-5 1.00000-5 1.00000-6 45.000000 .10000000
A1   00000 0.        0.        .04152000-5.84700-6-.04150000 9.24700-6 .59610000
A1   00    1.00000-6 1.00000-7 1.00000-7 1.00000-6 1.00000-6 1.00000-6 .00100000
EXPON00000 0.        1.0000000 0.       -1.0000000 0.
EXPON      1.00000-5 .10000000 .20000000 .10000000 .00030470
A3sqE00000 0.        0.        0.        0.        .00030470 7.81800-5-2.0110000
A3sqE00    1.00000-5 1.00000-5 1.00000-5 1.00000-5 5.00000-8 1.00000-8 .00100000
A5sqE00000 0.        0.        0.        0.        .00733100 0.        0.
A5sqE00 24 352800.+8 2.0000000 0.5000000 0.0000100 0.0000010 0.0000100 0.0000010
CHANN 0    29.264300 256.00000 .50000000
CHANN 0    118.08950 128.00000 .50000000
CHANN 0    480.78130 64.000000 .50000000
CHANN 0    1993.2745 32.000000 .50000000
CHANN 0    8582.3881 16.000000 .50000000
CHANN 0    40123.195 8.0000000 .50000000
CHANN 0    228645.95 2.0000000 .50000000
CHANN 0    2435278.3 2.0000000 .50000000
```

Figure 10. SAMMY input file for ^{nat}Ce Capture Yield

```
142Ceoxide transmission
142 Ce    141.909241 1.0000e-5 200403.00    0    1 0  0 0  0 0
reich-moore formalism
generate plot file a
twenty
fgm
ev
print capture area in lpt file
PRINT REDUCED WIDTHS
PUBLISH
energy uncertainties are at end of line in par file
use no cutoff for derivatives or cross sections
quantum numbers are in parameter file
shift GELINA resolution function to center

  307.0000 47.62000     0.0200    0.0000    0.0010
  5.900000 0.004523                        0.00000
transmission

ISOTOPIC ABUNDANCIES AND MASSES
135.907129 2.0000e-3 1.0000E-5 0 1
137.905989 2.0000e-3 1.0000E-5 0 2
139.905446 7.9300e-2 1.0000E-5 0 3 4 5
141.909250 9.2070e-1 1.0000E-5 0 6 7 8
13.0033550 2.0000e+0 1.0000E-5 0 91011121314151617

GEEL Resolution function parameters follow
BURST0     1.0000000 .10010000
TAU  00000 0.        0.        0.        0.       -.77220000 1363.8500-.53220000
TAU  00    1.00000-5 1.00000-5 1.00000-5 1.00000-5 1.00000-5 130.00000 1.00000-5
LAMBD00000 1.4460000 0.        0.        454.97200-.55077000
LAMBD      1.00000-5 1.00000-5 1.00000-6 45.000000 .10000000
A1   00000 0.        0.        .04152000-5.84700-6-.04150000 9.24700-6 .59610000
A1   00    1.00000-6 1.00000-7 1.00000-7 1.00000-6 1.00000-6 1.00000-6 .00100000
EXPON00000 0.        1.0000000 0.       -1.0000000 0.
EXPON      1.00000-5 .10000000 .20000000 .10000000 .00030470
A3sqE00000 0.        0.        0.        0.        .00030470 7.81800-5-2.0110000
A3sqE00    1.00000-5 1.00000-5 1.00000-5 1.00000-5 5.00000-8 1.00000-8 .00100000
A5sqE00000 0.        0.        0.        0.        .00733100 0.        0.
A5sqE00 24 352800.+8 2.0000000 0.5000000 0.0000100 0.0000010 0.0000100 0.0000010
CHANN 0    10.663700 64.000000 .50000000
CHANN 0    27.067200 64.000000 .50000000
CHANN 0    163.55620 64.000000 .50000000
CHANN 0    285.43520  8.000000 .50000000
CHANN 0    405.03600  4.000000 .50000000
CHANN 0    699.45070  4.000000 .50000000
CHANN 0   26349995.8  8.000000 .50000000
```

Figure 11. SAMMY input file for ^{142}Ce Transmission

```
Ce142 oxide capture with self-shielding & single-scattering
142 Ce    141.909241    100.0 2.0000E+05    0    1 0  0 0  0 0
reich-moore formalism
generate plot file a
twenty
fgm
ev
print capture area in lpt file
PUBLISH
energy uncertainties are at the end of line in par file
use no cutoff for derivatives or cross sections
quantum numbers are in parameter file
shift GELINA Resolution function to center
include double scattering  + single + self
no finite-size corrections to multiple-scattering
do not suppress intermediate printout
chi squared is wanted
normalize as yield rather than cross section
print reduced widths

  302.0000 58.59100    0.01674    0.0000    0.0010
  5.600000 0.004524                        0.00000
capture
    0.2850      2.99      0.00

ISOTOPIC ABUNDANCIES AND MASSES
135.907129 2.0000e-3 1.0000E-5 0 1
137.905989 2.0000e-3 1.0000E-5 0 2
139.905446 7.9300e-2 1.0000E-5 0 3 4 5
141.909250 9.2070e-1 1.0000E-5 0 6 7 8
13.0033550 2.0000e+0 1.0000E-5 0 91011121314151617

GEEL Resolution function parameters follow
BURST0     1.0000000 .10010000
TAU  00000 0.        0.        0.        0.       -.77220000 1363.8500-.53220000
TAU  00    1.00000-5 1.00000-5 1.00000-5 1.00000-5 1.00000-5 130.00000 1.00000-5
LAMBD00000 1.4460000 0.        0.        454.97200-.55077000
LAMBD      1.00000-5 1.00000-5 1.00000-6 45.000000 .10000000
A1   00000 0.        0.        .04152000-5.84700-6-.04150000 9.24700-6 .59610000
A1   00    1.00000-6 1.00000-7 1.00000-7 1.00000-6 1.00000-6 1.00000-6 .00100000
EXPON00000 0.        1.0000000 0.       -1.0000000 0.
EXPON      1.00000-5 .10000000 .20000000 .10000000 .00030470
A3sqE00000 0.        0.        0.        0.        .00030470 7.81800-5-2.0110000
A3sqE00    1.00000-5 1.00000-5 1.00000-5 1.00000-5 5.00000-8 1.00000-8 .00100000
A5sqE00000 0.        0.        0.        0.        .00733100 0.        0.
A5sqE00 24 352800.+8 2.0000000 0.5000000 0.0000100 0.0000010 0.0000100 0.0000010
CHANN 0    29.264300 256.00000 .50000000
CHANN 0    118.08950 128.00000 .50000000
CHANN 0    480.78130 64.000000 .50000000
CHANN 0    1993.2745 32.000000 .50000000
CHANN 0    8582.3881 16.000000 .50000000
CHANN 0    40123.195 8.0000000 .50000000
CHANN 0    228645.95 2.0000000 .50000000
CHANN 0    2435278.3 2.0000000 .50000000

DETECTOR EFFICIENCIES FOLLOW
1.00000000 .01000000 0 1
1.00000000 .01000000 0 2
1.00000000 .01000000 0 3 4 5
1.00000000 .01000000 0 6 7 8
.850988935 .01000000 0 91011121314151617
```

Figure 12. SAMMY input file for ^{142}Ce Capture Yield

APPENDIX B. SAMMY PARAMETER FILE

APPENDIX B. SAMMY PARAMETER FILE

```
PARTICLE PAIR DEFINITIONS
Name=136Ce+n      Particle a=neutron       Particle b=136Ce
     Za= 0        Zb= 0         Pent=1     Shift=0
     Sa=  0.5     Sb=   0.0     Ma=   1.008664920000000     Mb= 135.907511000000
Name=138Ce+n      Particle a=neutron       Particle b=138Ce
     Za= 0        Zb= 0         Pent=1     Shift=0
     Sa=  0.5     Sb=   0.0     Ma=   1.008664920000000     Mb= 137.905676000000
Name=140Ce+n      Particle a=neutron       Particle b=140Ce
     Za= 0        Zb= 0         Pent=1     Shift=0
     Sa=  0.5     Sb=   0.0     Ma=   1.008664920000000     Mb= 139.905454999998
Name=142Ce+n      Particle a=neutron       Particle b=142Ce
     Za= 0        Zb= 0         Pent=1     Shift=0
     Sa=  0.5     Sb=   0.0     Ma=   1.008664920000000     Mb= 141.909268999999
Name=16O+n        Particle a=neutron       Particle b=16O
     Za= 0        Zb= 8         Pent=1     Shift=0
     Sa=  0.5     Sb=   0.0     Ma=   1.008664920000000     Mb=  15.994915000000
Name=13C+a        Particle a=alpha         Particle b=13C
     Za= 2        Zb= 6         Pent=1     Shift=0
     Sa=  0.0     Sb=  -0.5     Ma=   4.002604000000000     Mb=  13.003355000000
     Q= -2215610.0000000000

SPIN GROUPS
  1       1    0  0.5 0.0000000
    1  136Ce+n     0  0.5
  2       1    0  0.5 0.0000000
    1  138Ce+n     0  0.5
  3       1    0  0.5 0.0000000
    1  140Ce+n     0  0.5
  4       1    0 -0.5 0.0000000
    1  140Ce+n     1  0.5
  5       1    0 -1.5 0.0000000
    1  140Ce+n     1  0.5
  6       1    0  0.5 1.0000000
    1  142Ce+n     0  0.5
  7       1    0 -0.5 1.0000000
    1  142Ce+n     1  0.5
  8       1    0 -1.5 1.0000000
    1  142Ce+n     1  0.5
  9       1    1  0.5 0.0000000
    1  16O+n       0  0.5
    2  13C+a       1 -0.5
 10       1    1 -0.5 0.0000000
    1  16O+n       1  0.5
    2  13C+a       0 -0.5
 11       1    1 -1.5 0.0000000
    1  16O+n       1  0.5
    2  13C+a       2 -0.5
 12       1    1  1.5 0.0000000
    1  16O+n       2  0.5
    2  13C+a       1 -0.5
 13       1    1  2.5 0.0000000
    1  16O+n       2  0.5
    2  13C+a       3 -0.5
 14       1    1 -2.5 0.0000000
    1  16O+n       3  0.5
    2  13C+a       2 -0.5
 15       1    1 -3.5 0.0000000
    1  16O+n       3  0.5
    2  13C+a       4 -0.5
 16       1    1  3.5 0.0000000
    1  16O+n       4  0.5
    2  13C+a       3 -0.5
 17       1    1  4.5 0.0000000
```

```
    1  16O+n       4  0.5
    2  13C+a       5 -0.5

RESONANCES are listed next
-3923178.00 43.2325900 25976950.0                        0 0 0     3
-2189734.00 43.7532800 1820293.00                        0 0 0     6
-8629.35600 .818049800 1318606.00                        0 0 0     6
-5409.27000 841.640500 9.94097500                        0 0 0     3
-96.1500000 110.000000 990.000000                        0 0 0     1
-79.0695400 21.4353000 316.759900                        0 0 0     6
-19.0230700 492.275400 .341364900                        0 0 0     3
-15.0000000 113.000000 1.67000000                        0 0 0     2
66.30000000 110.000000 66.0000000                        0 0 0     1
135.7000000 110.000000 630.000000                        0 0 0     1
140.0000000 113.000000 15.0000000                        0 0 0     2
181.0000000 110.000000 4.30000000                        0 0 0     1
187.0000000 110.000000 4.20000000                        0 0 0     1
232.0000000 110.000000 8.10000000                        0 0 0     1
250.0000000 113.000000 4.30000000                        0 0 0     2
274.0000000 111.000000 315.000000                        0 0 0     1
365.0000000 113.000000 4.20000000                        0 0 0     2
475.0000000 113.000000 8.10000000                        0 0 0     2
533.0000000 112.000000 810.000000                        0 0 0     1
575.0000000 113.000000 315.000000                        0 0 0     2
633.0000000 111.000000 1460.00000                        0 0 0     1
695.0000000 113.000000 810.000000                        0 0 0     2
820.0000000 113.000000 1460.00000                        0 0 0     2
876.0000000 112.000000 1390.00000                        0 0 0     1
965.0000000 113.000000 1390.00000                        0 0 0     2
1154.108000 216.780400 15.3345600                        0 0 0     8
1277.780000 84.2841600 69086.4200                        0 0 0     6
1689.164000 50.1073500 17.7857300                        0 0 0     7
1742.246000 24.0294100 71.3354500                        0 0 0     8
2544.130000 121.157100 694.786400                        0 0 0     4
2794.862000 83.9297200 16990.4000                        0 0 0     6
2941.948000 56.0545400 4.63241000                        0 0 0     8
2966.690000 183.808400 12.7693500                        0 0 0     7
3838.334000 117.484600 38644.8200                        0 0 0     6
4293.995000 100.376100 125.735700                        0 0 0     7
4524.799000 38.3140900 616.425100                        0 0 0     6
5188.784000 39.9800300 39.8043200                        0 0 0     8
5621.952000 47.4296500 1290.66400                        0 0 0     6
5640.149000 44.0541600 36.8433600                        0 0 0     4
5816.156000 475.761500 60.4277300                        0 0 0     7
5964.175000 104.185000 12.4194000                        0 0 0     8
6006.385000 55.6149100 919.952800                        0 0 0     3
6324.989000 24.2272400 5.42066700                        0 0 0     4
6425.918000 27.3872300 87.2900600                        0 0 0     8
6781.027000 56.3227600 151.505900                        0 0 0     4
7478.663000 22.6153400 58.5257600                        0 0 0     8
8151.346000 49.2146800 3216.66800                        0 0 0     7
8340.897000 39.4046000 93.2989200                        0 0 0     8
8392.399000 42.0374700 288.517000                        0 0 0     5
8404.316000 78.4950800 21359.6800                        0 0 0     6
8850.836000 661.562800 21.1867400                        0 0 0     8
9437.917000 18.5551000 330.387100                        0 0 0     8
9572.961000 92.7742400 53380.4100                        0 0 0     3
9645.449000 37.0460200 145.932600                        0 0 0     8
10330.22000 6.80975900 9.05248700                        0 0 0     5
10868.59000 50.1907500 48.7412700                        0 0 0     7
10923.26000 27.3323900 1402.39900                        0 0 0     6
11162.07000 1.07284600 34.4001700                        0 0 0     5
11182.08000 47.9851700 10614.1900                        0 0 0     6
```

11231.48000	99.5722400	343.923700	0	0	0	3
11323.10000	40.2285800	1967.52700	0	0	0	6
11354.58000	36.8816200	115.995500	0	0	0	8
11440.34000	57.0085100	17294.2400	0	0	0	4
11441.22000	21.9891600	9.17395100	0	0	0	4
11474.66000	49.4971800	70.6572900	0	0	0	5
11488.97000	28.2860400	54.7988400	0	0	0	7
11975.13000	89.3039500	3771.63400	0	0	0	6
12231.07000	29.0505400	158.130200	0	0	0	8
12405.84000	4.20699000	85.9655700	0	0	0	5
12480.90000	91.1170300	39614.1800	0	0	0	3
12484.58000	54.5536200	78.2674500	0	0	0	7
12534.44000	10.1149800	5.44803700	0	0	0	5
12782.27000	77.2672100	34011.0800	0	0	0	6
13039.70000	102.075600	59.7687700	0	0	0	7
13175.21000	36.2332900	34.0391400	0	0	0	5
13856.09000	30.9841000	52.8196800	0	0	0	8
13965.58000	22.9607500	136.328500	0	0	0	4
13977.60000	61.0406200	2146.37500	0	0	0	6
14017.25000	44.5827200	334.131100	0	0	0	5
14356.94000	55.7576400	39.1618900	0	0	0	7
15127.54000	37.6212600	50.9311300	0	0	0	8
15240.00000	115.427500	99148.0600	0	0	0	6
15671.13000	9.05068800	3.45811200	0	0	0	5
15845.89000	40.5771000	204.891000	0	0	0	7
16151.63000	38.0016800	6507.02600	0	0	0	4
16201.93000	62.3265500	46.7553700	0	0	0	8
16432.02000	28.7136500	1266.50500	0	0	0	5
16641.41000	37.2711400	3116.88000	0	0	0	6
17342.49000	32.4622900	13732.9700	0	0	0	7
17765.64000	34.7124700	332.907900	0	0	0	8
17827.83000	38.6841200	3956.56000	0	0	0	6
18021.61000	3.97087800	317.156000	0	0	0	5
18082.35000	6.69437700	299.447200	0	0	0	5
18117.43000	43.4776000	115.537000	0	0	0	4
18169.21000	103.541600	84604.0900	0	0	0	3
18237.91000	3.29098800	76.9866700	0	0	0	4
18780.32000	45.5618500	147.363700	0	0	0	5
19401.51000	39.4484800	1609.57300	0	0	0	6
19675.42000	5.93081000	19.0309100	0	0	0	5
19987.29000	52.6144900	75.9641600	0	0	0	8
20590.07000	67.4389400	22740.3500	0	0	0	7
20763.25000	21.6875400	638.630900	0	0	0	8
20816.56000	3.27707900	544.508700	0	0	0	4
21214.64000	60.2663800	3938.59200	0	0	0	5
21329.29000	2.39366600	29.9645400	0	0	0	8
21622.38000	478.512900	576340.600	0	0	0	3
22529.51000	20.4357200	19.4393300	0	0	0	4
22618.75000	183.504000	144514.000	0	0	0	7
22747.74000	33.8644200	1229.71100	0	0	0	8
23227.01000	318.177800	203987.700	0	0	0	7
23367.90000	10.0078200	18.8387300	0	0	0	4
23567.79000	100.522400	42.1980900	0	0	0	5
23879.39000	16.3797500	87.4906200	0	0	0	8
24110.74000	42.5045600	16.4224900	0	0	0	5
24489.89000	89.1652700	67.6076200	0	0	0	7
24737.43000	82.2149100	70829.9500	0	0	0	6
24801.91000	146.145900	71329.2300	0	0	0	3
25277.82000	360.444400	100.608000	0	0	0	4
25396.96000	14.0272300	751.612100	0	0	0	8
25407.13000	318.829800	401767.100	0	0	0	6
25611.77000	1.79145300	41.6741500	0	0	0	5
26004.02000	71.8880400	1756.52300	0	0	0	7

26042.51000	28.6859000	421.833000	0	0	0	4
26400.83000	149.216400	71.9921200	0	0	0	5
26577.85000	4.57249200	590.586500	0	0	0	4
27246.23000	20.5315100	72.1484600	0	0	0	5
27272.55000	90.2036300	377.328900	0	0	0	7
27662.72000	31.4570700	96.9654200	0	0	0	5
27916.29000	18.1613900	1243.38100	0	0	0	4
28053.07000	38.8113800	2707.46500	0	0	0	8
28209.36000	201.522300	104446.100	0	0	0	3
28480.40000	119.339500	201.154100	0	0	0	7
29001.18000	6.76735000	37.6416800	0	0	0	4
29066.85000	120.728800	83.4492900	0	0	0	4
29238.94000	15.0068000	540.814400	0	0	0	5
29324.12000	70.6149700	39388.3500	0	0	0	6
29624.47000	5.88347100	52.7326700	0	0	0	4
29894.10000	107.868700	1047.23500	0	0	0	3
29995.55000	41.3950000	2362.42400	0	0	0	8
30713.02000	44.5334200	23793.0800	0	0	0	3
30804.48000	90.7278900	612.452300	0	0	0	7
30826.93000	51.5056200	490.105200	0	0	0	5
30891.96000	93.5726200	32513.8200	0	0	0	6
31682.26000	56.1636800	86.1073300	0	0	0	8
32406.97000	37.7920200	1688.16900	0	0	0	8
32443.28000	88.1198300	85.9938200	0	0	0	5
33415.13000	45.7783300	173.689700	0	0	0	8
33510.04000	317.304300	45.0026300	0	0	0	5
33669.45000	354.652900	86.7372400	0	0	0	4
33812.15000	341.045300	87.0709000	0	0	0	5
34213.24000	65.3783200	366.018500	0	0	0	7
34638.21000	44.6861000	1785.24200	0	0	0	8
34678.90000	10.9883300	10053.4700	0	0	0	4
34975.40000	24.3239200	23.6847200	0	0	0	4
35406.17000	84.1075700	1263.17000	0	0	0	8
36120.90000	121.947000	764.516700	0	0	0	7
37684.64000	59.8685900	500.476600	0	0	0	8
38193.85000	144.316600	118539.600	0	0	0	6
38199.63000	17.6847100	5439.66600	0	0	0	5
38272.99000	18.6369400	65066.4400	0	0	0	3
38320.65000	41.7793000	29.2656000	0	0	0	5
38798.89000	56.7576300	636.954300	0	0	0	8
38870.49000	69.6353100	14912.0400	0	0	0	6
39160.79000	51.5829400	1000.00900	0	0	0	5
39687.43000	316.188700	238.475000	0	0	0	4
39700.46000	39.6753500	35253.3100	0	0	0	6
40207.24000	7.58344900	2834.89100	0	0	0	5
40335.30000	120.226900	734.872000	0	0	0	7
40981.17000	7.04917700	3137.77000	0	0	0	5
41175.93000	38.9222600	2890.49700	0	0	0	8
41514.84000	44.0664900	2506.23100	0	0	0	5
41814.63000	21.5557400	40.8006500	0	0	0	5
41950.11000	76.8591700	272719.100	0	0	0	3
42519.06000	165.210600	156.707800	0	0	0	4
42720.25000	9.38759400	1841.77300	0	0	0	5
42749.52000	92.8725900	41994.3000	0	0	0	6
43080.21000	70.6422600	472.749100	0	0	0	7
43408.60000	731.140200	377642.200	0	0	0	6
43720.17000	22.3346600	16.5288800	0	0	0	5
44336.28000	29.5339200	26.6053400	0	0	0	4
44354.06000	69.1293500	2145.19700	0	0	0	8
44725.34000	2.44610000	4250.01600	0	0	0	5
45148.02000	25.5239300	24.6725400	0	0	0	4
45236.80000	24.5807700	20.0584500	0	0	0	5
45565.48000	56.0314400	137.926900	0	0	0	8

45572.44000	31.9442800	31.4954500	0	0	0	4
46174.14000	103.906400	103.208600	0	0	0	4
46381.68000	197.016700	232.941700	0	0	0	7
46532.86000	17.1042800	13.2062700	0	0	0	5
46765.02000	22.7179200	25.2818600	0	0	0	5
47207.28000	6.40154700	671.866300	0	0	0	4
47660.71000	24.2340600	1310.20200	0	0	0	3
48665.69000	48.9901600	1717.41300	0	0	0	5
49301.21000	212.097100	92784.0700	0	0	0	6
49507.48000	126.072400	72541.1900	0	0	0	3
49708.33000	157.699700	174.765200	0	0	0	4
49884.64000	97.0460800	89.5991900	0	0	0	4
50263.90000	28.8117500	26.0254000	0	0	0	5
50624.35000	36.6688300	31.2457800	0	0	0	5
51111.73000	14.0172900	9.09636800	0	0	0	5
51350.28000	190.898100	952.198200	0	0	0	7
51523.87000	18.6727800	22.2150600	0	0	0	5
52289.03000	189.017700	200.891700	0	0	0	4
52467.56000	130.605000	470.172300	0	0	0	8
52678.21000	17.2206900	15.9809100	0	0	0	5
52860.07000	304.974400	149274.700	0	0	0	6
53021.72000	17.3668600	1771.96400	0	0	0	5
53170.80000	161.235800	604.267000	0	0	0	7
53292.17000	13.5146300	43360.6600	0	0	0	4
53522.11000	7.96062800	1647.23000	0	0	0	5
53689.68000	41.6727100	4212.41000	0	0	0	3
53717.15000	62.5809200	60.1503600	0	0	0	7
53791.54000	52.0259200	5734.18300	0	0	0	8
54237.27000	26.6510100	27.8659100	0	0	0	5
54601.25000	69.9874900	93.2905200	0	0	0	5
54939.07000	320.593900	175514.100	0	0	0	6
55276.00000	32.6326400	222986.900	0	0	0	3
55586.85000	193.345700	620.664100	0	0	0	7
55786.68000	16.2414800	981.491100	0	0	0	5
56070.71000	99.5313500	24818.6200	0	0	0	6
56295.66000	79.4173600	60.2566300	0	0	0	5
56753.50000	327.145800	48640.1800	0	0	0	6
57018.47000	124.702200	984.587400	0	0	0	7
57236.67000	94.5859800	263.668100	0	0	0	8
58056.49000	109.999100	5485.01200	0	0	0	7
58473.08000	133.729100	12021.0700	0	0	0	6
58489.08000	37.3752200	30.0311700	0	0	0	5
59077.35000	63.7895900	2348.98100	0	0	0	8
59472.94000	58.7924600	606.950600	0	0	0	8
59486.37000	36.5191900	30.8326700	0	0	0	4
59678.26000	25.9240900	18.4721400	0	0	0	5
59898.01000	45.2897900	47.7571500	0	0	0	5
60127.43000	53.6628900	735.987400	0	0	0	5
60249.23000	159.923600	61910.1500	0	0	0	7
60377.12000	24.2268600	62789.5900	0	0	0	3
60531.41000	84.1673500	11571.6000	0	0	0	8
60665.15000	175.787300	111627.200	0	0	0	6
60974.89000	108.633200	503.430200	0	0	0	8
61311.84000	267.554600	1040.17000	0	0	0	7
61537.72000	101.533900	81.8346700	0	0	0	5
61821.35000	55.3112700	332.884300	0	0	0	8
61986.07000	96.6864600	85.7165500	0	0	0	4
62191.78000	40.9366300	7678.76000	0	0	0	7
62570.25000	36.0426500	869.966000	0	0	0	8
62875.05000	198.990300	179979.100	0	0	0	6
63006.62000	304.961200	107359.300	0	0	0	3
63563.33000	81.1549800	908.735500	0	0	0	7
64071.85000	103.769900	417.162400	0	0	0	8

64448.88000	208.826500	175.319200	0	0	0	5
64479.17000	67.9159400	2226.85900	0	0	0	7
65138.06000	111.679100	1309.70100	0	0	0	7
65827.65000	82.5150300	439.269100	0	0	0	8
65974.10000	214.725500	18216.7100	0	0	0	6
66202.63000	40.3295600	1273.28700	0	0	0	8
66244.85000	101.107600	1785.70200	0	0	0	4
66328.56000	109.398500	1247.15800	0	0	0	7
66408.17000	38.8747600	3290.95100	0	0	0	5
66710.59000	83.9384900	2842.69900	0	0	0	8
66859.61000	167.787100	24757.9800	0	0	0	6
67287.55000	109.642700	10283.1400	0	0	0	7
68260.20000	4.68960300	4803.46400	0	0	0	5
68382.40000	79.5305600	1474.49500	0	0	0	8
68698.77000	119.531200	1464.17700	0	0	0	7
69286.10000	58.3505600	468.640200	0	0	0	8
69525.75000	488.532900	123.652200	0	0	0	5
69702.83000	32.7983400	25613.2400	0	0	0	4
69806.20000	140.333100	133984.800	0	0	0	6
69993.46000	27.2701900	2041.28500	0	0	0	8
70106.17000	76.0512100	1580.16700	0	0	0	7
70229.79000	15.9895900	935.809800	0	0	0	4
70726.51000	9.80102000	328.214100	0	0	0	5
71114.05000	31.7450700	10030.2000	0	0	0	8
71192.86000	116.921000	32.0736700	0	0	0	4
71479.47000	137.695800	1351.13300	0	0	0	7
71629.25000	83.1886700	1241.77500	0	0	0	8
71946.47000	92.3579900	519.908700	0	0	0	8
72238.22000	119.919600	1452.41900	0	0	0	7
72430.19000	202.403600	1069.99100	0	0	0	4
73048.09000	110.820000	681.726500	0	0	0	5
73301.64000	109.979000	978.248000	0	0	0	7
74001.41000	64.9174700	412.391500	0	0	0	8
74744.43000	60.5386800	6116.75600	0	0	0	5
74915.52000	23.9859700	8515.31100	0	0	0	5
75091.12000	110.656300	4991.31500	0	0	0	7
75322.17000	88.6400200	6906.66600	0	0	0	8
75428.76000	87.2992500	39782.7900	0	0	0	7
75561.56000	146.199300	83296.1900	0	0	0	3
75655.82000	22.8977300	1248.94400	0	0	0	8
75862.19000	22.4891100	1005.96100	0	0	0	7
75982.58000	535.823900	706118.400	0	0	0	6
76454.40000	47.4110600	6486.02900	0	0	0	7
76775.55000	106.458800	741.057600	0	0	0	8
76857.68000	7.99294400	12958.2400	0	0	0	5
77003.81000	164.644800	79373.0800	0	0	0	6
77340.09000	52.6424000	2649.81100	0	0	0	8
77476.62000	75.0546600	2952.53100	0	0	0	7
77613.36000	102.102900	3907.25500	0	0	0	8
77858.31000	197.247300	77914.4200	0	0	0	6
78395.07000	69.1708500	31600.0400	0	0	0	4
78574.81000	184.519900	58231.8100	0	0	0	3
79168.72000	206.072700	42668.7100	0	0	0	6
79608.46000	69.9061000	1553.31200	0	0	0	8
80810.95000	126.289800	1006.70000	0	0	0	5
81030.85000	727.887700	256843.900	0	0	0	6
81527.60000	1156.47900	202.791100	0	0	0	4
81868.42000	99.9496200	2303.06000	0	0	0	8
82095.85000	43.3792000	4136.90800	0	0	0	4
82426.58000	53.1664400	9670.84000	0	0	0	5
82795.45000	164.461800	2686.28700	0	0	0	7
83233.77000	111.717600	1444.54200	0	0	0	8
83758.56000	1384.28100	275.888400	0	0	0	4

84163.06000	41.7104300	6039.42800	0	0	0	5
84443.24000	108.150100	2093.09000	0	0	0	7
84970.60000	91.4302300	14950.2800	0	0	0	8
85380.21000	87.1068500	2411.34000	0	0	0	8
85909.64000	289.372400	2266.73200	0	0	0	7
86545.26000	33.3338600	2844.79200	0	0	0	5
86782.14000	148.776300	6264.01700	0	0	0	7
86943.87000	121.211900	28115.8900	0	0	0	8
87212.53000	37.9395700	22844.0600	0	0	0	4
87341.74000	170.849400	30330.2600	0	0	0	6
87934.17000	303.511800	146916.700	0	0	0	7
88315.14000	451.979000	312604.800	0	0	0	3
88806.19000	89.6360200	6011.38900	0	0	0	8
89282.97000	75.0573600	672.089300	0	0	0	5
89347.33000	104.643700	10577.5300	0	0	0	8
90238.30000	527.735000	255326.300	0	0	0	6
90550.53000	24.3552600	26869.1100	0	0	0	5
90734.35000	21.1884100	17503.3700	0	0	0	7
90872.11000	55.3651400	157028.900	0	0	0	6
91354.65000	82.6230400	5455.72200	0	0	0	8
91873.94000	255.478600	5468.91100	0	0	0	7
92065.79000	135.678200	4700.00500	0	0	0	8
92483.40000	137.830000	4354.24500	0	0	0	4
92805.22000	207.908600	1486.67000	0	0	0	7
93144.99000	1526.54100	721745.900	0	0	0	6
93364.09000	63.4745800	790.547800	0	0	0	8
93507.89000	46.4722100	284447.800	0	0	0	3
93904.68000	340.740400	54456.4400	0	0	0	7
94906.55000	177.285500	10170.0500	0	0	0	8
95284.09000	43.9052500	4309.71300	0	0	0	7
95808.94000	359.028600	61785.5600	0	0	0	4
96137.93000	48.5176100	250653.400	0	0	0	3
96348.34000	44.3420700	4299.82200	0	0	0	6
96772.43000	47.7286600	12769.5900	0	0	0	8
97189.93000	37.6096800	139802.400	0	0	0	6
97472.13000	198.309600	3775.28300	0	0	0	4
98741.00000	93.3368100	34164.4000	0	0	0	3
99845.58000	41.4992500	2499.65800	0	0	0	5
100376.8000	33.8039700	293451.300	0	0	0	6
100816.2000	51.4979000	70431.1000	0	0	0	7
102965.7000	54.3471100	17563.3600	0	0	0	8
103878.1000	2734.62800	38453.5300	0	0	0	7
104545.5000	31.4404100	597809.500	0	0	0	6
104925.8000	44.5726400	152.807700	0	0	0	4
105825.8000	47.4129600	10073.4700	0	0	0	7
105984.3000	32.1147500	4302.92200	0	0	0	5
107000.9000	14.5522600	7327.43400	0	0	0	5
107354.1000	33.0277800	286145.000	0	0	0	6
107808.8000	67.0569700	7565.53400	0	0	0	8
107901.6000	22.8488500	31247.6500	0	0	0	4
108621.4000	85.4707400	22482.3000	0	0	0	3
109190.2000	60.4062200	12210.4500	0	0	0	7
110522.1000	66.9099900	118327.600	0	0	0	7
110982.1000	35.4430700	370522.200	0	0	0	6
112076.6000	87.0809100	2016.94300	0	0	0	8
113016.2000	62.7520600	20760.9100	0	0	0	7
113661.7000	32.1568200	111349.400	0	0	0	6
114763.2000	27.0704200	10033.3000	0	0	0	4
115214.9000	48.8727500	6150.55300	0	0	0	7
115624.1000	64.1191000	313.972200	0	0	0	8
116841.6000	67.7759700	10202.4800	0	0	0	7
117243.3000	23.2729500	12279.3200	0	0	0	4
117481.8000	43.6203600	76016.0900	0	0	0	3

118033.8000	60.5530500	20852.0200	0	0	0	8
118297.8000	207.337400	53242.5500	0	0	0	5
120998.9000	119.887600	19582.8200	0	0	0	5
121242.4000	79.3221700	16814.1100	0	0	0	7
121336.4000	117.410500	114963.600	0	0	0	3
123058.4000	118.130300	7317.28900	0	0	0	8
124328.0000	60.2596900	9174.78200	0	0	0	7
124509.3000	63.4641500	144541.500	0	0	0	6
124904.6000	504.176800	1654.67700	0	0	0	4
126232.2000	268.470600	1518.95000	0	0	0	8
127058.8000	112.525400	532.394300	0	0	0	5
127276.5000	131.308400	83825.7000	0	0	0	7
127767.7000	106.879000	29073.5700	0	0	0	8
128288.2000	93.1552000	242533.600	0	0	0	6
129575.9000	55.8776800	195460.200	0	0	0	3
130948.0000	700.062300	102839.600	0	0	0	6
131539.2000	152.715900	8463.75100	0	0	0	5
131853.9000	269.239800	50999.6200	0	0	0	8
133256.6000	189.036800	9838.64200	0	0	0	6
133279.8000	20.1540300	4.66283500	0	0	0	5
133586.1000	292.290800	2918.23900	0	0	0	7
135293.1000	632.558400	1588.99200	0	0	0	8
136785.7000	66.3172100	126470.500	0	0	0	3
137255.4000	511.578700	91510.1000	0	0	0	8
138135.0000	206.503300	96343.7700	0	0	0	3
138437.7000	1202.23200	100894.500	0	0	0	7
140299.2000	353.691600	131146.700	0	0	0	6
140659.5000	166.612800	19124.1800	0	0	0	4
141953.3000	250.250300	2874.40600	0	0	0	7
143119.4000	149.176600	6.41129800	0	0	0	5
143293.5000	358.289500	43838.3100	0	0	0	7
144508.9000	132.620100	239892.800	0	0	0	3
145798.0000	572.664600	27639.7700	0	0	0	6
146537.3000	502.792100	49917.1100	0	0	0	8
147656.7000	47.1438400	84.3326400	0	0	0	4
148131.9000	530.130700	8615.95300	0	0	0	7
148618.6000	24.0568200	4.22971400	0	0	0	5
149336.4000	1494.79900	1020.88700	0	0	0	4
150489.7000	408.612400	736.719200	0	0	0	5
150759.4000	452.440100	10748.5700	0	0	0	8
151203.2000	74.1100800	84267.7600	0	0	0	3
151743.9000	19.4930900	32374.4000	0	0	0	5
153491.9000	274.908000	7299.84300	0	0	0	5
153825.5000	207.466800	943.731900	0	0	0	8
156923.7000	1022.84900	126442.700	0	0	0	6
157690.4000	19.4788900	1258.39300	0	0	0	4
157786.8000	612.470900	2329.04700	0	0	0	8
158261.4000	797.618500	78327.8500	0	0	0	7
158439.4000	50.1715900	15763.0400	0	0	0	3
159508.1000	105.947700	26398.2400	0	0	0	4
160709.6000	510.100100	16542.0800	0	0	0	8
161476.1000	76.3906500	4747.49100	0	0	0	5
162159.5000	1084.52000	21020.2100	0	0	0	7
163162.5000	713.753800	1097.28400	0	0	0	4
164871.7000	214.251200	2960.59300	0	0	0	5
165681.9000	258.320000	10143.5400	0	0	0	8
165903.9000	515.323500	53246.3200	0	0	0	6
166906.8000	786.551500	35859.9700	0	0	0	6
167053.3000	26.3159300	27944.0400	0	0	0	4
167347.1000	140.189100	103802.900	0	0	0	3
168209.3000	33.1279600	45700.9600	0	0	0	5
168723.1000	741.529700	18003.9700	0	0	0	7
169183.0000	879.214200	2153.74800	0	0	0	4

```
170359.7000 491.998600 4474.39200                       0 0 0     8
171221.3000 217.742400 59409.0300                       0 0 0     5
171472.7000 878.543000 25319.0100                       0 0 0     7
171697.1000 22.5124100 194884.800                       0 0 0     5
171994.1000 32.3167400 170689.600                       0 0 0     3
172227.3000 36.2838800 64837.1400                       0 0 0     3
173384.2000 335.831300 33544.2600                       0 0 0     4
174800.9000 61.7203400 21425.9800                       0 0 0     5
175281.5000 2855.24800 507310.100                       0 0 0     6
176266.9000 37.5742800 432753.500                       0 0 0     3
178448.3000 120.987300 14286.2700                       0 0 0     5
178656.7000 271.998300 3387.29200                       0 0 0     8
180957.2000 138.289900 54800.8400                       0 0 0     3
181023.2000 706.108800 298863.600                       0 0 0     6
182308.7000 1535.58600 740.050000                       0 0 0     4
184535.3000 340.208400 155.858300                       0 0 0     5
185842.7000 171.865800 24467.6900                       0 0 0     3
186283.1000 118.821100 62172.6200                       0 0 0     3
187306.2000 72.3921600 22289.2400                       0 0 0     4
187891.9000 37.3831000 1311.53700                       0 0 0     5
188286.1000 1906.39100 1619.15500                       0 0 0     4
189399.5000 31.0425900 275.515800                       0 0 0     4
190185.4000 474.673600 14094.2000                       0 0 0     7
191965.5000 419.796200 2200.23700                       0 0 0     8
192511.6000 34.6806500 589.580300                       0 0 0     4
192998.2000 815.566600 1442.92100                       0 0 0     5
193397.2000 190.771000 23228.1500                       0 0 0     7
193899.1000 24.7961100 41736.7400                       0 0 0     4
194648.2000 90.4551300 82984.9900                       0 0 0     5
195246.7000 280.630300 38991.3300                       0 0 0     8
195326.7000 41.0359100 311032.300                       0 0 0     3
197246.5000 745.199600 620.712500                       0 0 0     4
198908.8000 30.2675700 14647.1200                       0 0 0     5
199308.9000 70.2278300 5923.58500                       0 0 0     3
241153.6000 43.2539600 12782.0300                       0 0 0     3
241786.9000 43.3128500 170782.000                       0 0 0     6
409872.2000 43.1811500 574429.100                       0 0 0     6
423648.3000 43.0556900 19685.1300                       0 0 0     3
-12010000.0 250.000000 9075000.+3  0.0000              0 0 0 0   9
-4469100.00 250.000000 5410000.+3  0.0000              0 0 0 0   9
434310.0000 2700.00000 44410000.0  0.0000              0 0 0 0  11
1000220.000 250.000000 100360000.  0.0000              0 0 0 0  12
1309380.000 250.000000 43430000.0  0.0000              0 0 0 0  11
1651380.000 250.000000 4100000.00  0.0000              0 0 0 0  15
1689100.000 250.000000 270000.000  0.0000              0 0 0 0  14
1834090.000 250.000000 7790000.00  0.0000              0 0 0 0  12
1901440.000 250.000000 33500000.0  0.0000              0 0 0 0  10
2377880.000 250.000000 162370000.  0.0000              0 0 0 0   9
2888700.000 250.000000 220000.000  0.0000              0 0 0 0  13
3006900.000 250.000000 160000.000  0.0000              0 0 0 0  15
3211760.000 250.000000 1510000.00 9000.00000           0 0 0 0  14
3291010.000 250.000000 339630000. 170000.000           0 0 0 0  12
3438800.000 250.000000 620000.000 20000.0000           0 0 0 0  13
3441550.000 250.000000 1310000.00 7000.00000           0 0 0 0  14
3511910.000 250.000000 660210000. 26000.0000           0 0 0 0  11
3767000.000 250.000000 18530000.0 26000.0000           0 0 0 0  15
3989640.000 250.000000 276190000. 19150000.0           0 0 0 0  10
4060820.000 250.000000 105580000. 5230000.00           0 0 0 0   9
4180040.000 250.000000 92380000.0 9800000.00           0 0 0 0  12
4302790.000 250.000000 54300000.0 5770000.00           0 0 0 0  11
4311700.000 250.000000 43520000.0-440000.000           0 0 0 0  10
4467360.000 250.000000 16890000.0 3720000.00           0 0 0 0   9
4527360.000 250.000000 4990000.00 860000.000           0 0 0 0  13
```

```
4594830.000 250.000000 1390000.00 440000.000             0 0 0 0  16
4631210.000 250.000000 3200000.00 3880000.00             0 0 0 0  14
4820330.000 250.000000 58400000.0 2740000.00             0 0 0 0  11
5066300.000 250.000000 94500000.0-34360000.0             0 0 0 0  12
5123740.000 250.000000 23350000.0 2750000.00             0 0 0 0  15
5311000.000 250.000000 500000.000 4000000.00             0 0 0 0  10
5369270.000 250.000000 2780000.00 1250000.00             0 0 0 0  13
5574840.000 250.000000 191170000. 420000.000             0 0 0 0  11
5672620.000 250.000000 590000.000 15630000.0             0 0 0 0  14
5918630.000 250.000000 20500000.0 4190000.00             0 0 0 0  16
5993290.000 250.000000 14780000.0-210000.000             0 0 0 0  11
6076190.000 250.000000 3130000.00 2510000.00             0 0 0 0  17
6087440.000 250.000000 16040000.0 1920000.00             0 0 0 0  10
6207950.000 250.000000 4970000.00 109230000.             0 0 0 0  13
6332240.000 250.000000 3400000.00 181480000.             0 0 0 0  16
6400260.000 250.000000 26540000.0 29380000.0             0 0 0 0  15
6578030.000 250.000000 90640000.0 87940000.0             0 0 0 0  12
6672730.000 250.000000 1860000.00 19060000.0             0 0 0 0  14
6786120.000 250.000000 10570000.0 232540000.             0 0 0 0  13
6815170.000 250.000000 18940000.0 28360000.0             0 0 0 0  15
7168680.000 250.000000 129690000. 223850000.             0 0 0 0  15
7198370.000 250.000000 7860000.00 19700000.0             0 0 0 0  13
7294220.000 250.000000 26160000.0 5390000.00             0 0 0 0  10
7373310.000 250.000000 1890000.00  0.0000                0 0 0 0  10
11131720.00 250.000000 1511500.+4  0.0000                0 0 0 0  11
17223850.00 250.000000 772360000.  0.0000                0 0 0 0  12
19026720.00 250.000000 2575500.+4  0.0000                0 0 0 0  10

.200000000
Channel radii in key-word format
Radii=  5.210000,  5.210000    Flags=0, 0
   Group=  1   Chan=  1,
Radii=  4.900000,  4.900000    Flags=0, 0
   Group=  2   Chan=  1,
Radii=  6.064896,  6.064896    Flags=0, 0
   Group=  3   Chan=  1,
   Group=  4   Chan=  1,
   Group=  5   Chan=  1,
Radii=  5.396451,  5.396451    Flags=0, 0
   Group=  6   Chan=  1,
   Group=  7   Chan=  1,
   Group=  8   Chan=  1,
Radii=  3.400000,  3.728620    Flags=0, 0
   Group=  9   Chan=  1,
   Group= 10   Chan=  1,
   Group= 11   Chan=  1,
   Group= 12   Chan=  1,
   Group= 13   Chan=  1,
   Group= 14   Chan=  1,
   Group= 15   Chan=  1,
   Group= 16   Chan=  1,
   Group= 17   Chan=  1,
Radii=  6.700000,  3.728794    Flags=0, 0
   Group=  9   Chan=  2,
   Group= 10   Chan=  2,
   Group= 11   Chan=  2,
   Group= 12   Chan=  2,
   Group= 13   Chan=  2,
   Group= 14   Chan=  2,
   Group= 15   Chan=  2,
   Group= 16   Chan=  2,
   Group= 17   Chan=  2,
```

APPENDIX C. PLOTS OF EXPERIMENTAL DATA

APPENDIX C. PLOTS OF EXPERIMENTAL DATA

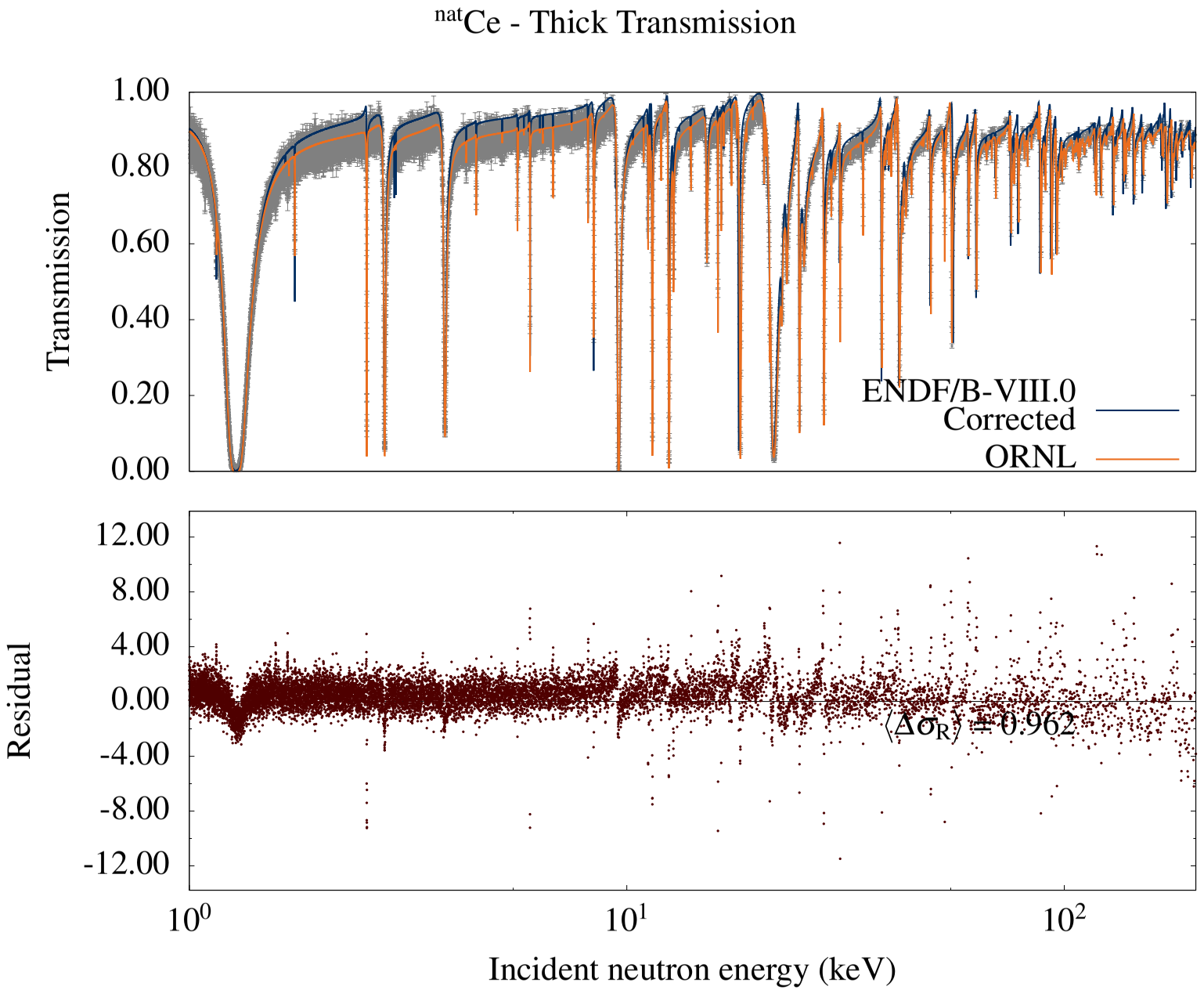

Figure 13. ^{nat}Ce Transmission - Thick Target - 1-200 keV

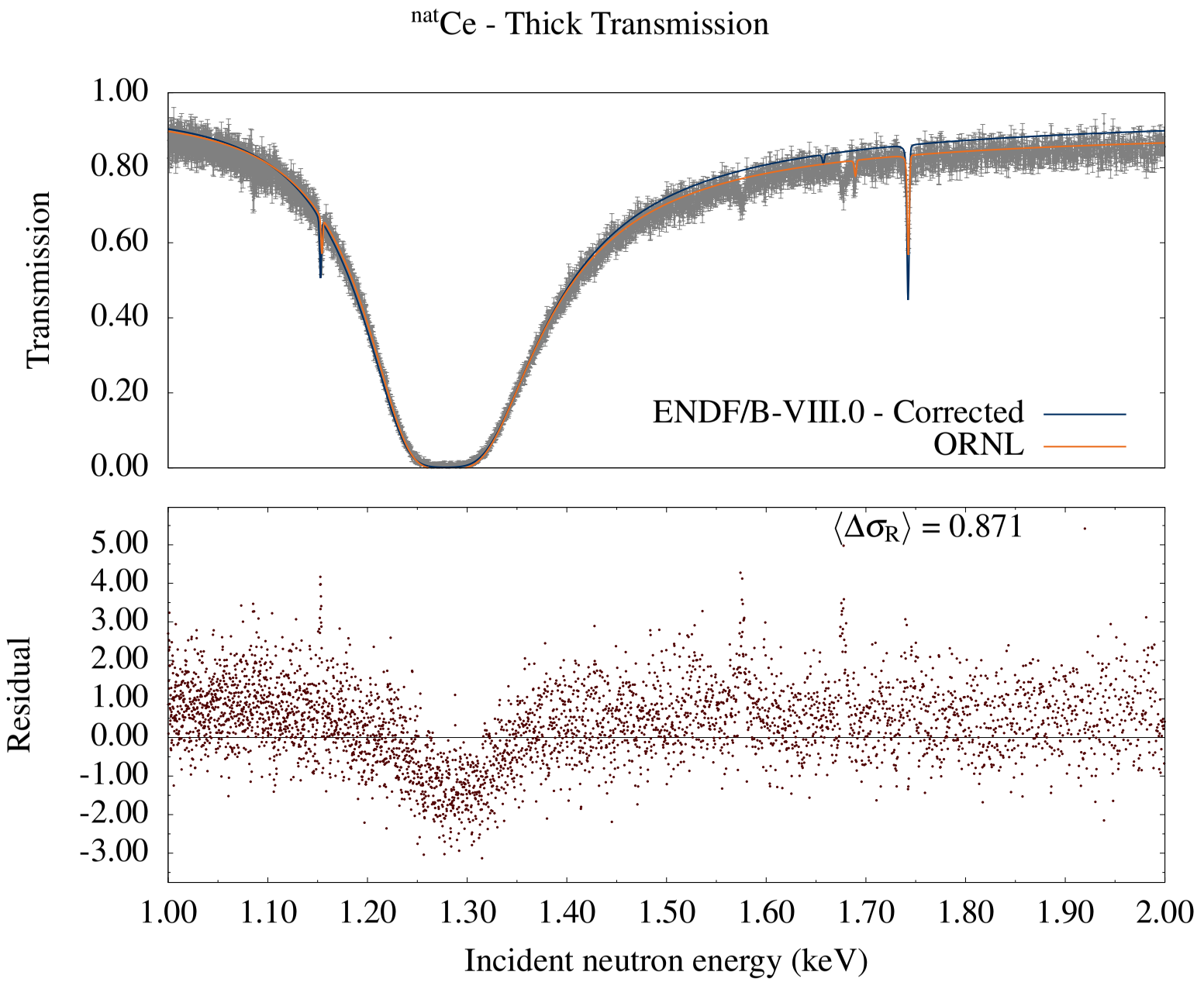

Figure 14. ^{nat}Ce Transmission - Thick Target - 1-2 keV. A discussion about the features at 1.58 and 1.68 keV can be found in Section 3.2

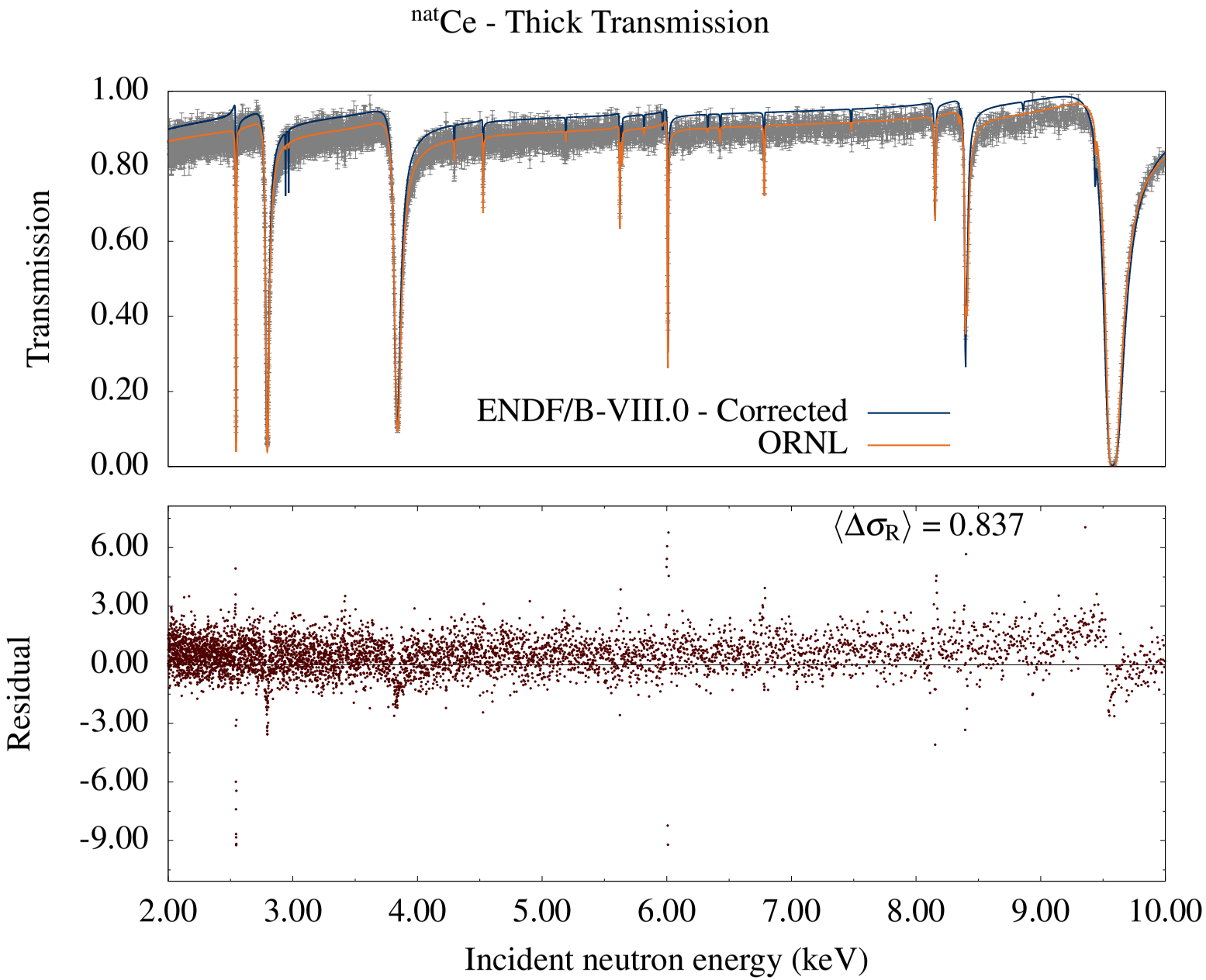

Figure 15. ^{nat}Ce Transmission - Thick Target - 2-10 keV

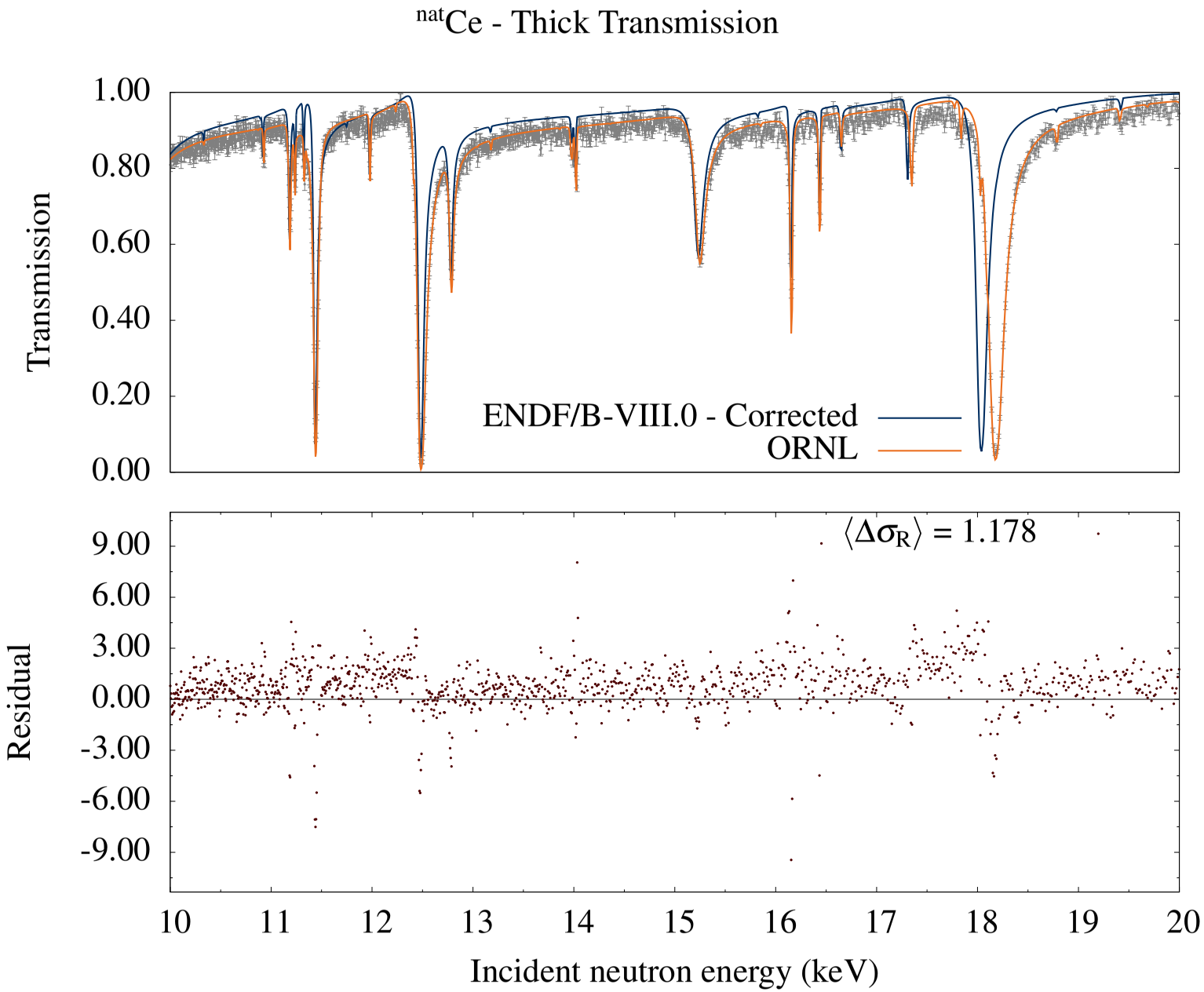

Figure 16. ^{nat}Ce Transmission - Thick Target - 10-20 keV

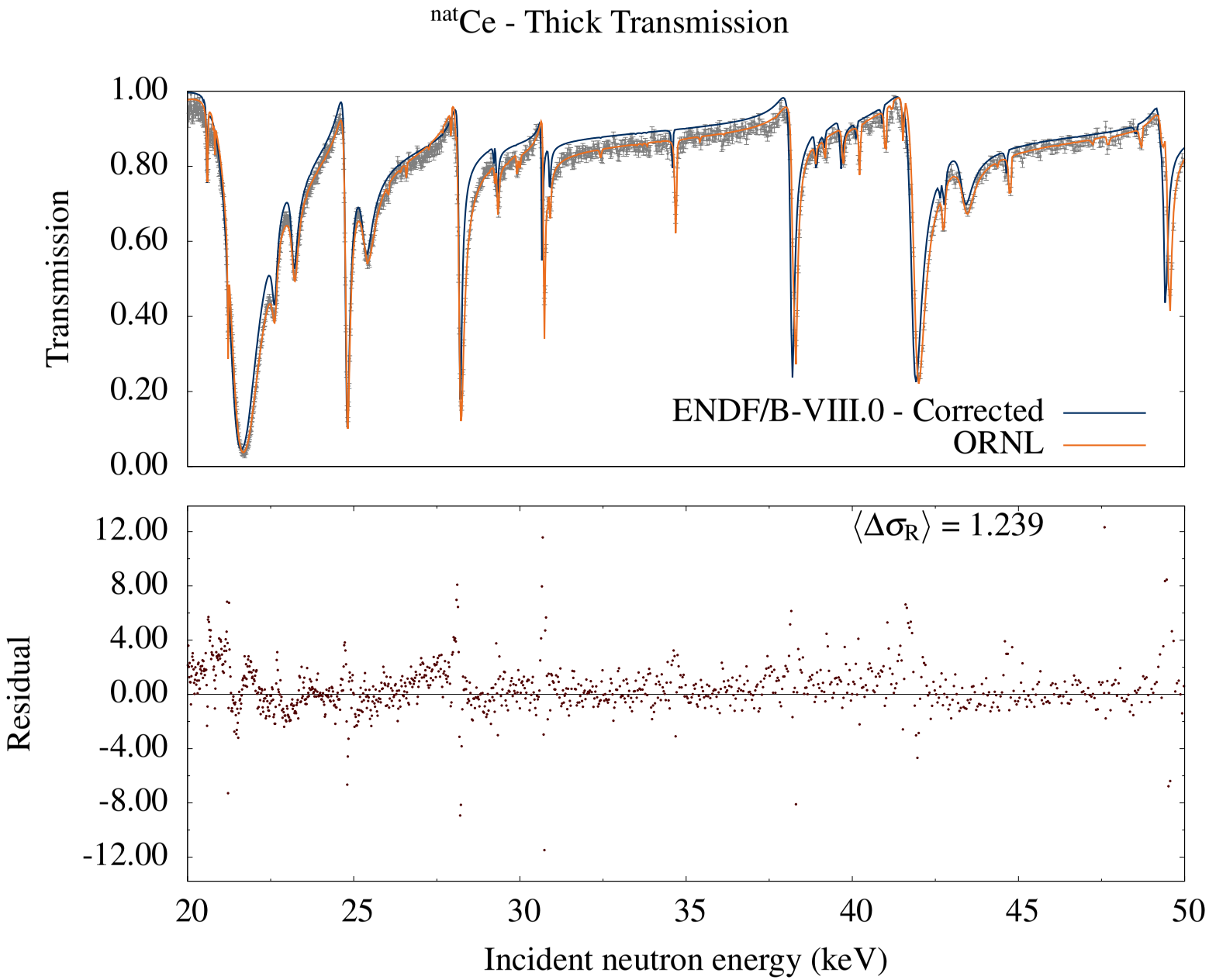

Figure 17. ^{nat}Ce Transmission - Thick Target - 20-50 keV

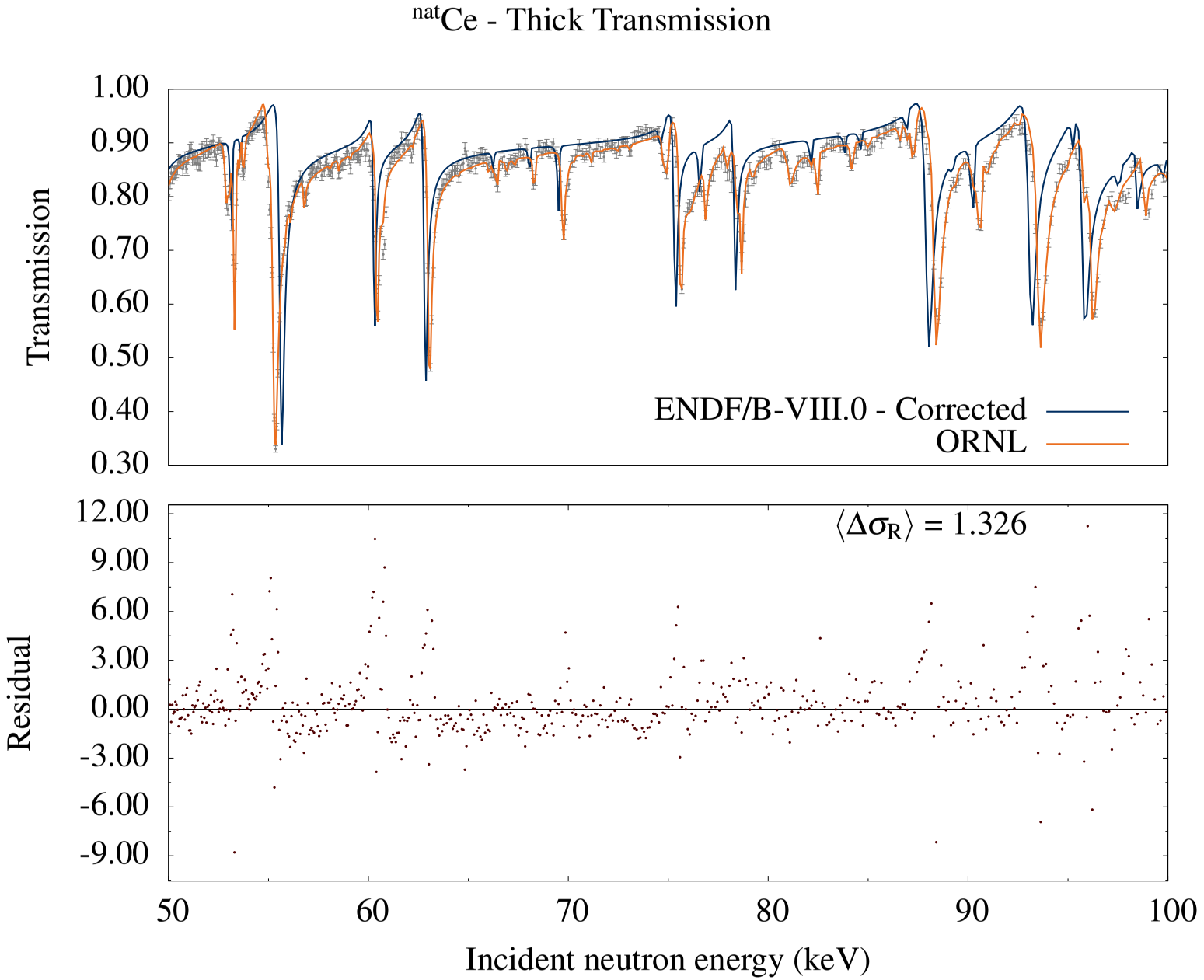

Figure 18. ^{nat}Ce Transmission - Thick Target - 50-100 keV

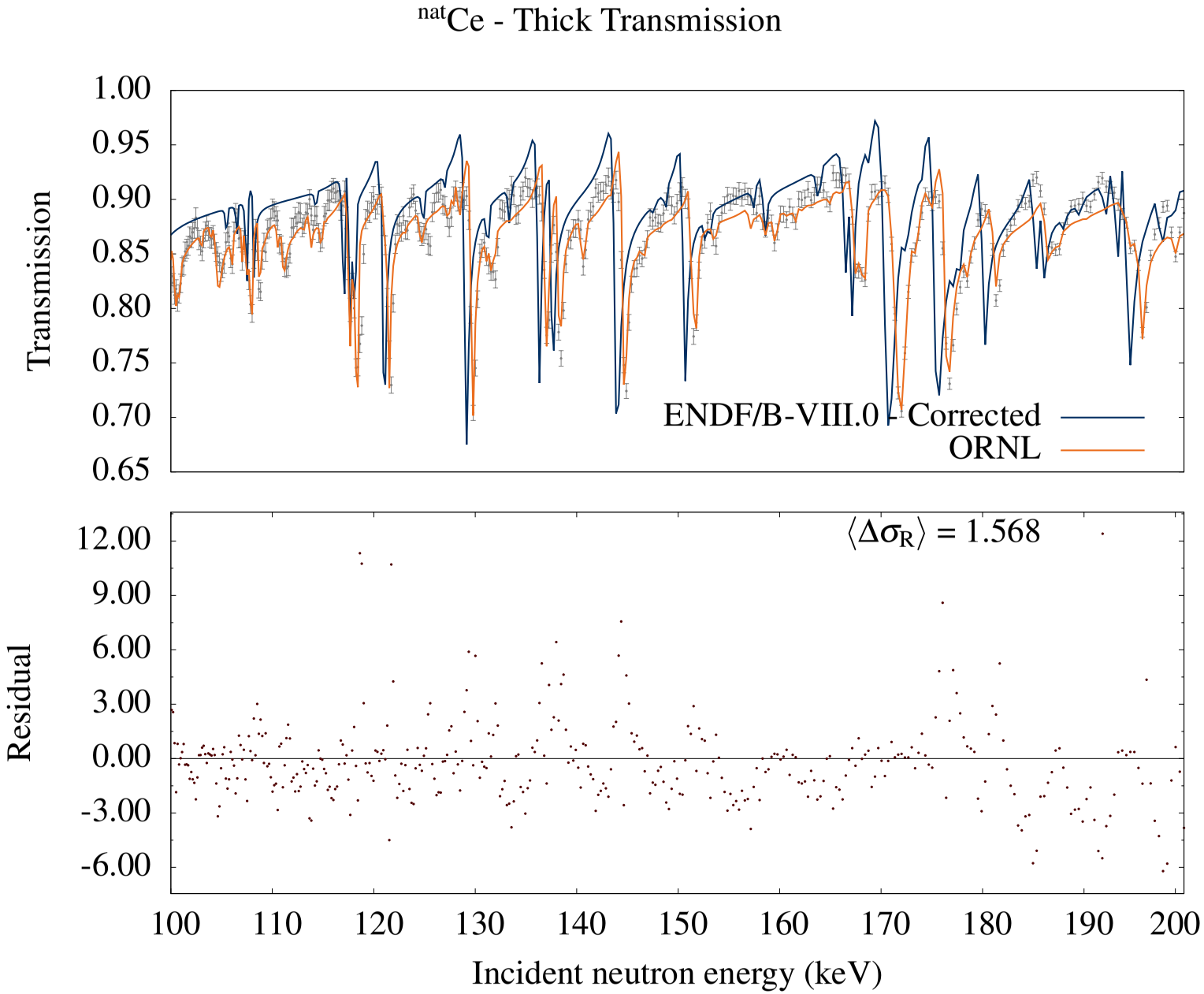

Figure 19. ^{nat}Ce Transmission - Thick Target - 100-200 keV

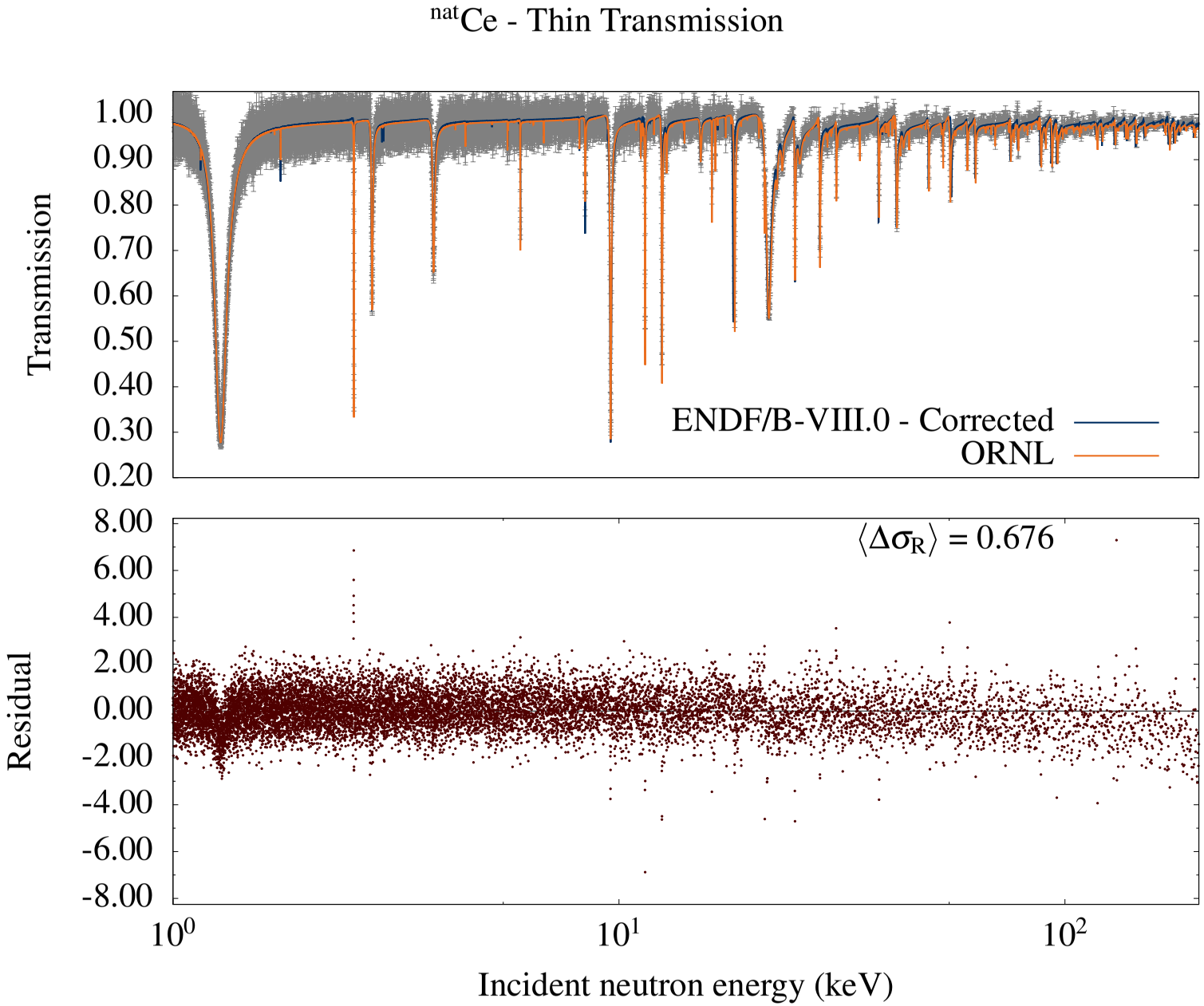

Figure 20. ^{nat}Ce Transmission - Thin Target - 1-200 keV

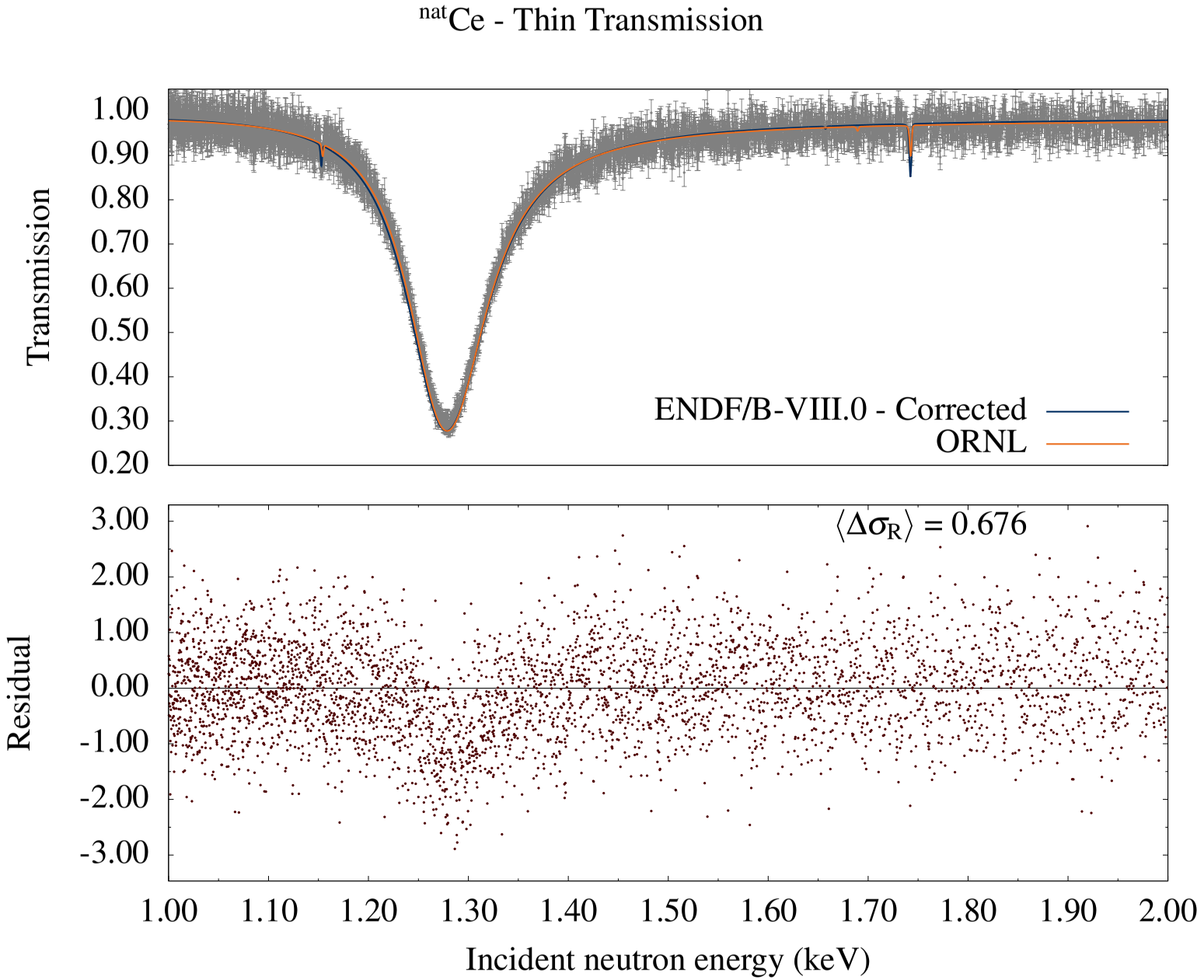

Figure 21. ^{nat}Ce Transmission - Thin Target - 1-2 keV

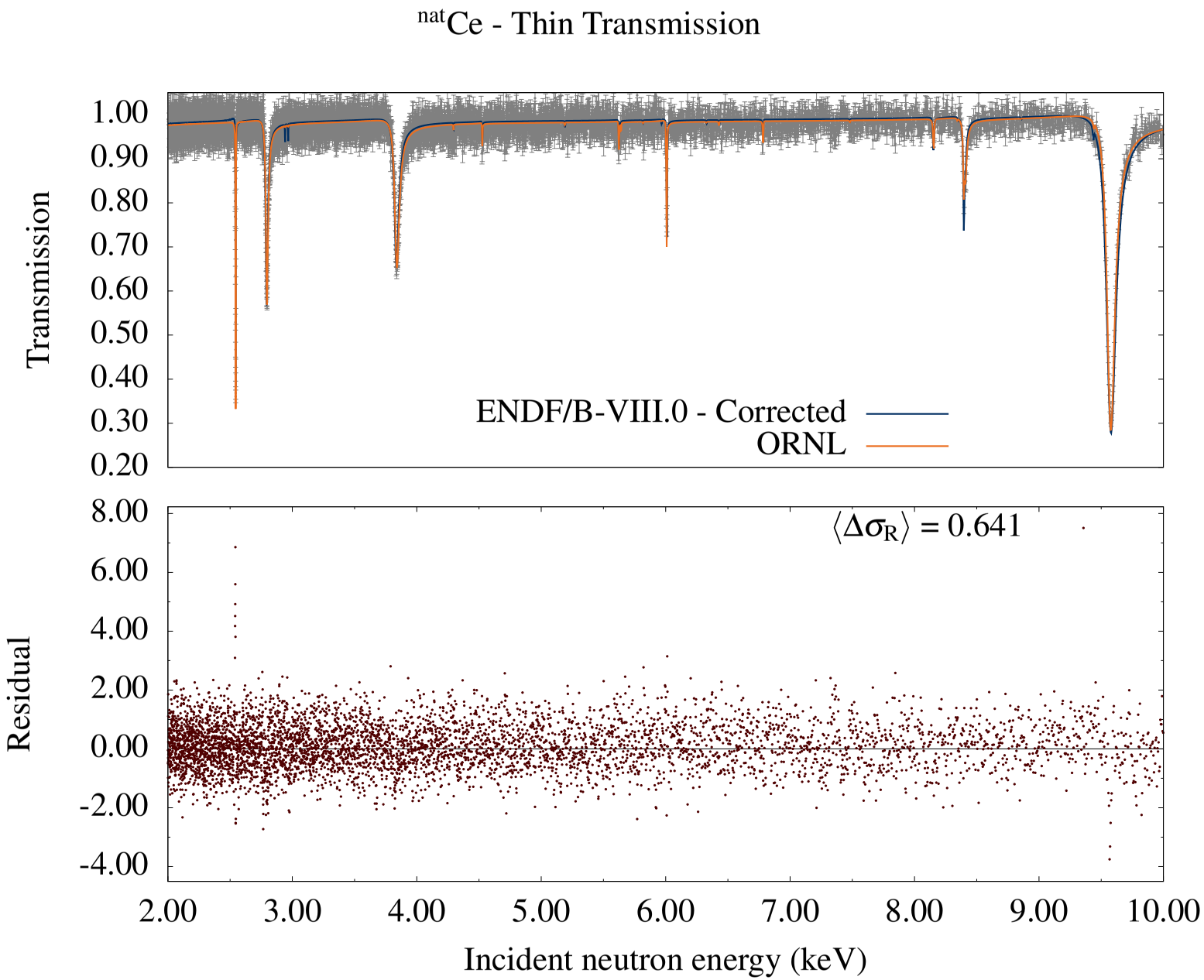

Figure 22. ^{nat}Ce Transmission - Thin Target - 2-10 keV

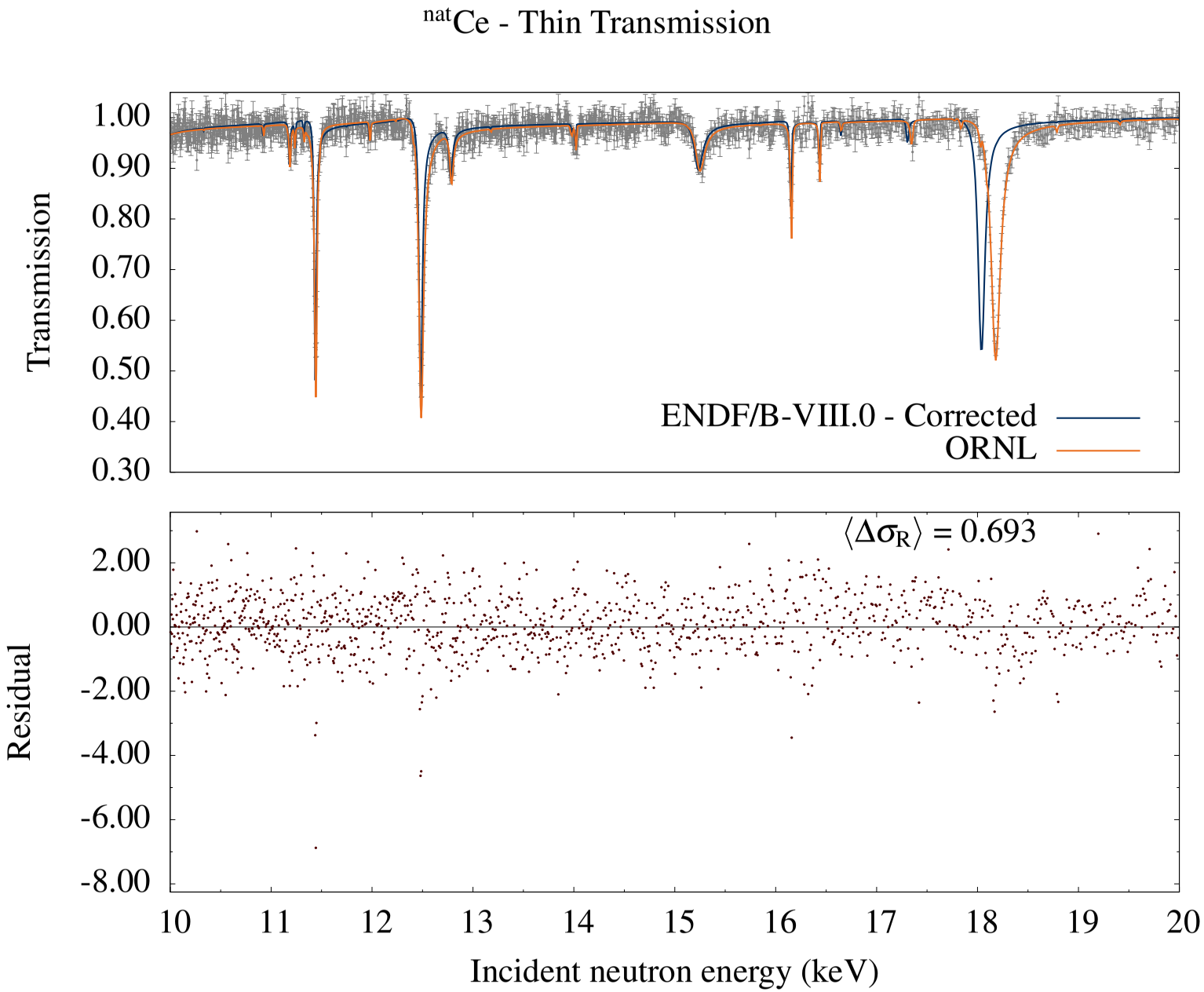

Figure 23. ^{nat}Ce Transmission - Thin Target - 10-20 keV

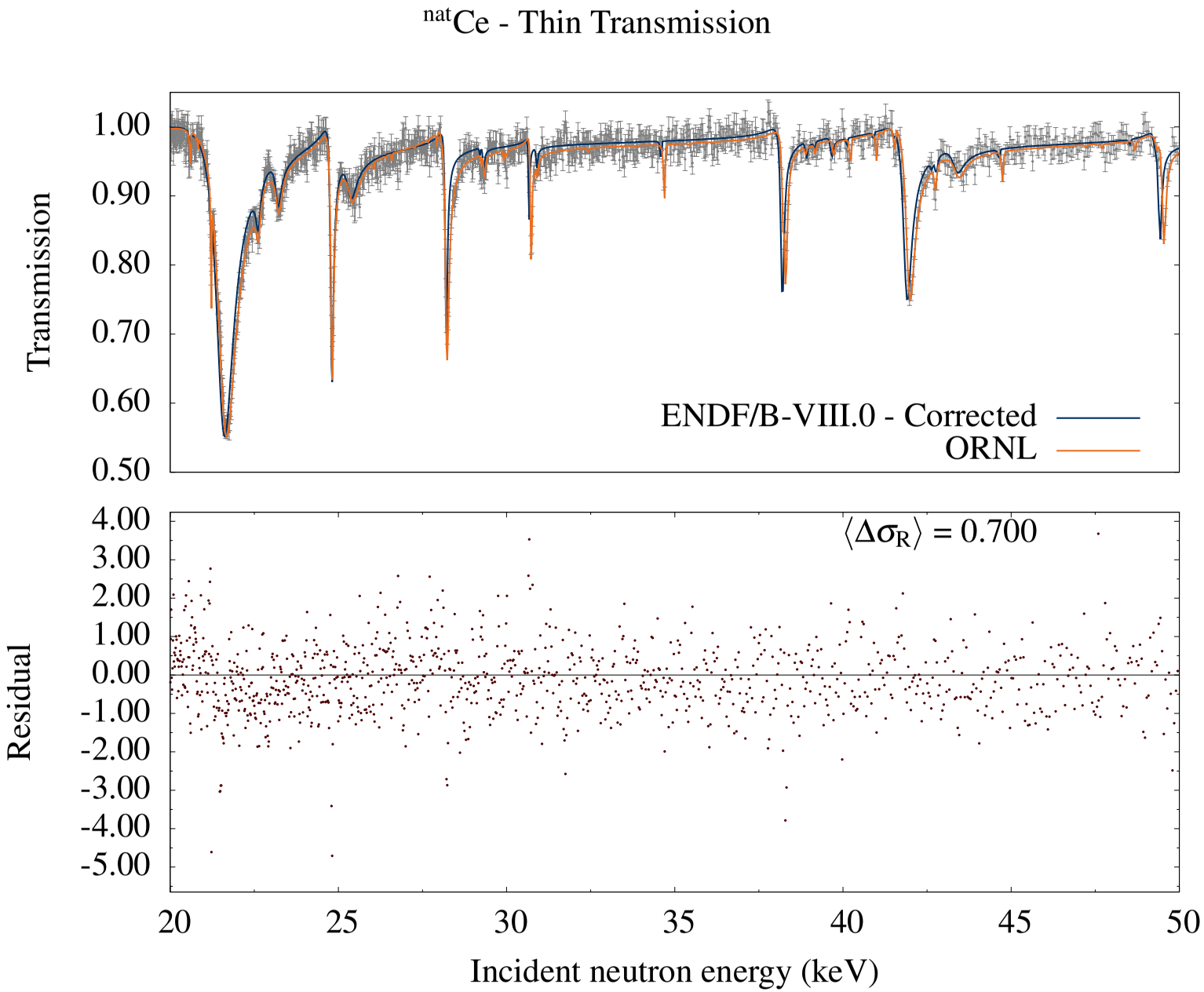

Figure 24. ^{nat}**Ce Transmission - Thin Target - 20-50 keV**

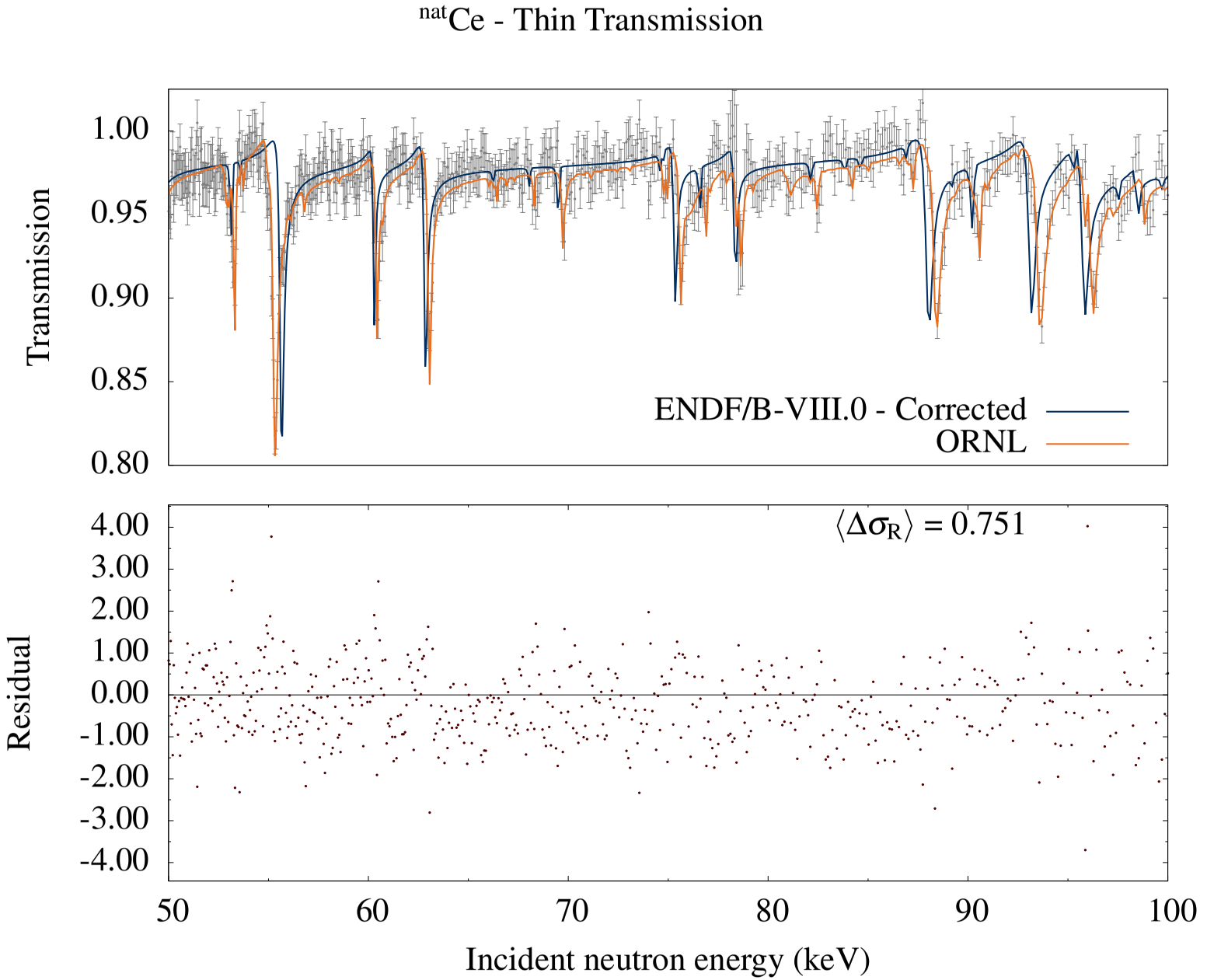

Figure 25. ^{nat}Ce Transmission - Thin Target - 50-100 keV

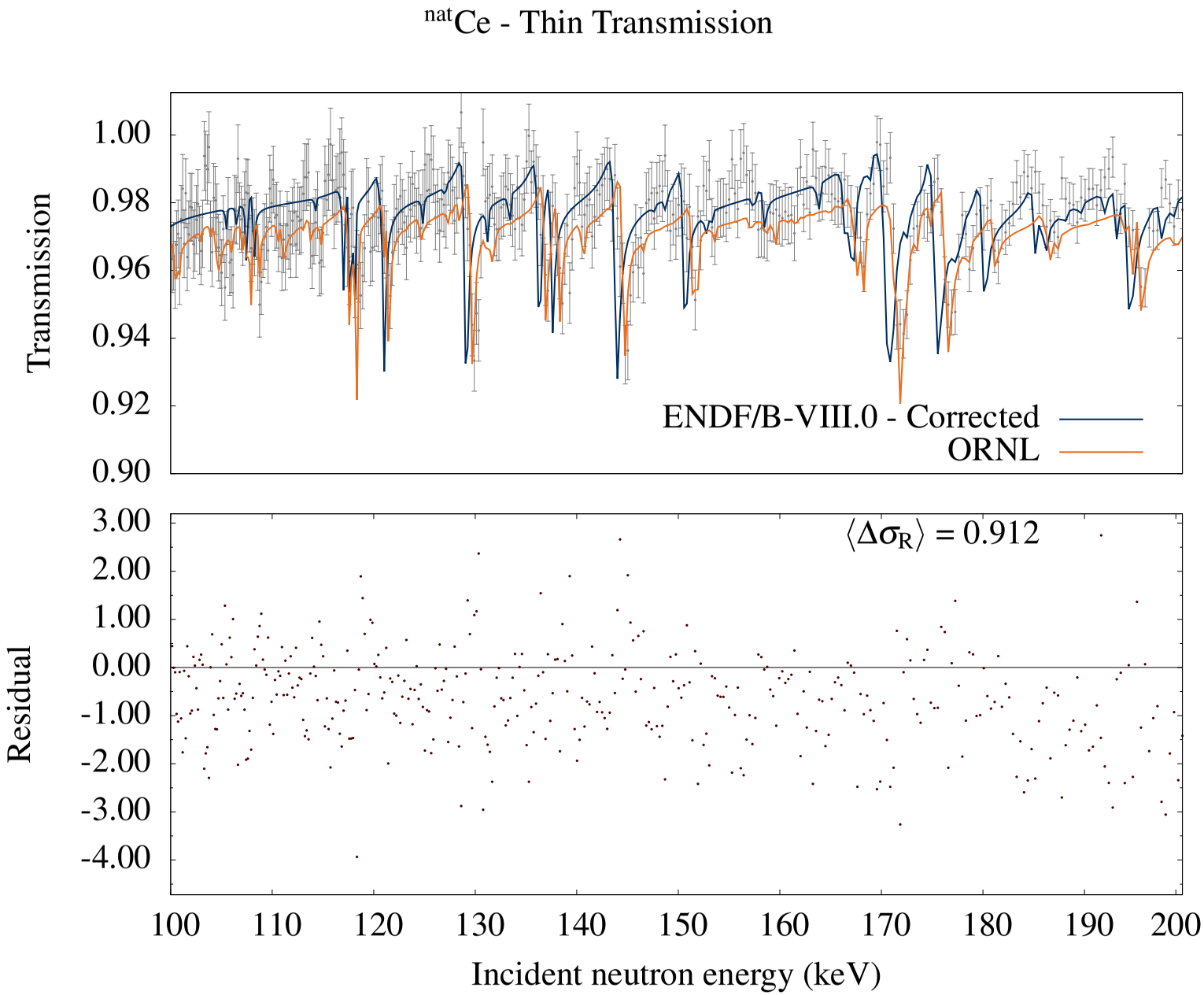

Figure 26. ^{nat}Ce Transmission - Thin Target - 100-200 keV

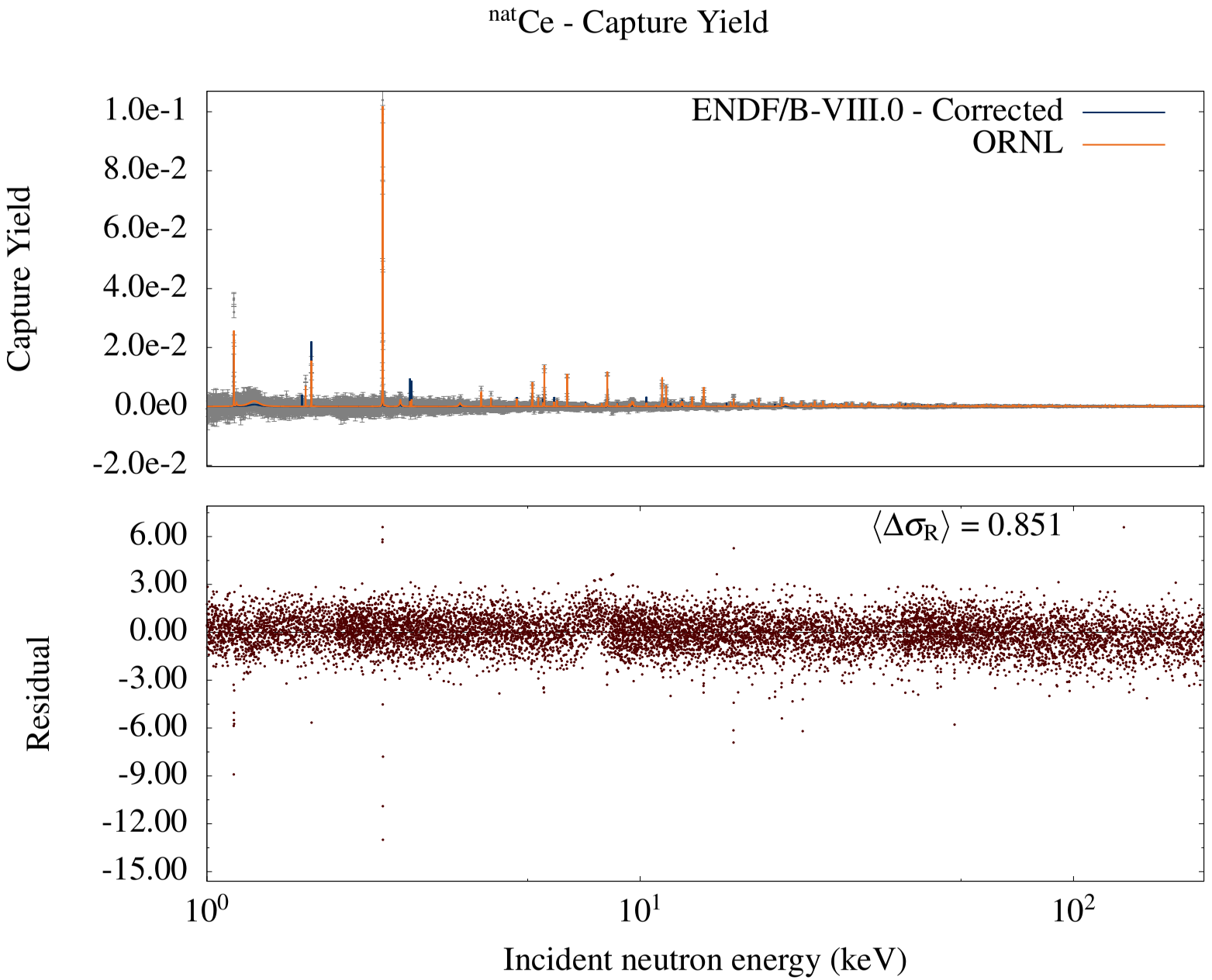

Figure 27. ^{nat}Ce Capture Yield - 1-200 keV

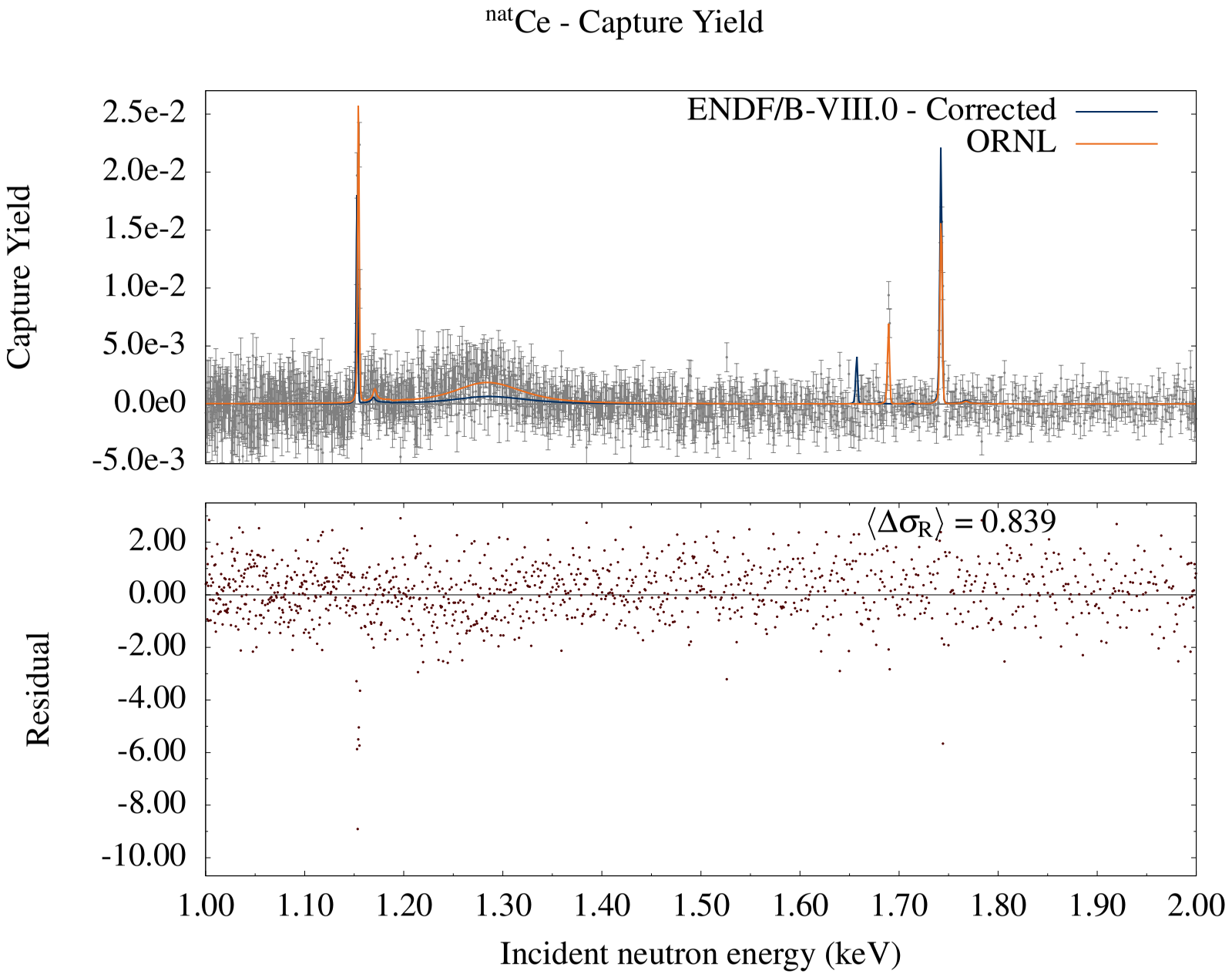

Figure 28. ^{nat}Ce Capture Yield - 1-2 keV

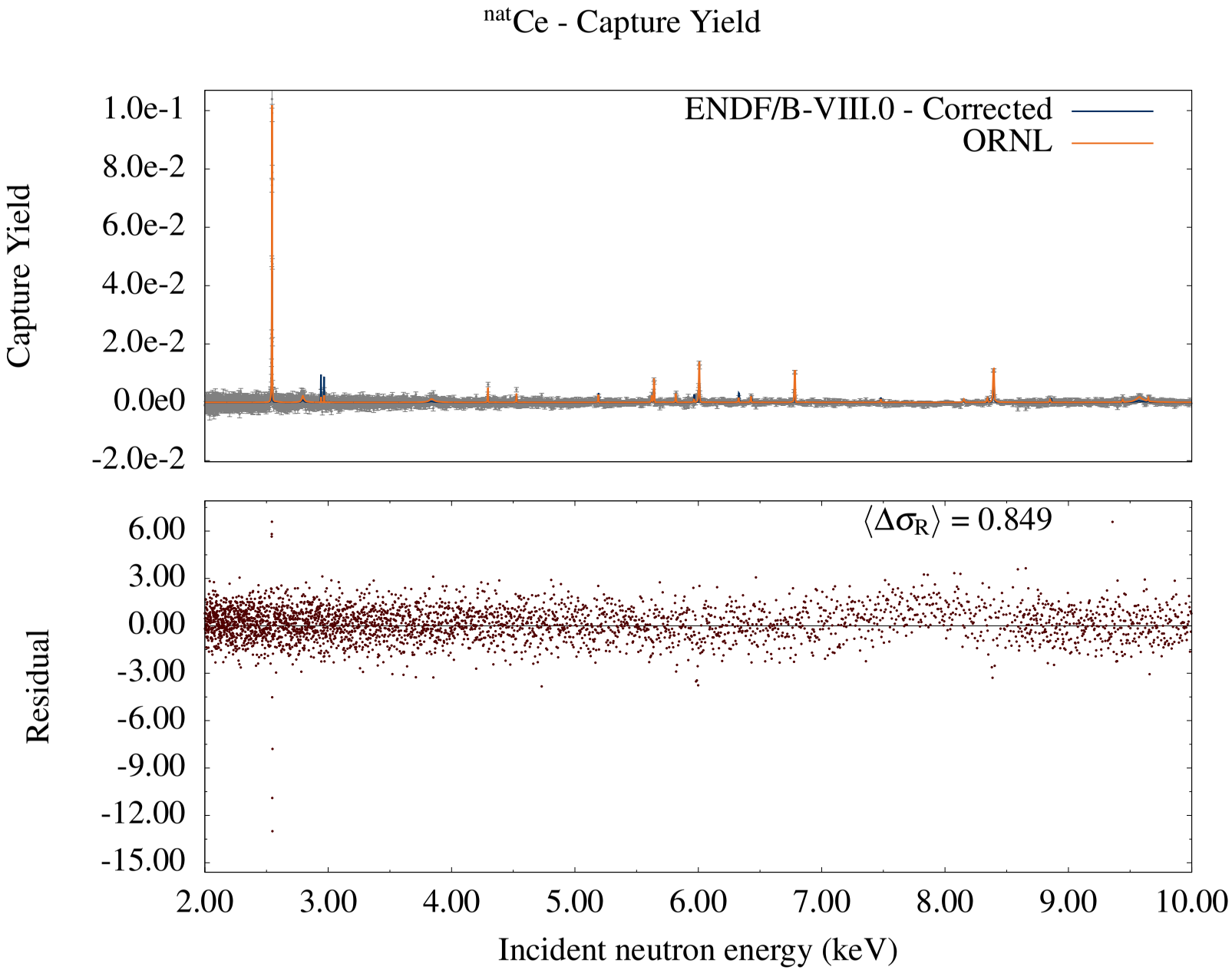

Figure 29. ^{nat}Ce Capture Yield - 2-10 keV

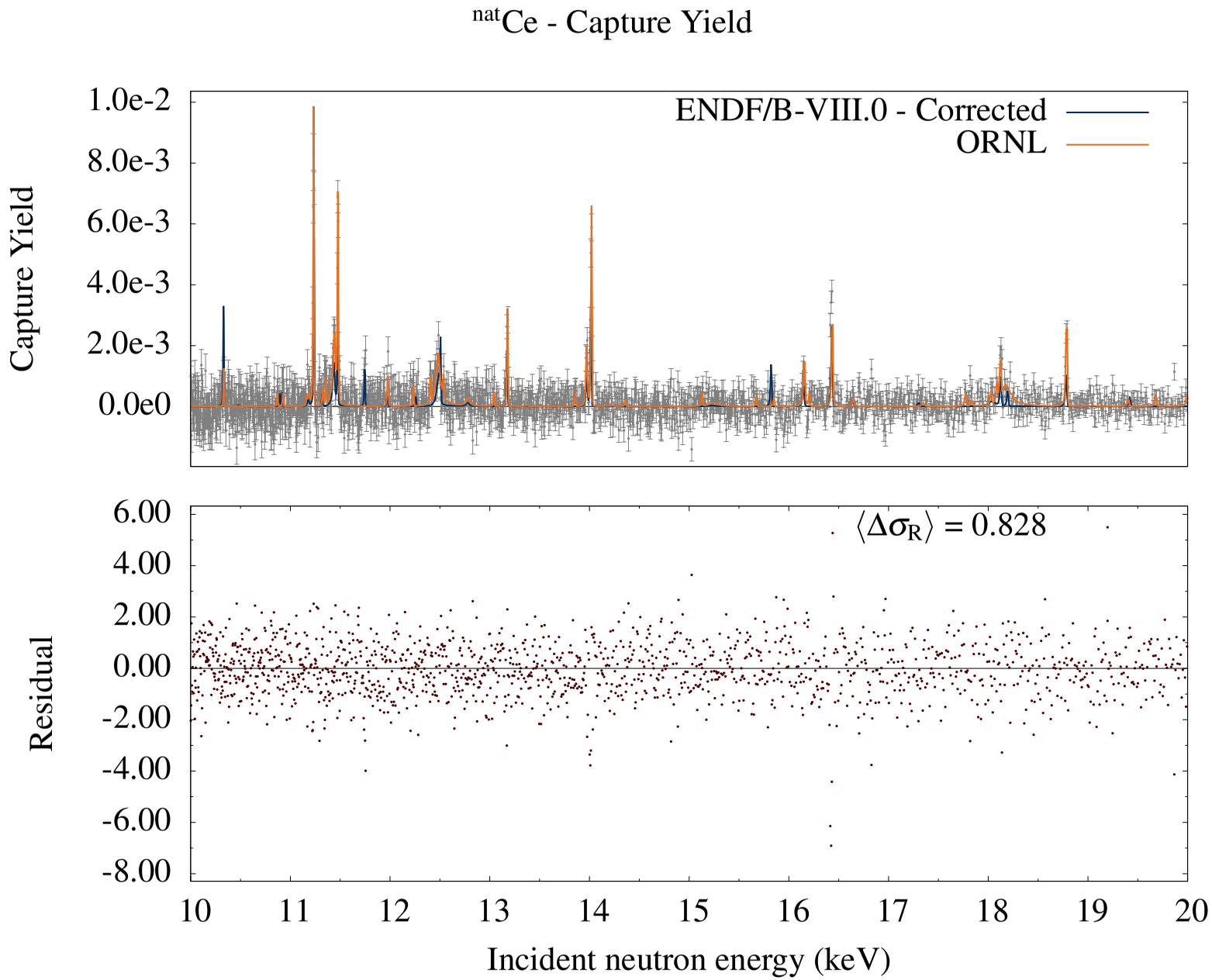

Figure 30. ^{nat}Ce Capture Yield - 10-20 keV

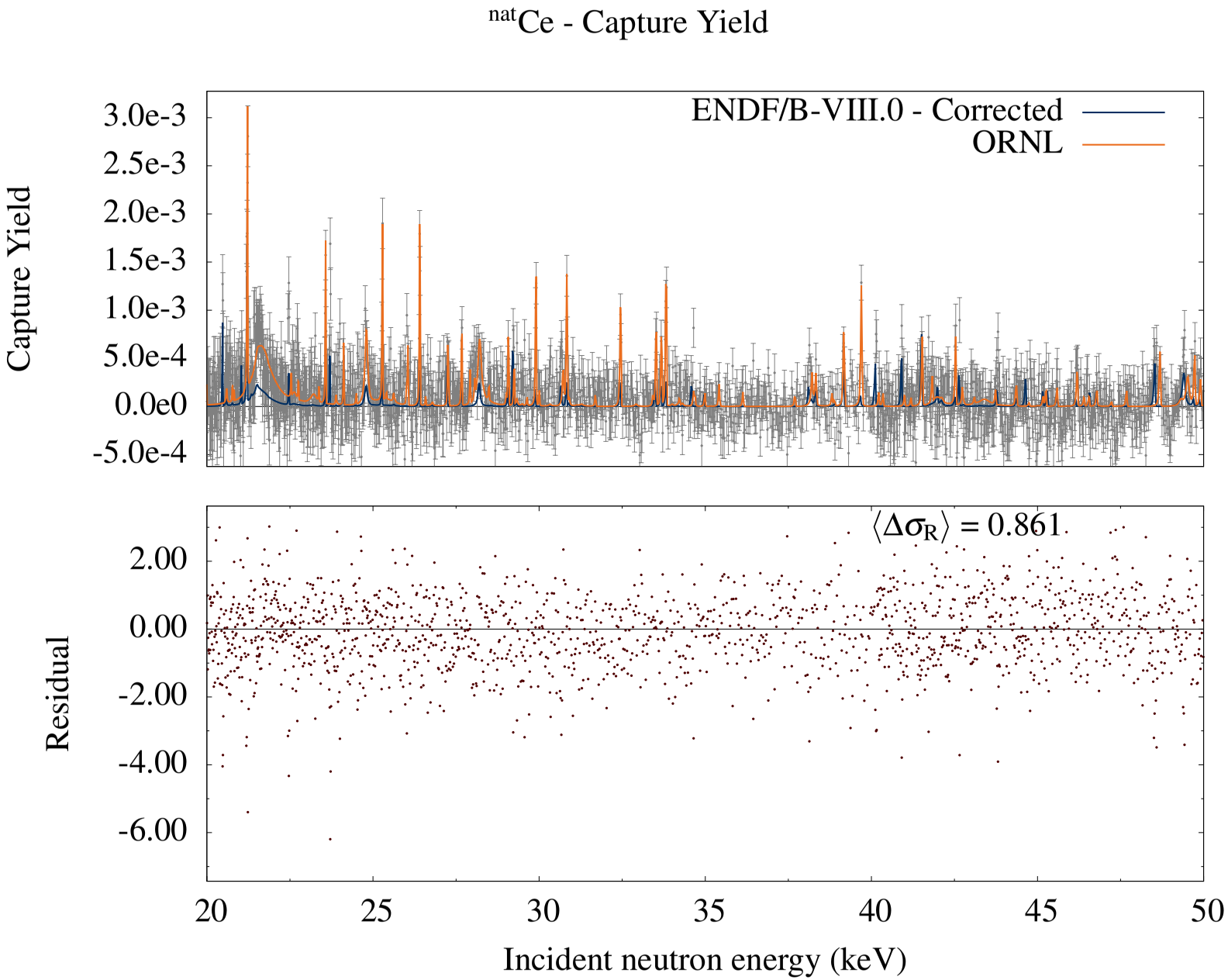

Figure 31. ^{nat}Ce Capture Yield - 20-50 keV

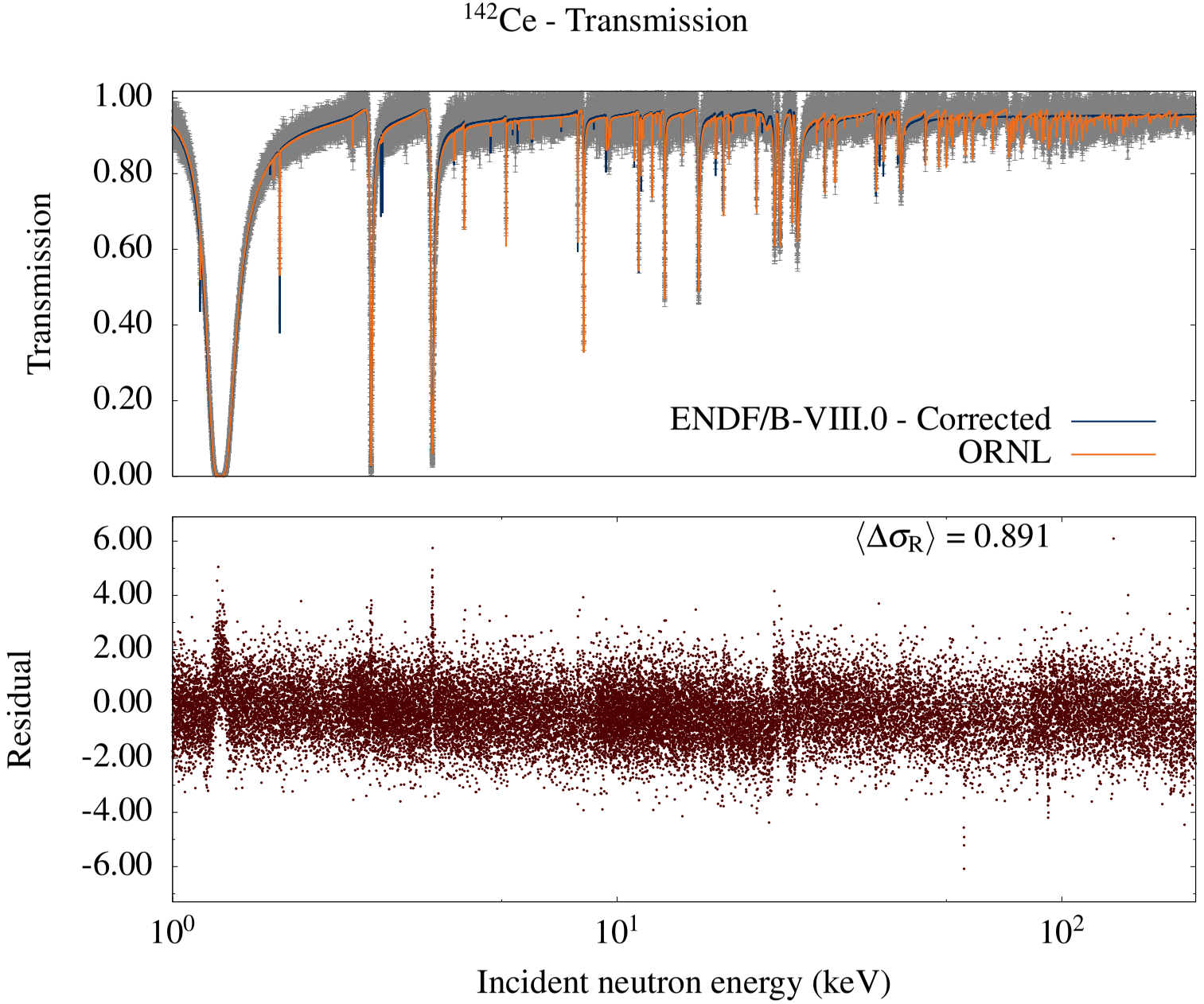

Figure 32. ^{142}Ce Transmission - 1-200 keV

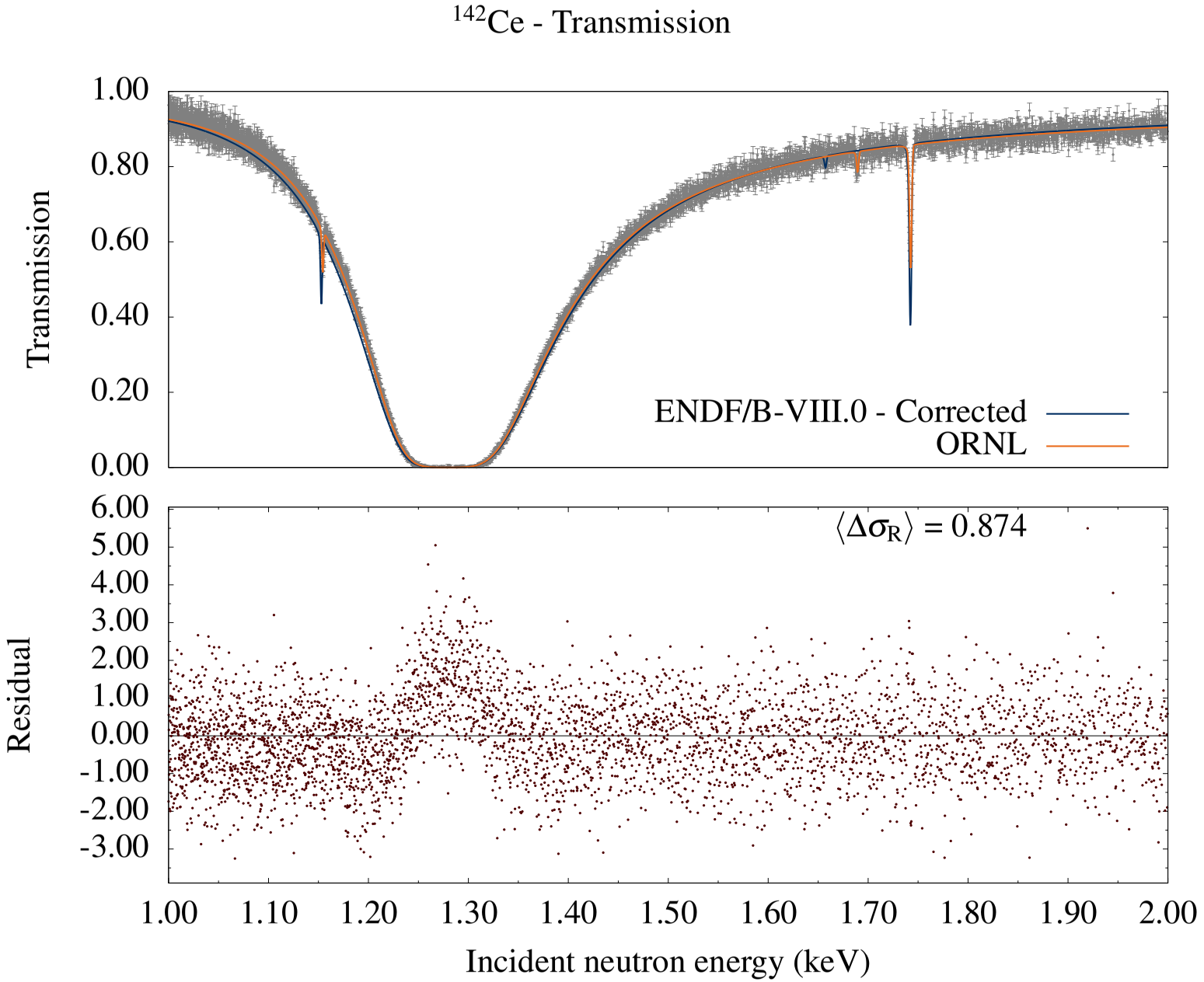

Figure 33. ^{142}Ce Transmission - 1-2 keV

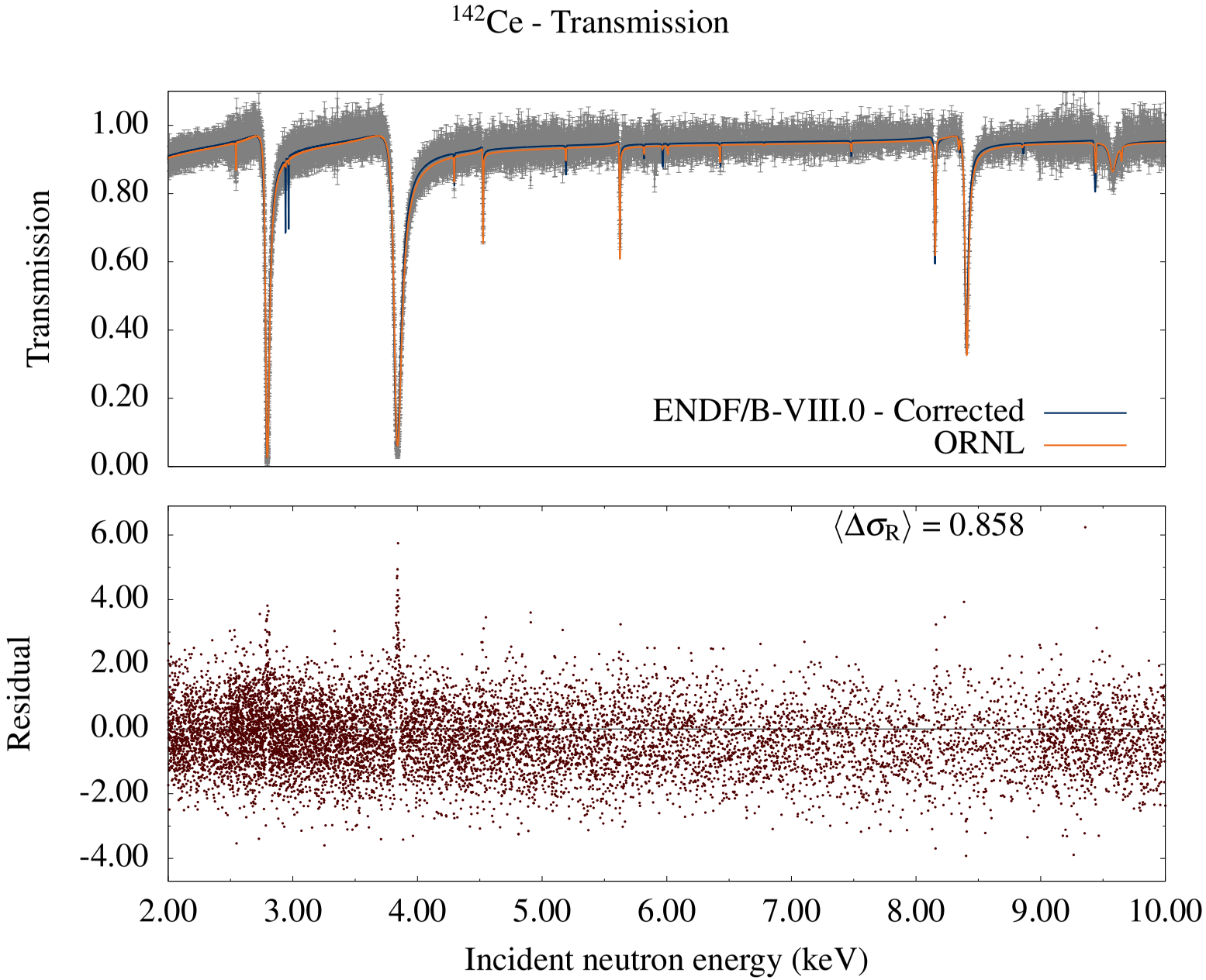

Figure 34. ^{142}Ce Transmission - 2-10 keV

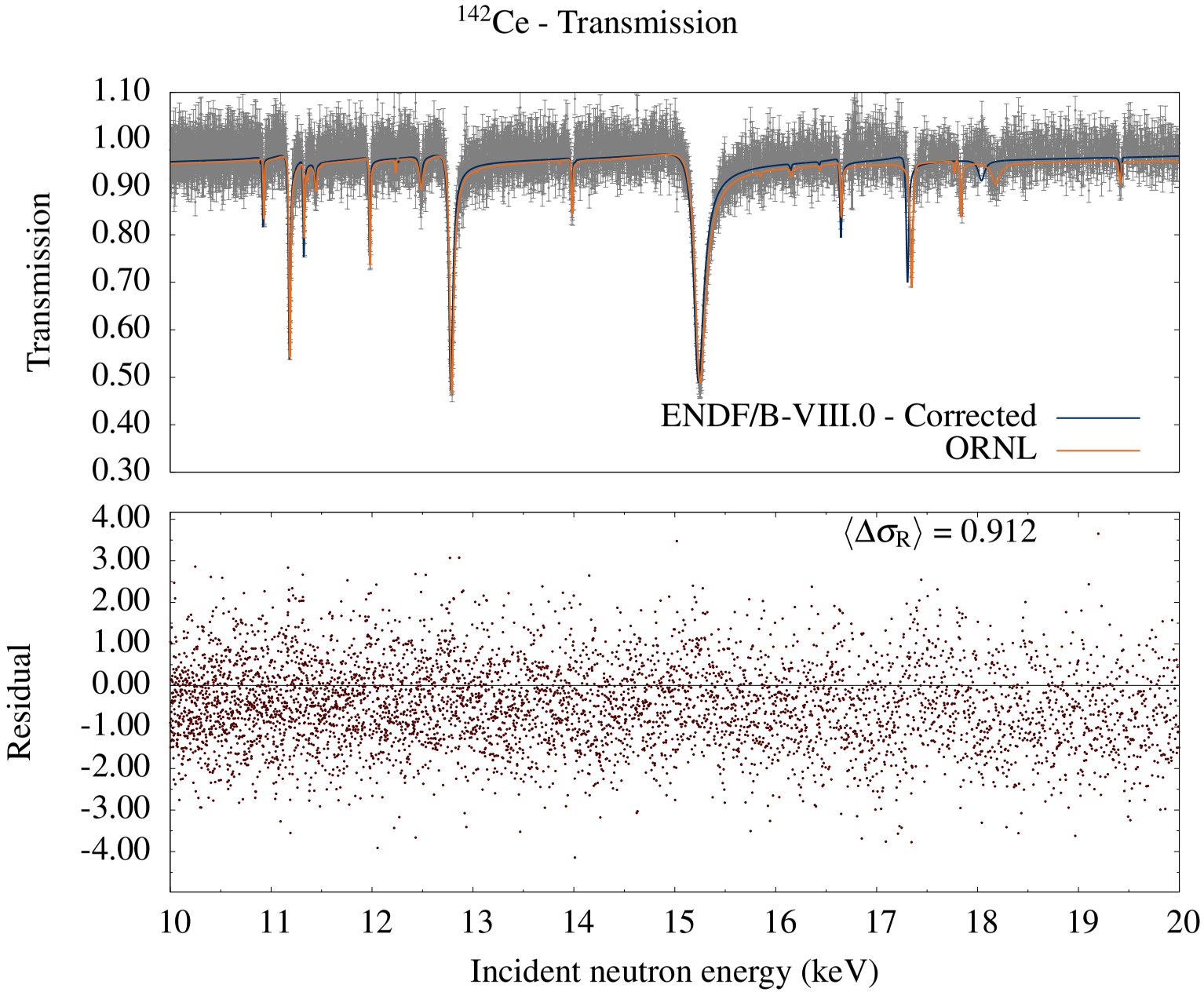

Figure 35. ^{142}**Ce Transmission - 10-20 keV**

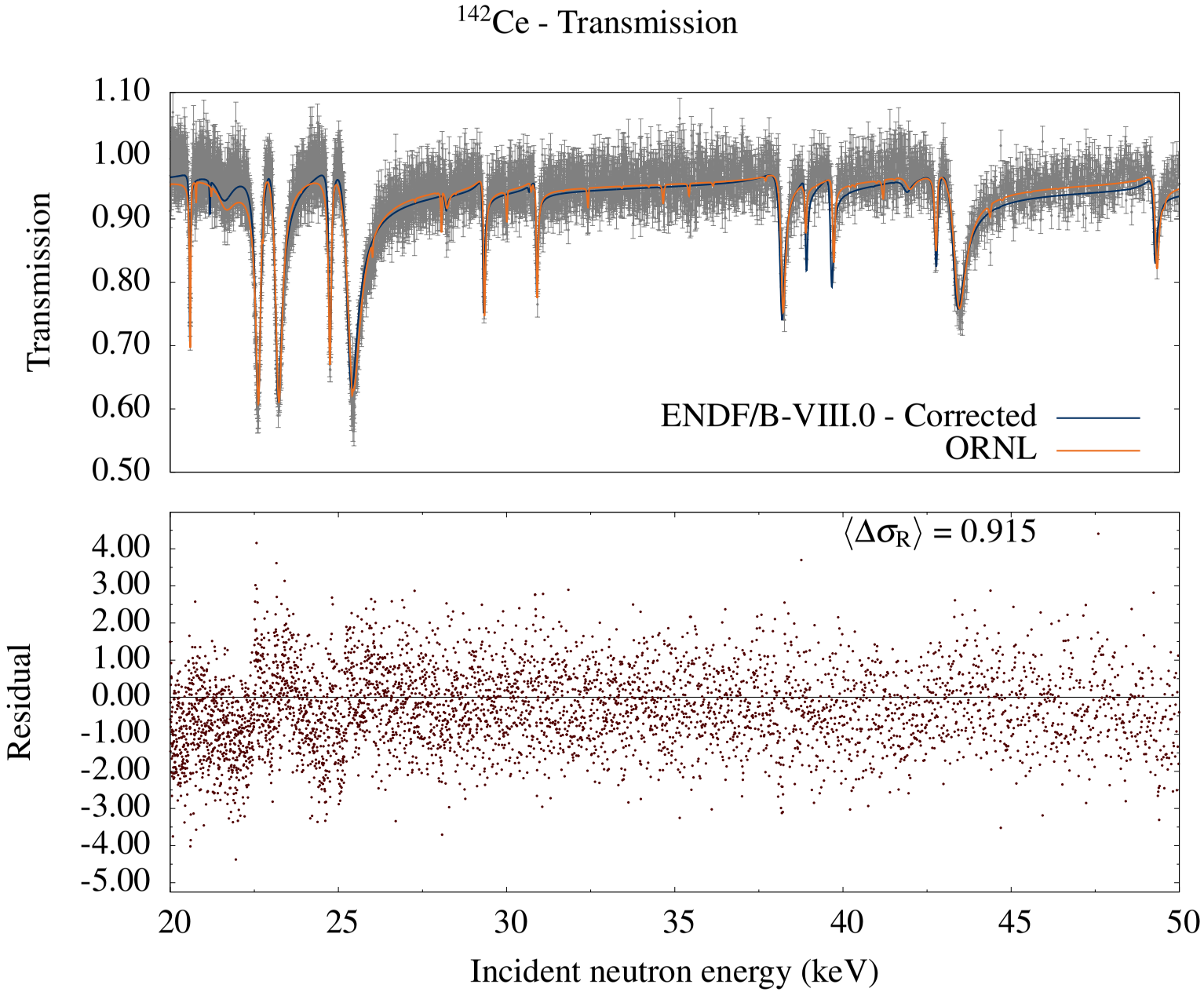

Figure 36. ^{142}**Ce Transmission - 20-50 keV**

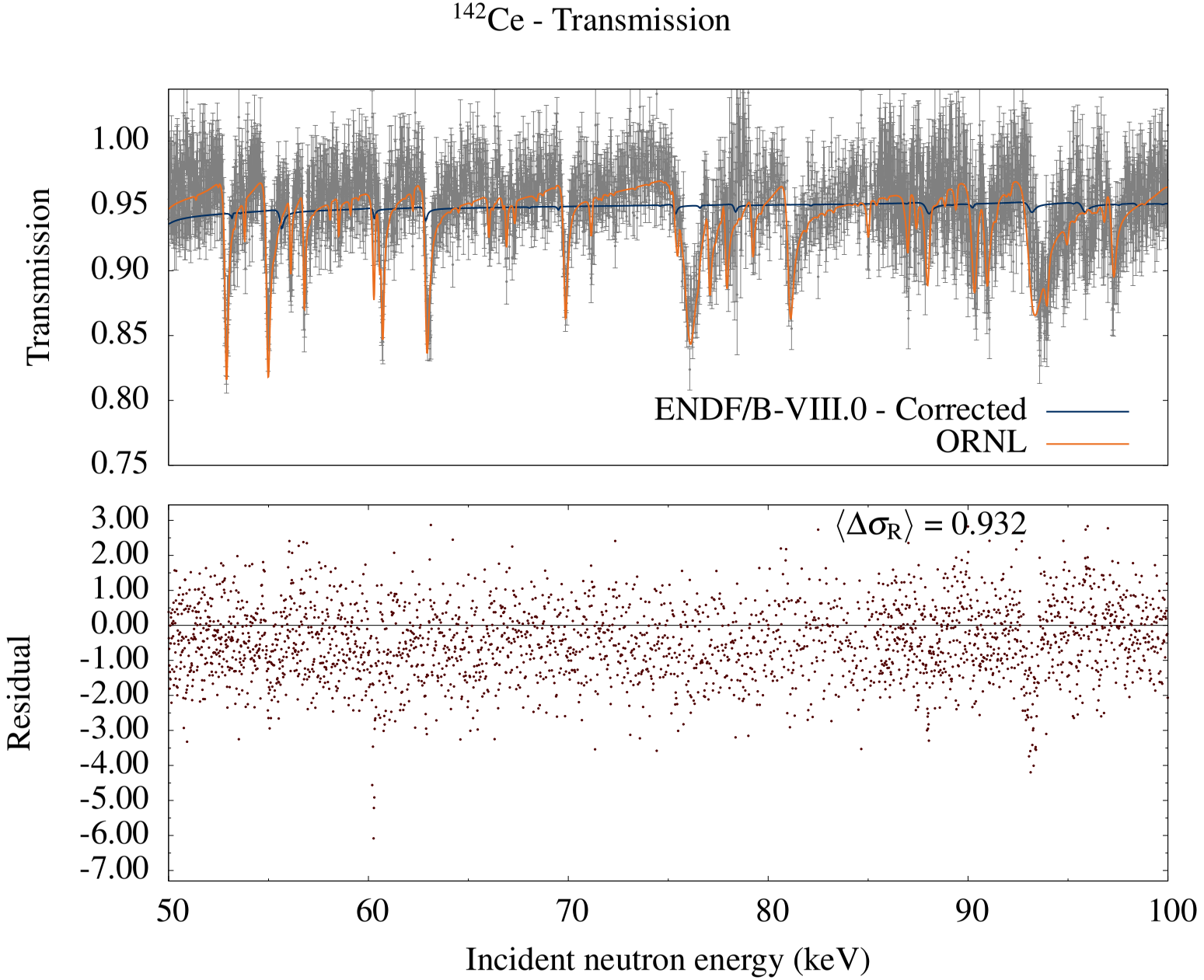

Figure 37. ^{142}Ce Transmission - 50-100 keV

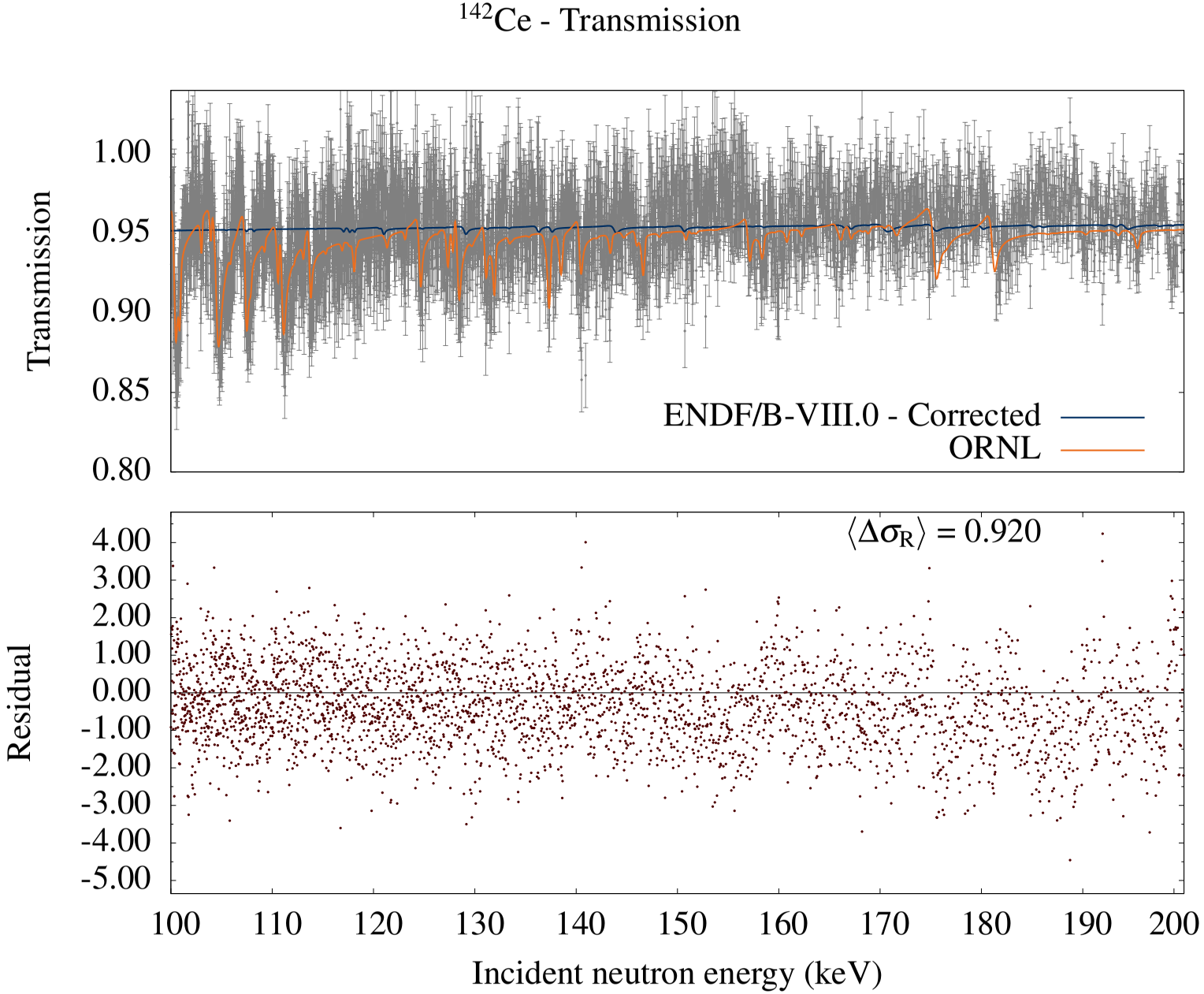

Figure 38. ^{142}Ce Transmission - 100-200 keV

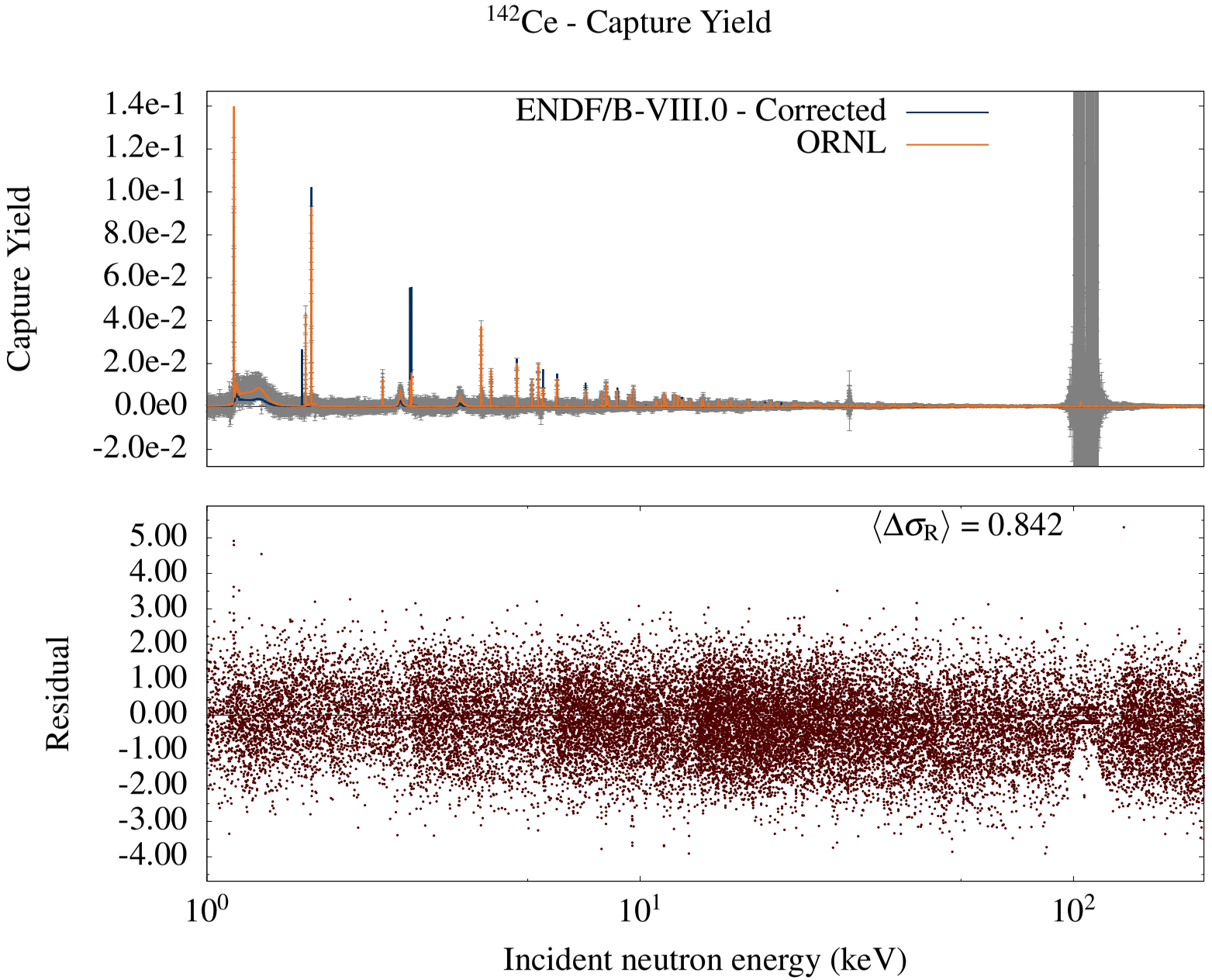

Figure 39. ^{142}Ce Capture Yield - 1-200 keV

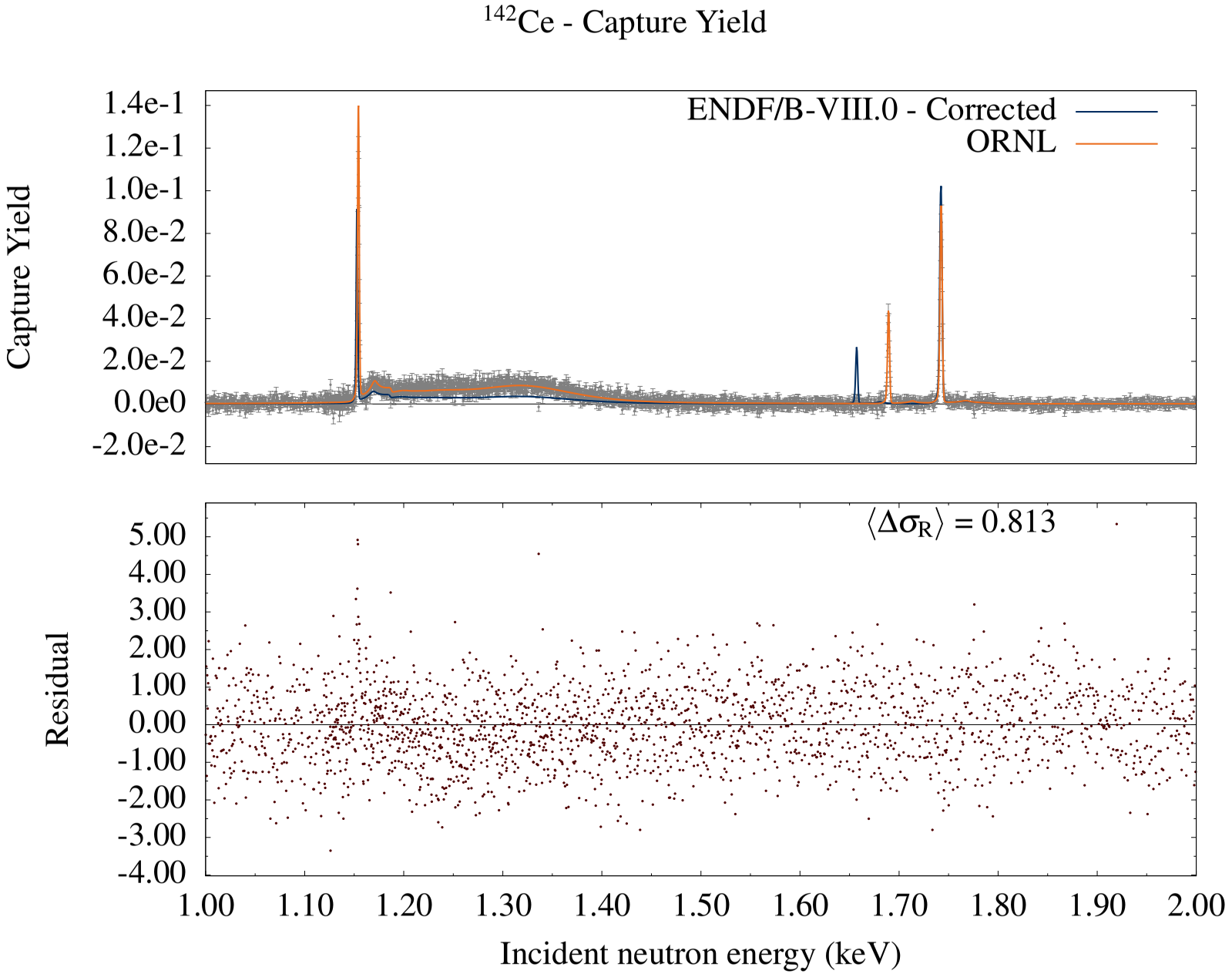

Figure 40. ^{142}Ce Capture Yield - 1-2 keV

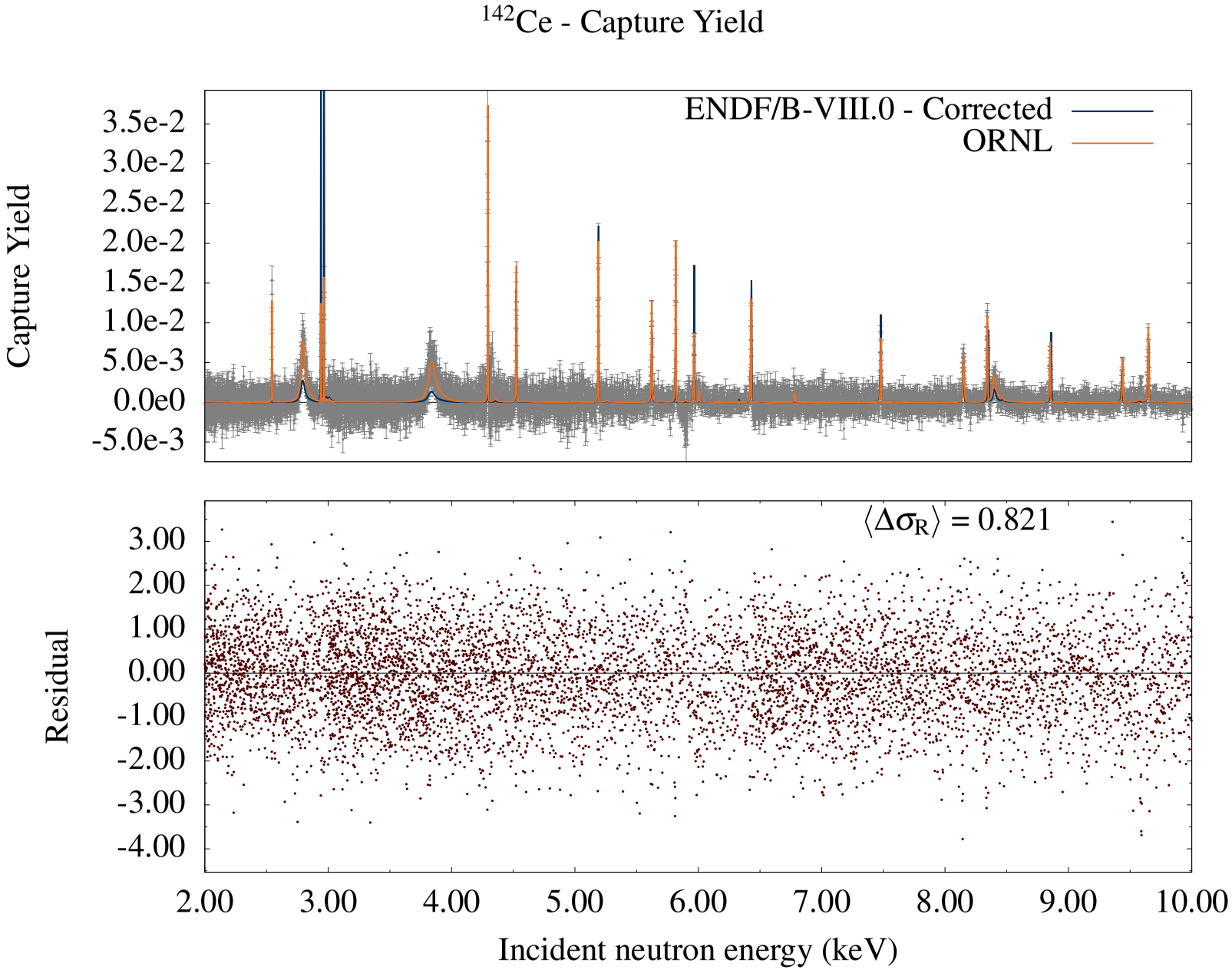

Figure 41. ^{142}**Ce Capture Yield - 2-10 keV**